PROCEEDINGS OF THE FIFTH PHOTOVOLTAIC SPECIALISTS CONFERENCE

VOLUME III

SOLAR POWER SYSTEM CONSIDERATIONS

20 October 1965

Held at the NASA-Goddard Space Flight Center
Greenbelt, Maryland

ARMY • **NAVY** • **AIR FORCE** • **AEC** • **NASA**

PROCEEDINGS OF THE FIFTH PHOTOVOLTAIC SPECIALISTS CONFERENCE

VOLUME III

SOLAR POWER SYSTEM CONSIDERATIONS

20 October 1965

Held at the NASA-Goddard Space Flight Center

Greenbelt, Maryland

FOREWORD

Continuing its interest in the photovoltaic area, the Interagency Advanced Power Group (IAPG) has published for the third time the proceedings of the Photovoltaic Specialists Conference. The content of these proceedings - a significant part of the information exchange activities of the IAPG - is of particular interest to members of its Solar Working Group.

This conference, the fifth of its kind, was cosponsored by IEEE, AIAA, and the NASA-Goddard Space Flight Center. Facilities for meetings and other arrangements were the responsibility of NASA-Goddard.

Presentations are included in the order in which delivered at the conference and were prepared from papers submitted to the Power Information Center (PIC) through the IEEE. Where papers have been authored by more than one person, cover sheets bear the name of the person who actually gave the presentation.

Presentations are arranged in three volumes and five sections reflecting the arrangement of the conference into three days and five sessions. Contents of the volumes are as follows:

Volume   I - Advanced Solar Cells

Volume   II - Thin Film Solar Cells and Radiation Damage

Volume III - Solar Power Systems Considerations

Transcriptions of the discussion periods following each presentation were prepared by Mrs. Marion Beckwith of Mr. Cherry's staff at NASA-Goddard. This effort is acknowledged as an important contribution to the proceedings.

Inclusion of a paper in these proceedings in no way precludes later publication in professional society journals.

PROCEEDINGS OF THE FIFTH PHOTOVOLTAIC SPECIALISTS CONFERENCE

Dates: 18, 19, and 20 October 1965

Place: NASA-Goddard Space Flight Center
        Greenbelt, Maryland

Attendance

Based upon information available at the time of publication, the following list represents those who attended at least one of the conference sessions:

IAPG Members Present:

Brancato, E. L.	NRL
Cherry, W. R.	NASA-Goddard
Fischell, Robert	APL
Hamilton, R. C.	IDA
Kittl, Emil	USAECOM
Potter, Andrew	NASA-Lewis
Schwarz, F. C.	NASA-ERC
Shapiro, S. J.	USAECOM
Smith, A. H.	NASA-HQ
Uchiyama, A. A.	JPL
Wise, J. F.	AF-APL
Yannoni, N. F.	AFCRL

Government:

Anderson, Donald	NASA-Ames
Brandhorst, H. W., Jr.	NASA-Lewis
Bullis, W. M.	NBS
Campbell, Frank	NRL
Cunningham, B. T.	NASA-Goddard
Danchenko, Vitaly	NASA-Goddard
Dawson, J. R.	NASA-Langley
Duncan, C. H.	NASA-Goddard
Ellis, W. E.	NASA-Langley
Fang, P. H.	NASA-Goddard
Faraday, B. J.	NRL
Ferris-Prabhu, A. V. M.	NASA-Goddard
Finger, H. B.	NASA-HQ
Foster, J. V.	NASA-Ames
Gallagher, D. J.	NASA-Goddard
Gdula, William	NASA-Goddard
Geiger, F. E., Jr.	NASA-Goddard

Government: (continued)

Goldsmith, Paul	JPL
Gordon, Frederick	NASA-Goddard
Green, Milton	USNUSL
Haynes, G. A.	NASA-Langley
Haynos, J. G.	NASA-Goddard
Hirschfield, Jule	NASA-Goddard
Hobbs, A. J.	NASA-Goddard
Janda, R. J.	NASA-Goddard
Jones, W. P.	NASA-Goddard
Kautz, H. E.	NASA-Lewis
Lambert, R. J.	NRL
Lillywhite, Malcolm	NASA-Goddard
Litynski, Z.	Library of Congress
Liu, Y. M.	NASA-Goddard
MacKenzie, C. M.	NASA-Goddard
Massie, L. D.	AFAPL
McCarron, S. G.	NASA-Goddard
Meszaros, George	NASA-Goddard
Mejia, N. V.	NASA-Goddard
Moses, E. G.	NASA-Goddard
Reetz, Art	NASA-HQ
Ritchie, D. W.	JPL
Salay, J. B.	NASA-Goddard
Schach, Milton	NASA-Goddard
Shepherd, J. M., Jr.	NRL
Shumaker, H. A.	NASA-Lewis
Sizemore, K. O.	NASA-Goddard
Slifer, L. W., Jr.	NASA-Goddard
Sokoloski, M. M.	NASA-Goddard
Spakowski, A. E.	NASA-Lewis
Statler, R. C.	NRL
Sullivan, R. M.	NASA-Goddard
Swartz, C. K.	NASA-Lewis
Tauke, Regina	NRL
Tucker, W. M.	NASA-Goddard
Waddel, R. C.	NASA-Goddard
Wannemacher, H. E.	NASA-Goddard
Wappaus, W. A.	NASA-Goddard
Weitzel, R. L.	NASA-Goddard
Yasui, Robert K.	JPL
Yuen, Joseph	NRL

Nongovernment:

Abrahams, Samuel	Fairchild Hiller
Adams, J. R.	Ball Brothers
Albright, George	Grumman Aircraft Corp.

Nongovernment: (continued)

Aldrich, R. W.	G.E. - Syracuse
Alexander, S. M.	Texas Instruments
Asbed, Norig	Hittman Associates
Augustine, Frank	Clevite Corp.
Bachner, R. L.	Solar Systems, Inc.
Baicker, J. A.	Princeton R&D Co.
Baker, J. K.	G.E. - Philadelphia
Barkley, D. W.	Libby Owens Ford
Barnhart, P. W.	Booz, Allen Applied Research
Barrett, Matt	Exotech, Inc.
Berry, Edwin	Aerospace Corp.
Bickler, Don	Hoffman Electronics Corp.
Blair, John	MIT
Boer, K. W.	Univ. of Delaware
Borson, E. N.	Aerospace Corp.
Burrill, J. T.	Ion Physics Corp.
Cain, Orison	Dow Corning
Chamberlin, R. R.	National Cash Register Co.
Chidester, L. G.	Lockheed M&S Co.
Close, J. R.	Minnesota Mining & Manuf. Co.
Cole, R. L.	Texas Instruments
Colehower, E. W.	Martin Co. - Baltimore
Cooley, W. C.	Exotech, Inc.
Cusano, D. A.	G.E. - Schenectady
Davis, Robert	Fenwal, Inc.
Downing, R. G.	TRW Systems
Downs, W. R.	Ball Brothers
Ellis, S. G.	RCA - Princeton
Feagin, R. B.	Texas Instruments
Feitknecht, J.	Allen Bradley Co.
Ferguson, G. D., Jr.	G.E. - Lynchburg
Flicker, H.	TRW Systems
Goldstein, Bernard	RCA - Princeton
Gould, J. A.	Clevite Research Center
Griffin, T. A.	Harshaw Chemical Co.
Halstead, R. E.	G.E. - Schenectady
Hangen, N. R.	RCA - Princeton
Hawkins, K. D.	Ryan Aeronautical Co.
Hicks, J. M.	Westinghouse Research
Hietanen, J. R.	Clevite Corp.
Hill, E. R.	Harshaw Chemical Co.
Holmes-Siedle, A. G.	RCA Labs. - Princeton
Hui, W. L. C.	RCA - Princeton
Holloway, H.	Philco Research
Hood, John	Dow Corning Corp.
Huffman, F. N.	Martin Co. - Baltimore
Ichikawa, Y.	Westinghouse - Youngwood
Iles, P. A.	Hoffman Electronics Corp.

Nongovernment: (continued)

Jilg, E. T.	Communications Satellite Corp.
Johnson, C. E.	Bellcomm Inc.
Julius, R. F.	Keltec Industries, Inc.
Kaye, S.	EOS, Inc.
Keramidas, B. G.	Harshaw Chemical Co.
King, W. J.	Ion Physics Corp.
Kling, H. P.	Hittman Associates
Lamb, A. H.	Atlantic Instruments & Electronics, Inc.
Ling, K. S.	RCA - Mountaintop
Lisak, L. R.	General Dynamics/Convair
Loferski, J. J.	Brown University
Luft, Werner	TRW Systems
Mann, A. E.	Spectrolab
Marks, B. S.	Lockheed M&S Co.
Martin, J. H.	Johns Hopkins Univ. - APL
Maxwell, K. H.	Philco Corp.
Medved, D. B.	EOS, Inc.
Mihm, F. I.	Heliotek
Miller, W. J.	G.E. - Lynchburg
Mlavsky, A. I.	Tyco Labs., Inc.
Mott, J. L.	Fairchild Hiller Corp.
Nelms, G. E.	Honeywell, Inc.
Nichols, Donald	General Atomic
Noble, E. B.	Westinghouse - Washington
Noel, G.	RCA - Princeton
Oman, Henry	Boeing Co.
Pearson, G. L.	Stanford University
Perkins, D. M.	RCA - Princeton
Pollack, S. R.	Univ. of Pennsylvania
Prince, M. B.	EOS
Ralph, E. L.	Heliotek
Rappaport, Paul	RCA - Princeton
Ratcheson, W. I.	Boeing Co.
Ray, K. A.	Hughes Aircraft Co.
Rensin, Ernest	ITT Federal Labs.
Reynard, D. L.	Lockheed M&S Co.
Riel, R. K.	Westinghouse - Youngwood
Rubin, Irwin	Solar Systems, Inc.
Runyan, W. R.	Texas Instruments
Sachs, I. M.	Optical Coating Labs.
Schaefer, J. C.	Harshaw Chemical Co.
Schlotterbeck, R. S.	G.E. - Lynchburg
Schwarz, F. R.	RCA - Princeton
Sequeira, Edward	EOS
Shirland, F. A.	Clevite Corp.
Skarman, J. S.	National Cash Register
Stanley, A. G.	MIT Lincoln Lab.

Nongovernment: (continued)

Stein, Irving	RCA - Princeton
Stevenson, R. D.	Douglas Aircraft
Stewart, Elmer	Harshaw Chemical Co.
Stonebraker, E. R.	Westinghouse - Youngwood
Stroebel, J. D.	Dow Corning Corp.
Tada, H. Y.	TRW Systems
Tarneja, K. S.	Westinghouse - Youngwood
Teener, J. W.	Johns Hopkins Univ. APL
Thomareas, Steve	Ryan Aeronautical Co.
Timberlake, A. B.	Battelle Memorial Institute
Toole, J. M.	RCA - Mountaintop
Uhler, E. F.	RCA - Harrison
Vette, James	Aerospace Corp.
Vineyard, Ray	Texas Instruments
Vohn, Paul	RCA - Princeton
Vrablik, E. A.	MIT - Lincoln Lab.
Wiener, Paul	RCA - Princeton
Williamson, E. M., Jr.	Libby Owens Ford
Winkler, S. H.	RCA - Princeton
Wolf, Martin	RCA - Princeton
Wysocki, J. J.	RCA - Princeton
Zehner, D. W.	Westinghouse - Baltimore
Zimmerman, Elizabeth	Philco Research Labs.

TAPG Secretariat:

Ashleigh, R. F.	PIC
Williams, F. E.	PIC

Program Committee

Paul Rappaport - Chairman
Robert E. Fischell - Secretary
Arvin H. Smith - Treasurer
William R. Cherry - Arrangements
Joseph J. Loferski - Technical Papers Coordinator

Robert Hamilton   Fred A. Shirland
Andrew E. Potter   Joseph F. Wise
Bernd Ross   Martin Wolf

VOLUME III

TABLE OF CONTENTS

PART E.   SOLAR POWER SYSTEM CONSIDERATIONS

*This paper was not made available for publication.

N66-17347

CALIBRATION OF SOLAR CELLS USING HIGH-ALTITUDE AIRCRAFT

Presented by

Henry W. Brandhorst, Jr.

NASA-Lewis Research Center

Cleveland, Ohio

20 October 1965

CALIBRATION OF SOLAR CELLS USING HIGH-ALTITUDE AIRCRAFT

Henry W. Brandhorst, Jr.
Lewis Research Center
National Aeronautics and Space Administration
Cleveland, Ohio 44135

Since June 1963 the NASA-Lewis Research Center has been using a high-altitude airplane to calibrate solar cells[1]. In this technique short-circuit currents of the solar cells are measured at different altitudes and then plotted logarithmically as a function of air mass. Extrapolation of these data to air mass zero yields the outer space short-circuit current of the solar cell.

The aircraft used in these studies is a B-57B as shown in Figure 1. It carries a crew of two - a pilot and a research observer. The solar cells are mounted in a collimating tube located in the aft fuselage (See Fig. 2). This area is not pressurized; hence, no window is placed over the test assembly. Because temperatures as low as -50°C are encountered on these flights, the solar cells are mounted on a block on which the temperature is thermostatically controlled.

The collimating tube is designed so that even with a variation of 2° in any axis during flight complete illumination would still be maintained over the sample holder which contains six cells. The tube is pivoted so that the angle of the tube will correspond to the solar elevation at the time of the flight. Once airborne, proper orientation of the tube to the Sun is assured by using an optical sight in the cockpit which is exactly parallel to the collimating tube in the aft section.

The outputs of the solar cells are measured as voltages across a 1-ohm load. In addition to the six short-circuit current voltages, there are several additional measurements relating to the temperature and solar intensity as shown in Figure 3. These voltages are indexed through a stepping switch and measured with a recording digital voltmeter system located in the cockpit and operated by the research observer.

The area for these flights is located 40° North latitude and 82° 30' West longitude, which is just east of Columbus, Ohio, The flights take place between 11:30 and 12:30 true solar time (approximately 12:00 to 1:00 EST) to ensure minimum air mass and minimum elevation change of the Sun.

On a typical run, as shown in Figure 4, measurements are made at altitudes ranging from 12,000 to 47,000 feet in 5,000-foot intervals. By knowing the time and location of each measurement, the solar elevation can be determined. Combining this with the altitude of each measurement yields the air mass of each point. Typical values of the air masses encountered

in this work range from 0.14 to 0.67 in June and 0.3 to 1.4 in January. The short-circuit currents so obtained are plotted logarithmically as a function of air mass and extrapolated to air mass zero.

Two corrections must be applied to this extrapolated current to obtain the true outer space short-circuit current. The first correction must be made because of the nonuniform distribution of ozone in the atmosphere. Roughly 80 percent of the ozone is still above 47,000 feet. While the major ozone absorption occurs in the ultraviolet region below the response of most solar cells, there is a weak absorption in the visible region between 0.4 and 0.7 micron known as the Chappuis band. The decrease in short-circuit current caused by this absorption can be calculated and is about 0.9 percent for typical n/p silicon cells. The second correction is normalization of the data to one solar constant, 139.6 milliwatts per square centimeter.

At the 1964 Photovoltaic Specialists Conference, a discrepancy amounting to several percent was reported between predictions based on balloon-flown [2] and airplane-flown cells with the airplane predictions being slightly lower. Also, the possibility of curvature of the Langley plot was noted. No explanation of these effects was possible at the time. In February 1965, the latter issue was clearly resolved, as shown in Figure 5. The break in the curve occurs at about air mass 0.6, corresponding to an altitude of 27,000 feet. Linear plots are obtained both above and below this point. It should be noted that extrapolation of the lower slope yields an outer space short-circuit current some 7 percent below the true value. The break is very abrupt and must, we felt, be associated with some peculiar property of the atmosphere.

A direct correlation between the location of the break in the Langley plot and the tropopause was made as shown in Figure 6. The tropopause is the boundary between the lower atmosphere or troposphere and the stratosphere. It is the altitude at which the ambient temperature either reaches a constant value (around -60°C) or the temperature lapse rate decreases to 2°C or less per kilometer. In the three cases shown in Figure 6, the tropopause, indicated by the arrow, was located at altitudes of 35,000, 38,000 and 31,000 feet corresponding to air masses of 0.37, 0.26 and 0.4, respectively. These data were taken over the period of March to April 1965. The correlation between the location of the tropopause and the break in the Langley plot is excellent.

In order to determine if variations in the tropopause effect the extrapolated short-circuit current, the same cell was flown at times when the tropopause was at air masses of 0.23, 0.25 and 0.34, as shown in Figure 7. All data have been normalized to one solar constant. It can be seen that the location of the tropopause has no effect on the extrapolated current provided the portion of the curve above the tropopause is used for extrapolation. Furthermore, the percentage difference between the upper curve extrapolation and the current obtained by using the line below the tropopause is variable and decreases as the height of the tropopause increases.

In order to obtain an accurate calibration, then, the flights must be made above the tropopause. Average height of the tropopause in the test area is about 36,000 feet. During the summer it rises to about 49,000 feet and in the winter it can go as low as 23,000 feet. While the B-57B has a service ceiling of 50,000 feet, sufficient data for accurate extrapolation of the Langley plot cannot be obtained when the tropopause is above 40,000 feet. Therefore, flights are limited to this condition and the altitude interval between data runs is variable from 2,000 to 5,000 feet, depending on tropopause location.

The physical origin of this break is not completely clear at the present time. Calculation of the solar cell short-circuit current as a function of altitude assuming nonuniform ozone and water vapor distributions in the atmosphere yields a curve which breaks in the opposite direction. Photographs of the solar image through the tropopause show no change in size. A recent paper[3] shows the presence of a "twinkle" layer in the atmosphere located near the tropopause; however, because of the size of the solar image, this effect should be negligible.

There does exist a haze layer at the tropopause, however, which may explain the effect. It is not visible to the naked eye while looking upward, but we have observed it while looking horizontally at altitudes near the tropopause. A paper by Kuhn and Suomi[4] confirms the existence of this haze layer and also shows that it can disappear in a few hours. We have observed a few curves that do not show a break at the tropopause but do show the high slope expected of data taken only above the tropopause. This behavior has been observed only in the summer.

In order to confirm the accuracy of the plots made above the tropopause, a series of flights was made on both primary and secondary balloon standard cells. The secondary standard cell that was flown was obtained from the Jet Propulsion Laboratory and had been calibrated with the technique described by Ritchie[5] last year. The results of this calibration are shown in Table I. All data are normalized to 28°C and 139.6 milliwatts per square centimeter. No break was observed at the tropopause. A calibrated monitor cell was also flown and its value did not deviate from its calibration value. The accuracy of the initial Jet Propulsion Laboratory calibration was ± 0.9 percent. The agreement between the two calibrations with the airplane results being slightly higher.

In summary, we have observed an unusual effect associated with the tropopause which causes an abrupt change in the slope of the solar cell Langley plot. Extrapolation of data taken above the tropopause to air mass zero yields consistent and accurate values of the outer space short-circuit current. Airplane calibrations of both primary and secondary balloon standard cells were carried out and show excellent agreement between the various techniques.

References

1. Brandhorst, Henry W., Jr.; and Boyer, Earle O.: Calibration of Solar Cells Using High-Altitude Aircraft. NASA TN D-2508, 1965.

2. Hadley, C. P.: Comparison of Flight and Terrestial Solar Measurements on Silicon Cells. Vol. II, Fourth Annual Photovoltaic Specialists Conf., NASA-Lewis Research Center, Cleveland, Ohio, June 2-3, 1964, Power Information Center, Penn. Univ., Phil., Penn., PIC-SOL 209/5.1, 1964. (NASA CR 59014, 1964)

3. Hudson, C. C.: Experimental Evidence of a Twinkling Layer in the Earth's Atmosphere. Nature 207, 247 (1965).

4. Kuhn, P. M.; and Suomi, V. E.: Airborne Radiometer Measurements of Effects of Particulates on Terrestial Flux. J. Appl. Meteor, 4, 246 (1965).

5. Ritchie, D. W.: Development of Photovoltaic Standard Cells for NASA., Vol. II, Fourth Annual Photovoltaic Specialists Conference, NASA-Lewis Research Center, Cleveland, Ohio, June 2-3, 1964, Power Information Center, Penn. Univ., Phil., Penn., PIC-SOL 209/5.1, 1964. (NASA CR 59014, 1964).

Fig. 1 B-57B Used in Solar Cell Testing Program

TABLE I. - AIRPLANE CALIBRATION OF SECONDARY STANDARD CELL

| CELL NUMBER	OUTER SPACE SHORT CIRCUIT CURRENT, $I_{SC,0}$*, mA		AIRPLANE AVERAGE, $I_{SC,0}$*, mA	GROUND CALIBRATION $I_{SC,0}$*, mA
	JULY 31, 1964	AUGUST 5, 1964		
NASA-182	48.3	48.3	48.3	48.45

TABLE II. - AIRPLANE CALIBRATION OF PRIMARY BALLOON STANDARD CELLS

CELL NUMBER	OUTER SPACE SHORT CIRCUIT CURRENT, $I_{SC,0}$*, mA		AIRPLANE AVERAGE, $I_{SC,0}$*, mA	BALLOON CALIBRATION, $I_{SC,0}$*, mA
	MARCH 11, 1965	APRIL 19, 1965		
1A	52.9	53.0	52.95	52.8
1B	59.0	59.1	59.05	58.7
2A	47.0	47.4	47.2	46.8
2B	52.3	52.4	52.35	52.0
3B	44.6	44.9	44.75	44.5

PIC-SOL 209/6.2

Fig. 2 B-57B Used in Solar Cell Testing Program
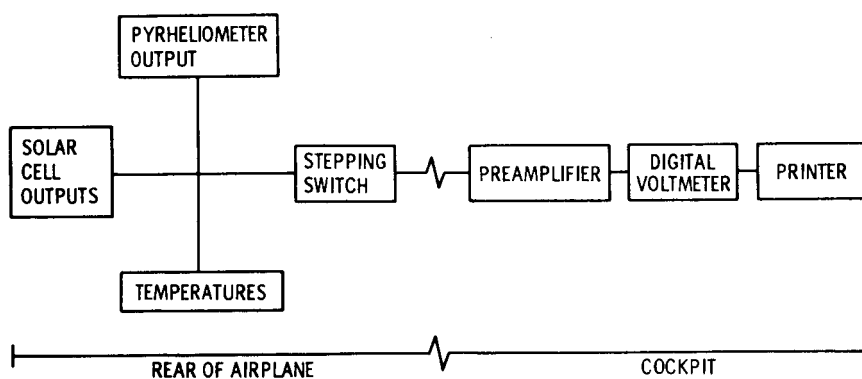
BLOCK DIAGRAM OF DATA ACQUISITION SYSTEM.

Figure 3.

FLIGHT PATTERN FOR B—57B SOLAR CELL TESTING FLIGHTS
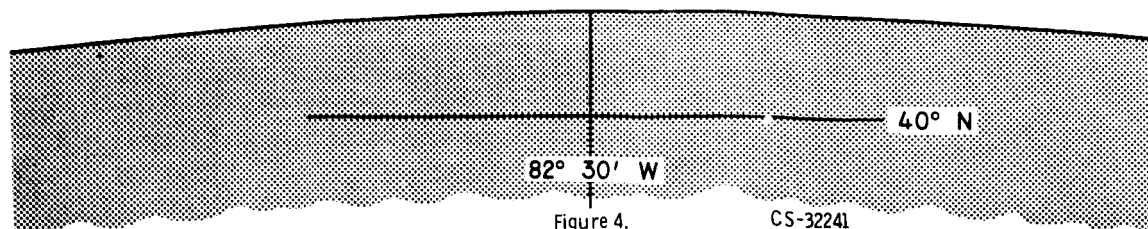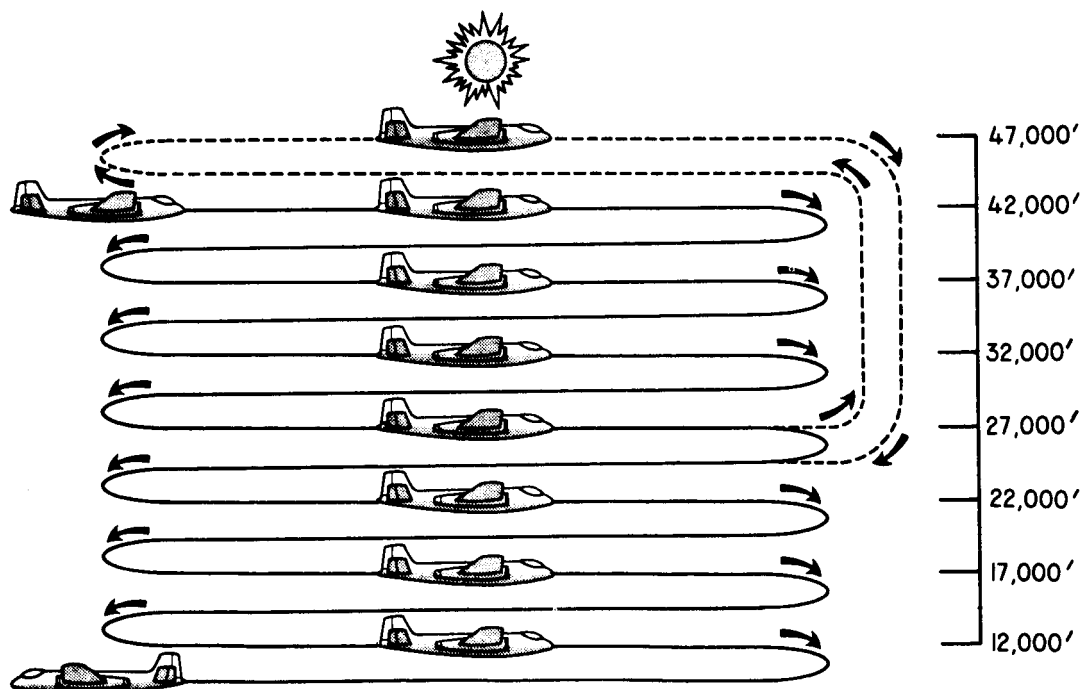

Figure 4.   CS-32241

CORRELATION BETWEEN TROPOPAUSE AND THE ANOMALOUS LANGLEY PLOT
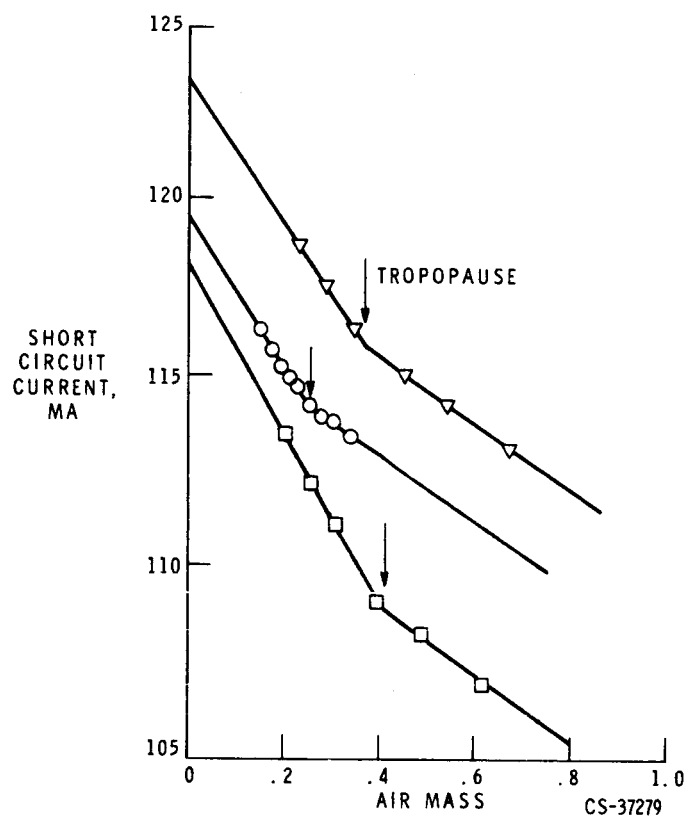

Figure 6.

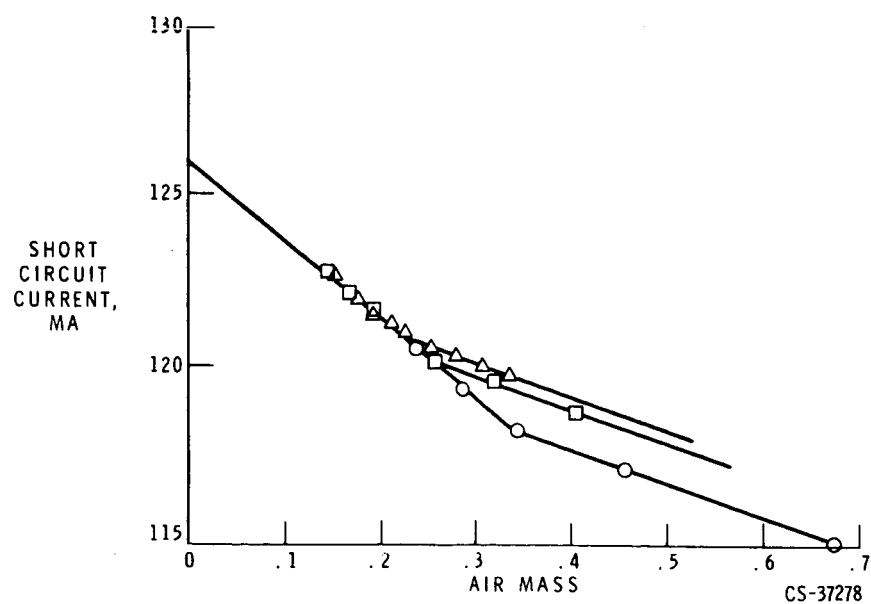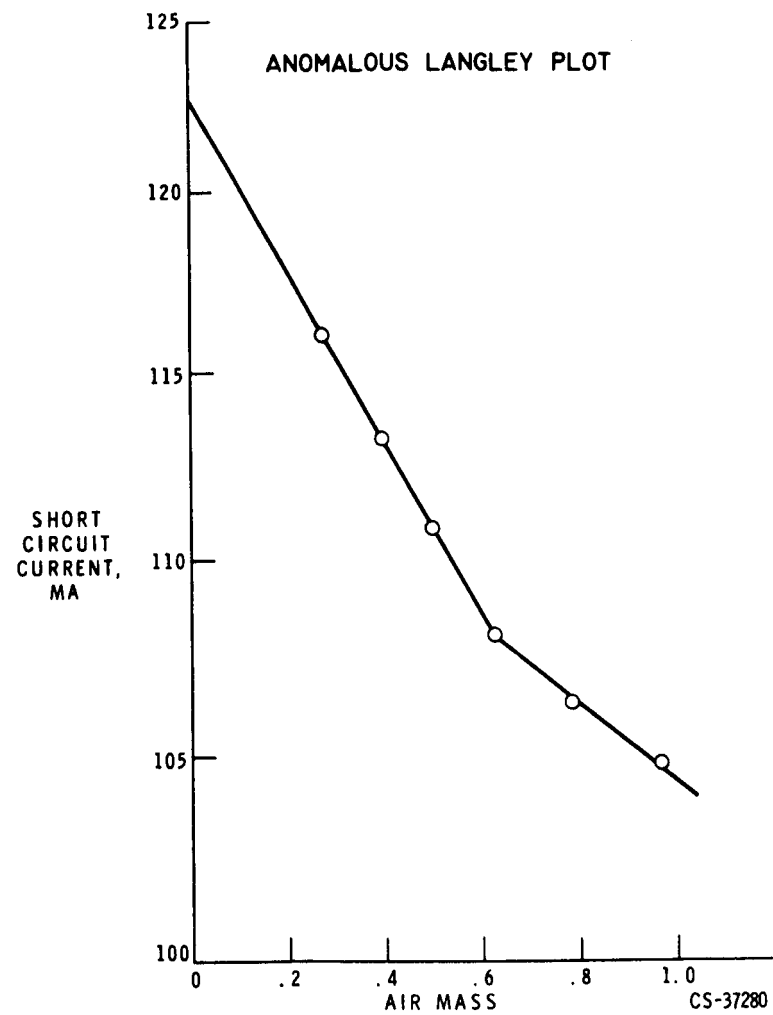EFFECT OF TROPOPAUSE ON THE OUTER SPACE SHORT CIRCUIT CURRENT

Figure 7.

Figure 5.

Discussion

Reynard: Questions, please.

Flicker - TRW: It seems fairly obvious that since you are already measuring the integrated power with a pyrheliometer, the only problem at the tropopause must be in the distribution. Have you tried sending up a set of interference filters in front of your pyrheliometer?

Brandhorst: Instead of putting interference filters in front of the pyrheliometer, which unfortunately is extremely broad band and a relatively inaccurate device, let me say - that's on tape, I'm sorry - (laughter), we have anticipated putting various filters over cells themselves, in hopes of observing some blue to red ratio shift through the tropopause. We have not had the time to do this as yet.

Haynes - NASA-Langley: Your tropopause - is this a locally occurring phenomenon?

Brandhorst: No. The tropopause is a universal phenomenon of the atmosphere.

Haynes: I see. Then you couldn't change your location and thereby rid yourself of a high tropopause.

Brandhorst: We can. Curiously enough, the tropopause reaches an average maximum height around 50,000 feet at the equator and descends to an average value of about 24,000 feet at the North Pole. I don't like the thought of going to Thule, Greenland and flying. (laughter) There is a variation in tropopause height: the farther north you go, the lower it gets.

Tada - TRW Systems: Do you have any feeling about difference in the spectral irradiance at the lowest altitude and the highest altitude that you go?

Brandhorst: We have no idea of the spectral distribution. We have, as I said, made measurements of the solar intensity with the pyrheliometer as a function of altitude. We unfortunately haven't been able to make any spectral distribution measurements.

Yuen - Naval Research Lab: Do you take into consideration whether you're using blue response or red response cells?

Brandhorst: We've flown a number of different spectral response solar cells ranging from the p on n red-shifted cells to the current, extremely blue-shifted n on p cells - some that are made at Lewis. We've also flown cadmium sulfide cells. The only correction that we make for spectral response is in the ozone correction. It changes it slightly. It's about eight-tenths percent for a typical p on n cell, about 1.1

percent for gallium arsenide, 1.2 percent for cadmium sulfide, as I recall offhand.

Yuen: But I was thinking about this tropopause effect. Do all cells have the same effect?

Brandhorst: Yes. Regardless of cell type, there is always an abrupt shift at the tropopause. The only effect that the different spectral responses would have would be to perhaps change the slopes of the curve slightly.

Yuen: Another question. Do all the cells have cover slides on them?

Brandhorst: No, we have flown with and without cover slides on them and we see no difference in the results as far as the tropopause is concerned.

B. Cunningham - GSFC: In one of the slides you showed a favorable comparison between aircraft data - I think balloon data - and then in the last column - the column furthest to the right - you showed a ground calibration column. It again compared favorably with the balloon and aircraft. What do you mean by "ground calibration"?

Brandhorst: This ground calibration was done by Don Ritchie at Table Mountain. These are the secondary standards that he generated against the primary balloon cells as described last year. This is why I referred to it as the ground calibration - it is the secondary standardization.

Cunningham: I see. OK. Thank you.

*SKY EFFECT ON SOLAR CELLS USING HIGH ALTITUDE AIRCRAFT

Presented by

D. W. Ritchie

Jet Propulsion Laboratories

Pasadena, California

20 October 1965

*This paper was not made available for publication in these proceedings.

N66-17348

PREFLIGHT CALIBRATION AND MATCHING OF SOLAR CELLS

FOR A BAND-PASS FILTER EXPERIMENT

Presented by

E. L. Ralph

Heliotek, Division of Textron Electronics, Inc.

20 October 1965

Abstract

This solar cell calibration experiment has been designed to evaluate solar cell performance in space over various wavelength regions. A detailed matching and calibration program was carried out to select an essentially identical group of solar cells. The solar cells were to be flown on a satellite without recovery capabilities, so it was necessary to obtain duplicate units which could be maintained on the ground and be calibrated indirectly by the telemetry data from the space units.

This paper describes the preflight measurement and matching program which was carried out to provide several complete standard units of essentially identical cell characteristics. The primary criteria for selection was the matching of cell spectral response over a temperature range of 10 to 90°C. Also, measurements and matching of cell current output at load point at various temperatures were made. After final selection of the cells to be used in the experiment and the encapsulation in the flight package, a final correlation ratio was determined between all cells when illuminated with various light sources. The matching program resulted in at least five cells of each of the five filter types being matched to within ± 2% over a wide temperature range. The flight cell and at least one cell on the ground of each type were matched to within ± 1%.

In conclusion, several predictions of the space performance of these cells were made based on present-day earth to space extrapolation techniques. A comparison of the calibration data obtained from space to these predictions gives a good check on the validity of the extrapolation techniques typically used.

PREFLIGHT CALIBRATION AND MATCHING OF SOLAR CELLS
FOR A BAND-PASS FILTER EXPERIMENT

E. L. Ralph
Heliotek, Division of Textron Electronics, Inc.

Introduction

At the time this band-pass filter experiment was conceived, the knowledge of the expected performance of solar cells in space sunlight was still somewhat uncertain even though the general claim was that performance to within about $\pm 5\%$ was known. Several attempts to try and improve upon this uncertainty have been made, but in every case an extrapolation technique has been used.[1] [2] [3] [4] It was felt that a space calibration experiment with some additional spectral information would be very useful to verify previous calibration studies and, in addition, supply spectral calibration data for checking out solar simulators.

This experiment utilized four quartz windows with different interference type band-pass filters. These filters were placed over four closely matched cells and one additional cell had a quartz window without a filter. Thus, a complete standard set analyzed four wavelength regions within the cell response range in addition to the over-all response analysis. Figure 1 shows the typical filter transmission curve for the four wavelength regions. Also shown is the typical spectral response curve of the cells used in the experiment. It can be seen that the four filters were designed to essentially cover the complete cell response region. Each filter width was chosen so that about one-fourth of the total cell output was obtained. Since the experiment was to be flown on a non-recoverable satellite, it was important to prepare standard units similar to the flight units which would remain on the ground to be used as working standards. The objective was to match and select all cells and filters as closely as practical so that temperature effects, angles of incidence, spectral variations, etc. would have the same effect on all cells and the filtered units. This extremely close match would then allow one to obtain meaningful space calibration data over a wide range of conditions. One would then be able to duplicate these conditions in the laboratory with the working standards and set up and calibrate solar simulators. The proper over-all intensity, as well as the proper cell output for the four discrete wavelength regions, could then be achieved.

To accomplish the above goals a detailed measurement and matching program was performed prior to the selection of the cells for the standard sets. The following sections describe the tests performed and the resulting match of thirty solar cells which made up six complete standard sets of five cells each.

Measurements

The initial selection of the N/P 10 ohm cm solar cells to be used in this experiment was based on an efficiency classification in a 2800° Kelvin tungsten light source. Cells from one efficiency grouping were then remeasured in the

tungsten source at 28°C and the cells were classified into one milliamp groups. Two hundred fifty-eight cells within a one milliamp group were then used to make up the population for the spectral response matching program.

The first spectral response measurement was made on the 258 cells using the band-pass interference filter spectral response equipment described in a previous publication.[5] Because of the large number of cells to be tested, only five wavelengths (filters) were compared for this preliminary screening. Measurements were made at 28 and 90°C to indicate the best match with regard to spectral response changes with temperature. A distribution diagram of the results of this test is shown in Fig. 2. It can be seen that the distributions are better formed near the center of the solar cell response range. At both the blue and red ends the distribution had a double mode indicating at least two distinct and different characteristics being present. The blue end differences are probably due to antireflection coating variations. Since all the cells for this experiment were to be as similar as possible, cells were selected from only one mode in the extreme wavelength cases. For all other wavelengths the distribution was within ± 5% of the mean so a preliminary spectral response match of ± 2% seemed possible. To match a group of cells for a particular band-pass filter, the response was compared at the two temperatures and at the wavelengths that were applicable for the particular band-pass filter which would be used (see Fig. 1). As a minimum, six cells for each of the five filter types were desired, so 39 cells were selected at this point to allow for future losses.

These 39 cells were then retested at 28°C using all thirteen wavelengths available in the spectral response equipment. This verified the previous measurement and also supplied a complete spectral response curve for each cell.

Each of the 39 cells were then soldered onto a metal substrate with a thermal expansion coefficient similar to silicon. This provided good thermal contact and a mechanical method for mounting in the flight package after final matching. Figure 3 shows the cell substrate assembly as well as the flight package and a quartz window.

After the soldering and mounting of the 39 cells the spectral response was remeasured at all thirteen wavelengths and at 10°, 28°, 60° and 90°C. This measurement provided the data from which the best match could be determined. Each of the four filter types and the over-all response wavelength ranges were then assigned specific cells based on temperatures. The cells selected for each filter type were identified by group numbers I through V corresponding to the filter type.

Spectral response measurements were repeated twice after this classification into groups to insure reliability in the selection. These two measurements were done at 28° and 90°C for the first retest and 28° and 60°C for the second retest.

A final grouping and selection was then made based on the analysis of all of the above spectral response measurements. Figure 4 is a summary table showing the maximum spread in spectral response for each group of six (or seven) cells, for each filter type, making a total of 32 cells selected. The data is tabulated for the four temperatures investigated. At 28° and 60°C the cells within each group are matched very well and have a maximum spread of less than 4% (± 2%) for all wavelengths in the cell-filter response region. The spread between the three best matched cells of each group was typically one-half the total spread, thus giving a match within about ± 1% at all wavelengths shown.

The data at 10°C and 90°C shows a larger spread than that obtained at 28° and 60°C. This could be expected for various reasons. First, the measurement repeatability (typically ± 0.5%) was not as good when the test temperature deviated substantially from room temperature. This was primarily due to differences in cell test temperatures. Since each cell had to be placed in a temperature controlled test fixture and subsequently allowed to reach an equilibrium temperature, slight variations in the thermal coupling and heat transfer caused significant temperature differences. This would be expected to cause the most problem in matching both the long and the short wavelength response regions since these regions of the cell spectral response are the most sensitive to temperature changes. Review of the data in Fig. 4 indicates that nineteen of the 21 data points having greater than 4% spread occur in these regions. To further complicate the measurements the cell response is very low at the extreme wavelength regions, thus reducing the measurement accuracy further. In addition to the above the spread in response would be expected to have the most variation cell-to-cell at the extreme wavelength regions because of the basic physical factors contributing to the cell response. Minority carrier lifetime and resistivity variations from one silicon slice to another would be expected to cause significant variations in the long wavelength region. Antireflection coating and diffusion process variations would be expected to have the largest effect on the response in the short wavelength region. Therefore it is understandable that the center wavelength region showed little increase in response spread for 10° and 90°C while the long and short wavelength regions experienced an increase in the spread, thus making cell matching more difficult in these regions.

Subsequent to the spectral response measurements and grouping of the matched cells, measurements were made in a D1203 Sunlight Simulator at 10°, 28° and 90°C. For this test the six best matched cells from each filter type group were measured with its respective filter type placed over the cell (i.e., the same physical filter window placed on all cells of a group). The short circuit current and the current at 250 mV (corresponding to load conditions in the flight experiment) were measured and the maximum spread in the data determined for each group of six cells per filter type. Information at 250 mV was needed since the previous matching was based on short circuit current which did not insure similar I-V characteristics. Short circuit current values were also measured in sunlight on Table Mountain, California, at 28°C with the proper filter covering each cell. These measurements are summarized in Fig. 5. It can be seen that the short circuit currents of all cells at all three temperatures are matched within 5%. This corresponds well

with the spectral response data (which is actually a short circuit current measurement). The current at 250 mV was highly dependent on the I-V curve shape so this data showed more spread. The 10° and 28°C data for both short circuit current and current at 250 mV had a very small spread of less than 4%. The 90°C data showed a larger spread at 250 mV. This was expected since at 90°C and at 250 mV; the knee of the I-V curve has a predominant effect on the current output and a substantial deviation from short circuit current is experienced.

From the simulator data above, the temperature dependence of short circuit current and current at 250 mV was obtained. The resulting curves are shown in Fig. 6. The deviation of the current at 250 mV from short circuit current at high temperatures can be seen readily from these curves. At lower temperatures such as those expected in space, (actual space operational temperatures were typically about 5°C) the two are identical and the temperature dependence is predictable so that reliable temperature corrections can be made. Subsequent to the original temperature calibration a repeat measurement was made on the Spectrosun X-25, a more advanced solar simulator with a better air mass zero spectrum match, and the additional data points at 5° and 28°C were obtained. Therefore, between these temperatures the data has been refined and should be representative of the temperature effect in M = 0 sunlight.

The above measurements constituted the pre-encapsulation selection and matching program. The cells were then encapsulated in the flight package with prematched and selected filters. A prematched and selected load resistor was then soldered across the cell terminals. The output voltage of each of the six standard sets (consisting of one each of the five filter types) was then measured in sunlight on Table Mountain, California, and the output from each cell was correlated to one particular cell for each filter type. Figure 7 shows the correlation ratios (voltage output ratios) obtained for all standard sets at 28°C relative to the APL standard set which was maintained as a laboratory standard. This correlation ratio constituted the final check of the sets and indicated the degree of matching that was accomplished in their operational state. One cell (Heliotek standard, filter type II) was obviously changed during mounting or assembly so that it was no longer as closely matched to the other cells from the filter Type II group. All other cells were matched to within the 4% that was expected based on the previous measurements.

As a further check of the success in matching, three standard sets were measured in the D1203 Solar Simulator and in a tungsten (2800°K) light source. The correlation ratios (Fig. 7) show that the close matching was maintained even though these two sources represent a very large variation in spectrum.

Results

The matching and selection program described above provided six sets of standards which were very similar in response and output. At least one of the sets was matched to within ± 1% of Flight Set No. 2, which was orbited

and returned space calibration data. The flight results of this experiment are described in another paper.[6] Assuming telemetry and data acquisition errors to be negligible (which may not be the case) this one working standard set would be space calibrated to within $\pm$ 1%. By applying the corresponding correlation ratio for each cell, all standard sets should be calibrated to better than $\pm$ 1% which would represent a significant improvement over calibrations previously available.

In addition to the matching measurements discussed above, several measurements and extrapolations to M = 0 conditions were made on an unfiltered Type V cell. This was done by several different techniques typically used for predicting solar cell output in space. The first test involved a Table Mountain measurement at 100 mW/cm^2 intensity (M = 1) based on a pyrheliometer standard. The output was then extrapolated to M = 0 (140 mW/cm^2) conditions using a K factor of 1.21 (determined by a theoretical ratio of the cell spectral response multiplied by the M = 0 and M = 1 spectral distributions).[7] The resulting M = 0 current output for the Heliotek Standard Type V cell at 28°C was 61.0 mA (or 244 mV across the 4 ohm load resistor).

The second test involved a Table Mountain measurement made simultaneously with a measurement of NASA (JPL) secondary balloon standard cell No. 188. The extrapolation to M = 0 conditions was made by using a direct proportionality relationship based on the M = 0 (140 mW/cm^2) calibration value of Standard No. 188.[8] This technique resulted in the Heliotek Standard Type V cell current output at 28°C being 60.8 mA (or 243 mV across the 4 ohm load resistor).

The third test was to set up the X-25 Solar Simulator to the proper M = 0 (140 mW/cm^2) intensity using Standard No. 188 then measuring the output of Heliotek Standard Type V cell at 28°C. In this case the output was 244 mV across the 4 ohm load resistor.

The fourth test was an M = 0 extrapolation from Table Mountain sunlight based on simultaneous measurements with JPL primary balloon standard No. BFS17A. The M = 0 (140 mW/cm^2) calibration of the Heliotek Standard Type V cell at 28°C was 242.9 mV across the 4 ohm load resistor.[9]

All four M = 0 extrapolation techniques above showed good agreement with the mean value being 243.5 mV. Preliminary data from the space calibration experiment indicates that the calibration value of Flight Set No. 2 Type V cell in space at 28°C was 245 mV. Application of the voltage output ratio, corresponding to the Heliotek Standard and the Flight No. 2 Type V cell, (Fig. 7) to the space data, gave a space calibration value for the Heliotek Standard Type V cell of 244 mV. Therefore, good agreement between the various extrapolation techniques and the space calibration was obtained.

Acknowledgements

References

1. John A. Zoutendyke, "A Method for Predicting the Efficiency of Solar Cell Power Systems Outside the Earth's Atmosphere", Technical Report No. 32-259, Jet Propulsion Laboratory, April 10, 1962.

2. Henry Oman, "Solar Cell Calibration by Means of Balloon Flights", Proc. Solar Working Group Conference, 28 February 1962.

3. J. A. Zoutendyke, "The Space Calibration of Standard Solar Cells Using High Altitude Balloon Flights", Proc. 4th Photovoltaic Specialists Conference, 3 June 1964.

4. Henry W. Brandhorst and Earle O. Boyer, "Calibration of Solar Cells Using High-Altitude Aircraft", NASA TND-2508, February 1965.

5. E. L. Ralph and M. Wolf, "Effect of Antireflection Coatings and Cover-glasses on Silicon Solar Cell Performance", Proc. 4th Photovoltaic Specialists Conference, 2 June 1964.

6. W. E. Allen and R. E. Fischell, "Use of Solar Cells and Band-Pass Filters for Calibration of Solar Simulators", 1965 Photovoltaic Specialists Conf. October 18-20, 1965.

7. "Extrapolation of Table Mountain Measurements to Air Mass Zero Conditions", Heliotek Technical Paper, Revised 1 June 1964.

8. D. W. Ritchie, "Development of Photovoltaic Standards for NASA", Proc. Fourth Photovoltaic Specialists Conf., 3 June 1964.

9. The calibration against JPL Balloon Standard BFS17A was done through the courtesy of Mr. D. Ritchie of JPL.

RELATIVE SPECTRAL RESPONSE DISTRIBUTION FUNCTIONS
OF 258 N/P SOLAR CELLS FOR FIVE WAVELENGTHS OF
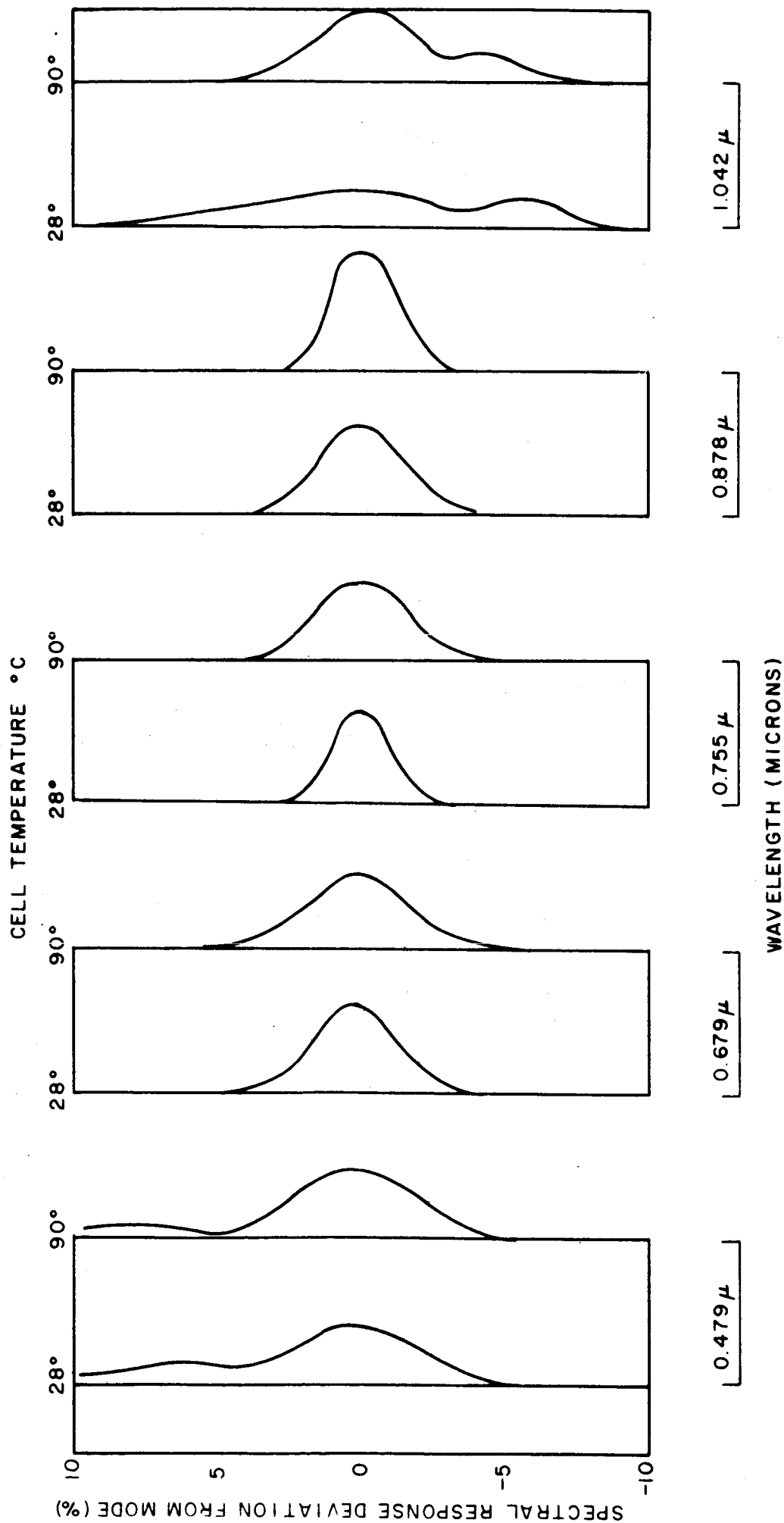LIGHT AND TWO CELL TEMPERATURES
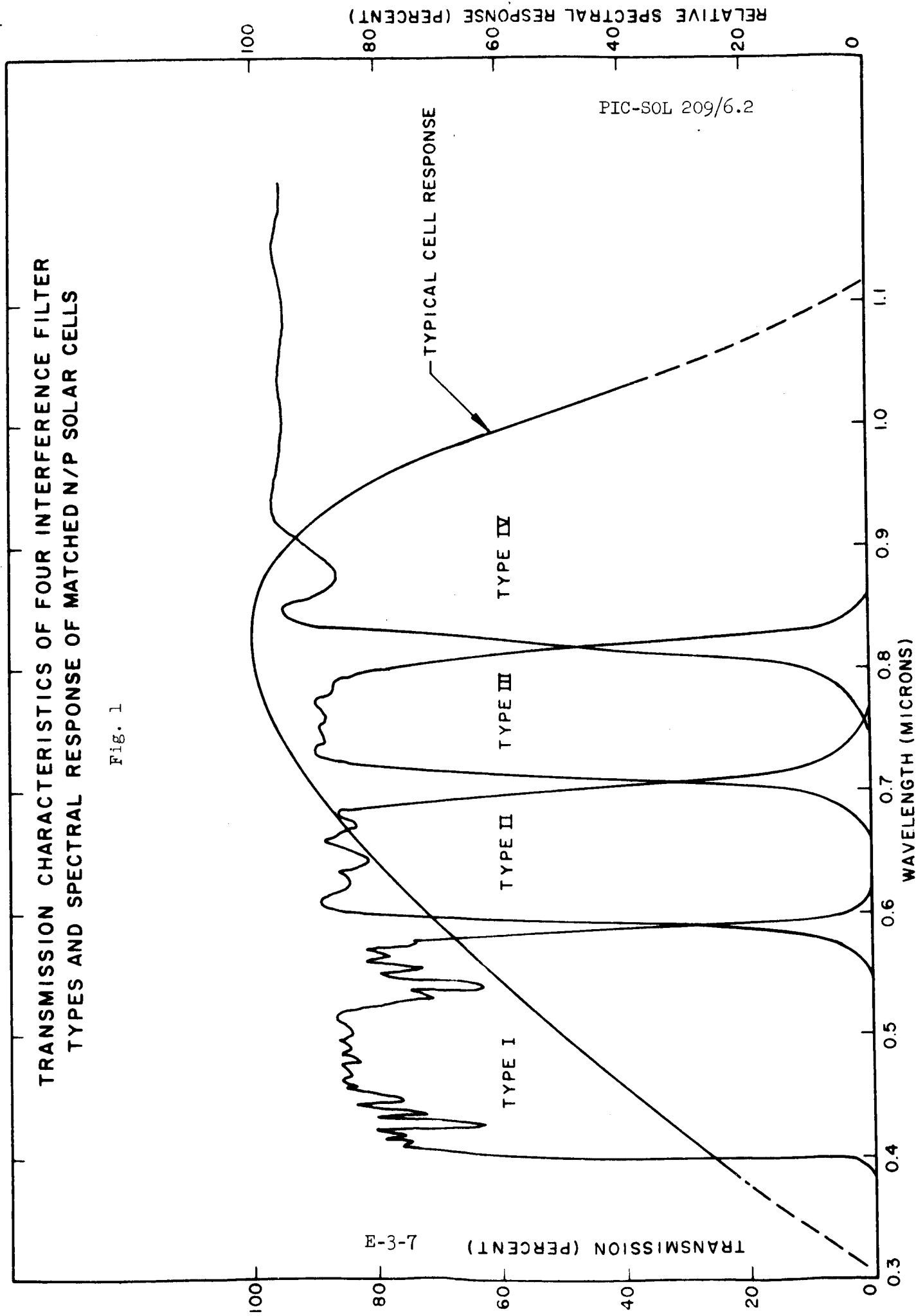
Fig. 2

TRANSMISSION CHARACTERISTICS OF FOUR INTERFERENCE FILTER
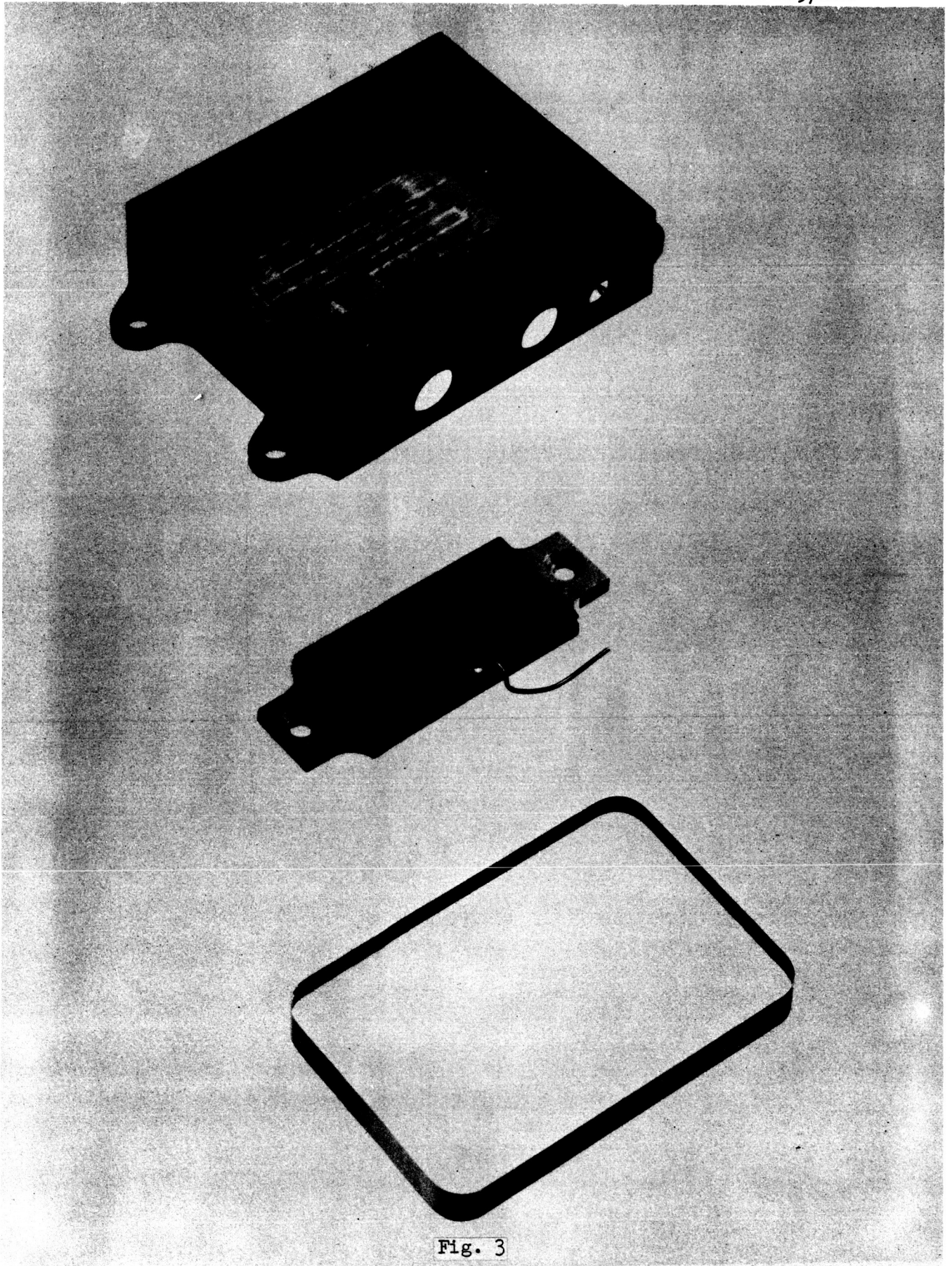TYPES AND SPECTRAL RESPONSE OF MATCHED N/P SOLAR CELLS

Fig. 1

PIC-SOL 209/6.2

TYPICAL CELL RESPONSE

TYPE I

TYPE II

TYPE III

TYPE IV

WAVELENGTH (MICRONS)

RELATIVE SPECTRAL RESPONSE (PERCENT)

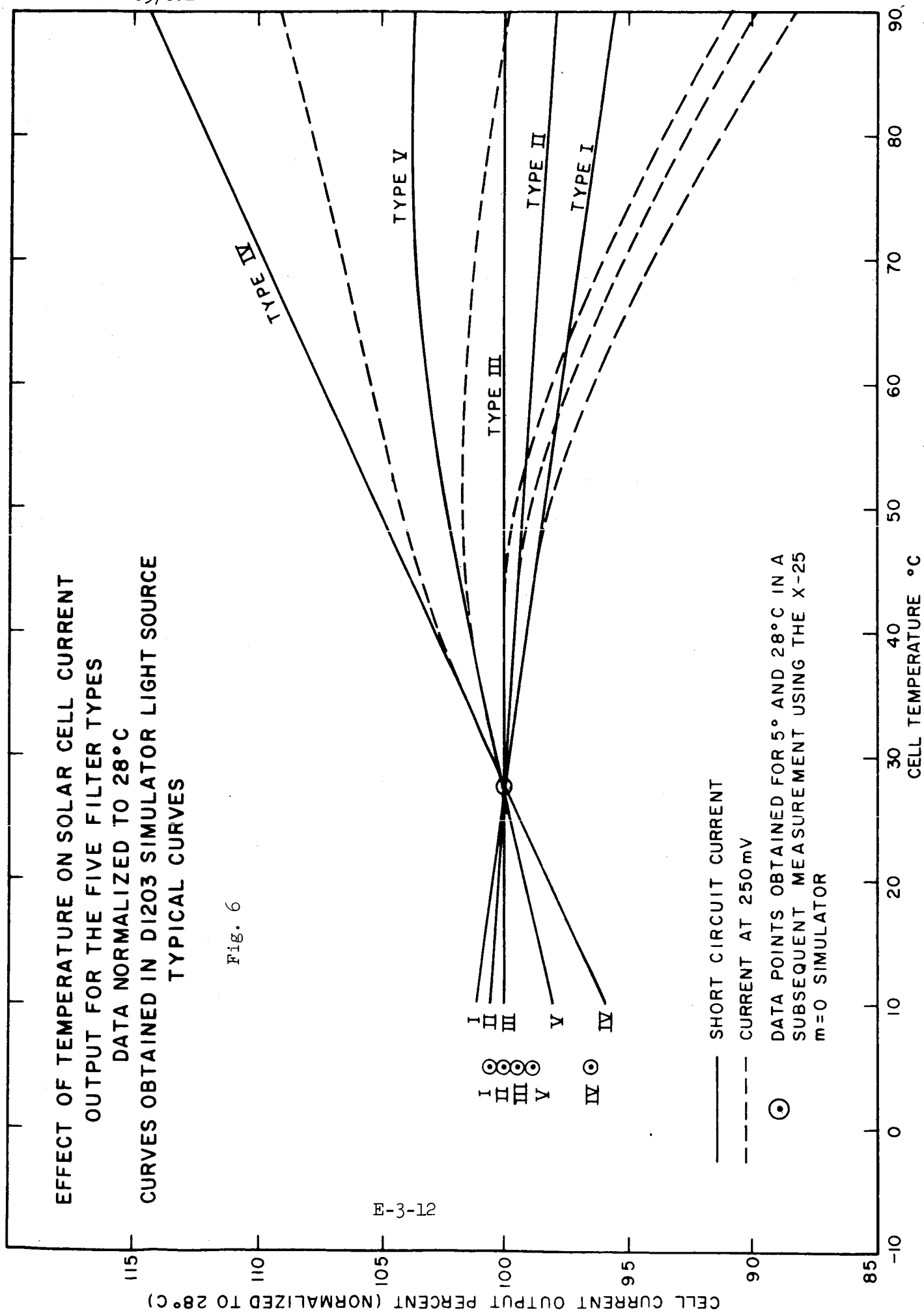TRANSMISSION (PERCENT)

E-3-7

Fig. 3

SPECTRAL RESPONSE MATCH AT VARIOUS TEMPERATURES

Cell Temperature °C	Group Identification	Number of Cells in Group	Maximum Spectral Response Spread (Percent) Wavelength (micron)													
			.436	.479	.500	.596	.679	.709	.755	.804	.878	.911	.965	.992	1.042
10	I	6	3.7	2.4	2.6	2.0	1.1								
	II	6		1.7	3.4	(5.8)	2.8	3.1	3.1						
	III	7				1.6	1.6	2.1	1.6	1.8	(4.3)				
	IV	7							2.1	2.3	3.1	3.4	(4.9)	2.4	(6.6)
	V	6	(6.8)	2.3	2.4	2.1	1.9	2.2	2.3	3.0	(5.4)	(4.6)	2.8	(7.8)	(8.7)
28	I	6	3.1	1.0	2.0	2.3	1.8								
	II	6		1.2	1.7	1.5	1.6	2.3	2.0						
	III	7					2.2	1.7	2.5	2.0	3.8				
	IV	7							1.6	1.7	2.5	1.8	2.6	3.2	3.7
	V	6	3.1	2.4	1.4	1.3	1.4	1.4	1.9	1.9	1.8	2.0	2.9	3.2	3.6
60	I	6	3.3	1.1	1.6	2.5	1.4								
	II	6		2.6	2.4	1.0	0.9	1.0	1.1						
	III	7					1.1	1.1	1.5	0.8	1.2				
	IV	7							3.1	2.3	2.9	2.9	3.5	3.9	3.8
	V	6	1.9	2.7	2.6	1.6	2.3	2.0	2.4	2.5	2.6	3.2	2.7	2.3	2.0
90	I	6	(6.0)	1.2	(5.0)	3.7	1.6	(4.4)							
	II	6		1.7	(5.5)	(6.4)	1.2	(4.8)	1.6						
	III	7				2.0	2.0		2.0	3.4	2.2				
	IV	7							1.7	4.0	3.3	(4.2)	(5.7)	(7.4)	3.4
	V	6	(5.4)	1.9	3.7	3.4	1.0	2.3	1.1	3.5	3.1	3.1	(4.3)	(6.0)	0.6

Fig. 4

EFFECT OF TEMPERATURE ON SOLAR CELL CURRENT
OUTPUT FOR THE FIVE FILTER TYPES
DATA NORMALIZED TO 28°C
CURVES OBTAINED IN DI203 SIMULATOR LIGHT SOURCE
TYPICAL CURVES

Fig. 6

E-3-12

CURRENT MATCHING IN M=O SIMULATOR AND M=1 SUNLIGHT

Cells Covered with Filter Type	Voltage at which I measured mV	Maximum Spread of Current Output in D1203 Solar Simulator (Percent)			Current Spread on Table Mountain (Percent)
		10°C	28°C	90°C	28°C
I (6 cells)	0	3.8	3.0	3.1	0.9
	250	3.8	3.0	3.1	---
II (6 cells)	0	2.5	3.7	4.9	0.9
	250	2.5	3.7	7.5	---
III (6 cells)	0	0.9	3.6	4.5	1.9
	250	3.6	2.7	11.7	---
IV (6 cells)	0	1.9	2.8	3.3	2.9
	250	1.9	2.8	10.7	---
V (6 cells)	0	1.5	1.2	1.7	1.1
	250	1.2	1.2	4.0	---

Fig. 5

E-3-11

CORRELATION OF ENCAPSULATED STANDARDS

RELATIVE TO APL STANDARD SET

Light Source	Identification of Standard Set	Voltage Output Ratio (R)* (28°C) Filter Type				
		I	II	III	IV	V
Table Mountain Sunlight (APL Meas.)	Flight #1 Std.	1.009	0.980	1.007	1.002	0.997
	Heliotek Std.	1.010	0.934	0.995	0.991	0.997
	Flight #2 Std.	0.980	0.994	1.010	1.034	1.004
	Spare #1 Std.	0.981	1.000	1.001	1.027	1.003
	Spare #2 Std.	0.969	1.011	1.037	1.023	1.000
D1203 Solar Simulator (Heliotek Meas.)	Flight #1 Std.	0.995	0.984	1.000	1.000	1.000
	Heliotek Std.	1.005	0.939	0.995	1.000	1.000
Tungsten 2800°K (Heliotek Meas.)	Flight #1 Std.	0.977	0.992	1.000	1.005	1.000
	Heliotek Std.	1.000	0.931	1.004	0.997	1.009

$$*R = \frac{\text{Voltage Output of Standard Unit}}{\text{Voltage Output of APL Unit}}$$

Fig. 7

CALIBRATION OF SOLAR CELLS USING BAND PASS FILTERS *

Presented by

R. E. Fischell

Johns Hopkins University - Applied Physics Laboratory

Silver Spring, Maryland

20 October 1965

* This paper was not available at the date of publication of these proceedings.

N66-17349

A COMPARISON OF GALLIUM ARSENIDE AND SILICON SOLAR CELLS FOR A SOLAR MISSION[*]

Presented by

John V. Foster

NASA-Ames Research Center

Moffett Field, California

20 October 1965

A COMPARISON OF GALLIUM ARSENIDE AND SILICON SOLAR CELLS FOR A SOLAR MISSION

John V. Foster,[*] James R. Swain,[*] Seymour H. Winkler,[**]
and Ferdinand R. Schwarz[***]

Introduction

The Ames Research Center of the National Aeronautics and Space Administration has been investigating a mission whose broad objectives include obtaining detailed information on fields, particles, radiations, and other solar phenomena in interplanetary space. The mission was extensively studied in 1963 by three 4-month studies conducted by industrial contractors - the Missile and Space Division of General Electric at Valley Forge, Pennsylvania; and the Martin Company, Space Programs Division, Baltimore, Maryland; and the Western Development Laboratories of Philco Corporation, Palo Alto, California. In addition, the Honeywell Company studied the mission and made the results available to NASA. A summary of these results was presented in a paper by H. F. Matthews and M. D. Erickson of Ames at the National SAE-ASME meeting, New York, April, 1964. These studies indicated that one of the major problems associated with the close-Sun mission is the development of a suitable electrical power system. The present Pioneer spacecraft (A through D) utilizes a spinning cylindrical structure with silicon solar cell arrays mounted around the outside of the cylinder. The mission of the present series will carry the spacecraft into about 0.75 of an astronomical unit (AU) from the Sun. Studies have shown that modification of the present array would allow trajectories as close as about 0.5 AU. For missions with trajectories placing the perihelion closer to the Sun (as close as 0.1 AU is desired), some other techniques are necessary.

With the above factors in mind, Ames has pursued several courses of action in searching for a solution to the power supply problem. A method of thermal control of the solar array, by the addition of reflective surfaces, is under study by contract with Philco Corporation. A despun thermal shield, which adjusts the area of solar cell exposure as the mission nears the Sun, has been studied at Ames. The thermal aspects of this approach have been studied by contract with Philco. The results of this study are being reported by another paper in this session by M. W. Cobb, W. S. Cummings, and J. W. Fairbanks of Philco. As part of the investigation, Ames decided to investigate the advantages and disadvantages of gallium arsenide solar cells for the close-Sun missions. Consequently, a study contract was negotiated with Radio Corporation of America, Astro-Electronics Division, Princeton, New Jersey. The remainder of this paper presents the results of this study.

[*]Research Scientist, National Aeronautics and Space Administration, Ames Research Center, Moffett Field, California.
[**]Engineering Group Leader, Radio Corporation of America, Astro-Electronics Division, Princeton, New Jersey.
[***]Engineer, Radio Corporation of America, Astro-Electronics Division, Princeton, New Jersey.

Discussion and Results

The specific solar missions considered involved perihelions of 0.51 AU,** 0.4 AU, 0.291 AU and 0.09 AU (sample trajectories Figure 1). The trajectory approaching 0.4 AU was for a spin-stabilized cylindrical vehicle with 55 watts end-of-life power output.+ The solar-cells for this mission would be bonded to the surface of the spacecraft (Figure 2). The 0.51 AU, 0.291 AU and 0.09 AU trajectories were for a Sun-oriented vehicle with 285 watts end-of-life power output.++ The solar cells for this mission would be bonded to panels which are attached to the spacecraft (Figure 3). A design requirement was that the solar array provide a continuous power output, not falling below the end-of-life level, for the entire duration of these missions. Thus, the possibility of varying the system duty cycle to fit the mission profile was not considered. However, such a possibility must be kept in mind. The solar-cell output will slowly vary as the spacecraft approaches the Sun, and a saving in array area could be realized by matching the system power requirements to these variations.

An important part of the effort involved analyzing the effects of environmental factors on solar-cell operation. Specific factors considered for each of the four trajectories were high temperature, charged particle (proton) irradiation, ultraviolet irradiation, micrometeorite bombardment, and solar wind. The high temperature and charged particle environments are the most damaging of the above list. Thus, the thermal effect and the charged particle effect will by the only degradation factors discussed here and the charged particle effect will be only briefly discussed.

The charged particle radiation environment that the solar cells will experience is assumed to consist primarily of solar-flare protons. This assumption is based on the information (Figure 4) provided by the NASA-ARC solar flare model. The flare particle count is specified as 8.5×10^{10} protons/cm^2 - year, at energies greater than 20 mev and isotropic at 1 AU (solar flare protons received in the vicinity of the Earth). Assuming that the yearly dose given in Figure 4 is the result of continuous emission from the Sun throughout the year, the dose received by the solar cells at any given time as a function of vehicle trajectory is computed by applying the $1/R^2$ law where R is the Sun-probe distance in AU. Charged particle flux encountered for each trajectory was calculated and converted to a damage equivalent of normally incident 17.6 mev proton flux. Output characteristics of gallium-arsenide (air-mass-zero efficiency 8.6%) and silicon (air-mass-zero efficiency 10.5%) solar cells were calculated as functions of monoenergetic flux.

**AU - "astronomical unit", where one AU is defined as the mean distance from the Earth to the Sun.
 +End-of-life assumed to be 6 months.
++End-of-life assumed to be 12 months.

at the day of launch. The silicon array, because of charged particle irradiation damage to the solar-cells, has a minimum output at the end of the mission (180 days).

The use of a maximum power-point-tracker would supply a greatly increased power demand near perihelion, if the spacecraft experiments or communications required an added number of watts at this time. Both the gallium-arsenide and silicon arrays can fulfill the mission power requirements although the gallium-arsenide array can provide greater power at the closest Sun approach.

Table 1 presents the array size (square feet of active solar cell area), cost of solar cells, weight of array and power available at perihelion for gallium-arsenide and silicon solar-arrays, designed to provide a minimum of 55 watts of output power during the 180-day mission.

The weight of the array is based on the values of 1.11 lbs/ft^2 for a silicon array and 1.30 lbs/ft^2 for a gallium-arsenide array. These values represent a reasonably good design which has been achieved in practice with a 0.9 packing factor. All array components including cover glass, cells, panel substrate, thermal emissive coating, electrical components and mounting hardware are represented in the array weights.

The cost of the solar cells shown in Table 1 is an estimate based on production quantities manufactured in 1968.

Using the array power versus probe-Sun distance curve (Figure 6), the total array size and packing factor were determined for the spinning cylindrical array for Sun approaches of less than 0.4 AU. Table 2 presents the calculated silicon and gallium-arsenide solar-array sizes and packing factors. The gallium-arsenide cells may be used for missions having a perihelion of 0.15 AU and silicon cells for Sun approaches as close as 0.2 AU.

For the silicon cells, the operating temperature was limited to 450°K at all calculated Sun approaches by varying the packing factor. At this operating temperature, the efficiency of the silicon cell is 2%. Since trajectory information was not available for Sun approaches closer than 0.4 AU, charged-particle irradiation damage incurred beyond 0.4 AU was neglected.

Solar-Array Parameters for the 0.51 AU Mission

The 0.51 AU mission was assumed to have a flat panel solar cell array which is maintained normal to the Sun vector during the 360-day design mission.

This array orientation can be used to provide a maximum power/array-area ratio because at the closest Sun approach of 0.51 AU the array operating temperature is only 468°K. At this temperature, both silicon and gallium-

Thermal control of the solar-cell array is required to maintain array constructed materials within an acceptable design temperature range, and to maintain a temperature range for the solar cells which results in the desired array power output for the closer Sun approaches.

Solar-Array Parameters for the 0.4 AU Mission

The vehicle considered for the 0.4 AU mission was spin-stabilized. The solar-cell array was assumed to be cylindrical with circular cross section. The spin axis of the spacecraft is coincident with the cylinder axis and is perpendicular to the Sun vector during the duration of the mission (180 days). Solar cells are mounted only on the lateral cylindrical surface, are in good thermal contact with the high-conductivity array substrate material, and are thermally insulated from the remainder of the spacecraft structure. The $\bar{\alpha}/\bar{\epsilon}$ ratio of the solar cells are assumed to be 0.95 and the output power was calculated on the basis of watts per square foot of active cell area. From the proton energy-range relationship it is known that approximately nine mils of fused silica will stop protons with energies below five mev. This thickness of glass shielding was selected for both the silicon and gallium-arsenide cells for the four missions under consideration because protons with energies below five mev cause a disproportionately large amount of damage to the solar cells.

Both the silicon and gallium-arsenide solar cells considered are one-by-two centimeters in area, twelve-mils thick and have nine mils of Corning 7940 fused-silica cover glass for irradiation protection and high thermal emissivity. The charged particle flux degrades the silicon solar cell about 20 percent during this six-month mission, but does not affect the gallium-arsenide power output.

The environment-degraded output density for gallium-arsenide and silicon solar cells was calculated for numerous points along the trajectory. The results are plotted in Figure 5. The two power plots represent the output at the maximum power-point of the solar cell I-V curves. In order to realize this power, a maximum power-point tracker circuit would have to be used in the power supply subsystem. The maximum power-point tracker is a pulse-width-modulated device which allows the power-conditioning subsystem to utilize maximum power capability of the solar-cell array by forcing the subsystem to operate on that point of the array output characteristic (I-V curve) which produces the largest current-voltage product. Another feature which may be incorporated in the power supply subsystem allows operation from a point on the array I-V curve which produces just the amount of input power required to supply the load demand and power supply losses. This feature minimizes dissipation of unused power when the array capability exceeds total power demand, aiding in the reduction of system operating temperature. The solar-cell operating temperature as a function of days in the trajectory is also shown in Figure 5.

Inspection of the power density curves shows that the gallium-arsenide array has its minimum power at the greatest Sun-probe distance, which occurs

arsenide solar cells have a power output. Silicon conversion efficiency at this temperature is about one percent and gallium-arsenide efficiency is about 3.5 percent.

The same solar cell $\bar{\alpha}/\bar{\epsilon}$ ratio (0.95), packing factor (0.9), and cover glass thickness (9 mils) as those of the 0.4 AU probe are specified for this mission. The silicon solar-cell power output was degraded about 25 percent by the charged particle flux encountered over this one-year mission, while the gallium-arsenide solar-cell power output was not affected. Thermal radiation from the rear side of the solar panel was assumed at an emissivity of 0.88.

The power density (watts per square foot of active solar-cell area) for both silicon and gallium-arsenide solar-cell versus days in the trajectory is plotted in Figure 7. Also shown are the solar-cell temperature versus time and the power density versus time for a hybrid array consisting of a 70% quantity of silicon cells and a 30% quantity of gallium-arsenide cells. All three power density curves represent the maximum power output of the array and would require the use of a minimum power-point-tracker to realize this output.

The array was sized to provide the required output of 285 watts at the time minimum output occurred.

By combining both silicon and gallium-arsenide solar-cells in a hybrid array, a flatter curve can be obtained for the available array power versus time data. A more sophisticated power conditioning system would be required to integrate the two contributions from the hybrid material array.

Table 3 represents the array size (square feet of active solar cell area), cost of solar cells, weight of array and maximum available power at perihelion for the silicon, gallium arsenide, and hybrid arrays. The data presented in this table are based on arrays designed to produce a minimum power output of 285 watts during the life of the mission. Basis of weight and cost is the same as for the 0.4 AU mission.

Solar-Array Parameters for the 0.291 AU Mission

The 0.291 AU mission uses a flat panel solar-cell array with nine mils of fused silica cover glass shielding and a maximum power-point-tracker in order to obtain maximum available power from the array for a 350-day mission. A value of $\bar{\alpha}/\bar{\epsilon}$ ratio of 0.7 is specified for the solar cells, with thermal emission from both sides of the solar cell panel.

Charged-particle flux is insufficient to degrade the shielded gallium-arsenide cell power output, but the silicon solar cell degrades about 30% during this one-year mission.

Figure 8 shows the gallium-arsenide and silicon solar-cell array power density versus days in the 0.291 AU trajectory. These two curves

represent the power output of a normally-oriented array without the employment of a temperature control technique. The array operating temperature versus time in the trajectory is also shown.

Based on the solar-cell output power calculations the power density plots show that the gallium-arsenide array can readily supply the 285 watt mission power requirement with normal solar-panel orientation, but the high temperature at the near-Sun approaches causes the silicon cell efficiency to drop to zero. The simplest technique which will reduce the array temperature sufficiently to allow silicon solar cells to operate during the entire mission is tilting the solar panel with respect to the Sun vector. With an angle of 60 degrees between the array normal and the Sun vector, the silicon array will produce a minimum of 8.5 watts per square foot of active solar-cell area.

Table 4 presents the array characteristics calculated for the 0.291 AU mission. The gallium-arsenide array maintains normal orientation throughout the mission. Its size is determined by its minimum power output, which occurs at the time of launch. The silicon array has an incidence angle of 60 degrees throughout the mission. A hybrid array consisting of a 50% quantity of gallium-arsenide cells and a 50% quantity of silicon cells will provide the required 285 watts with normal orientation and the least array size and weight. A packing factor of 0.9 was assumed for each array. The array weights are 1.1 and 1.30 pounds per square foot for the silicon and gallium-arsenide arrays, respectively. Solar-cell costs are based on the estimates used for the mission previously described.

Solar-Array Parameters for the 0.09 AU Mission

The 0.09 AU mission encounters the most severe environmental factors of the four missions considered here. Because of the close Sun approach (0.09 AU), the operating temperature of the flat panel array is so high that array cooling techniques must be used for the gallium-arsenide solar cells. These array cooling techniques limit the cell temperatures to 500°K. Silicon solar cells cannot be used for this mission because even with temperature control mechanisms which limit the temperature to 500°K, the silicon solar-cell efficiency is completely destroyed. Using these temperature control mechanisms, a 285 watt minimum power output for a 350-day mission can be accomplished.

Temperature Control Mechanism for the 0.09 AU Mission

Thermal Control by Tilting the Solar-Array with Respect to the Sun Vector. Figure 3 illustrates the thermal analysis model of a flat array which can be tilted with respect to the Sun. The tilt angle (θ) is defined as the angle between the panel normal and the Sun vector. Thermal calculations were performed varying the following two parameters.

. Tilt angle

. AU from Sun (or number of solar constants)

The $(\bar{\alpha}/\bar{\epsilon})$ value selected was 0.7 as representative of a narrow band-pass blue-red filtered cell.

Figure 9 shows array temperature as a function of number of solar constants. Figure 10 shows array power output per unit cell area as a function of number of solar constants. The temperature curve indicates that as the tilt angle increases, the temperature decreases; the most significant reductions result for tilt angles of 60° and greater. The power output curves indicate that as the tilt angle is increased, the power output is reduced in the range of 1 to 10 solar constants. Above 10 solar constants and over specific ranges of tilt angle, power output increases as the tilt angle increases. It should be noted that these power values, which are based on I_{sc} being cos θ dependent, are optimistic at the higher tilt angles since reflection may lower the power output to zero at $\theta \approx 85^\circ$ depending on filter characteristics.

Thermal Control Using a Deployable Sun Shield. Figure 11 illustrates the thermal analysis model of the Sun-shield configuration. The system consists of a fixed-position solar-cell array normally oriented to the Sun, and a multilayer, metallic-foil Sun-shield which can be deployed parallel to the array when required. The Sun-shield is composed of "n" layers of thin metallic foil (such as titanium to withstand the high temperature application) which are physically separated to produce the insulation effect desired. The shield is perforated with a regular hole pattern that permits a fixed percentage of solar energy to be passed to the solar-array. Near uniform illumination of the array at reduced solar intensity is achieved by proper relationship of the hole size and spacing, and by displacement distance of the deployed shield from the array.

The Sun-shield remains in the stowed position until the power output of the Sun-oriented array begins to drop due to the increasing temperature at higher solar constants (refer to Figure 12; Figure 12 indicates a deployment intensity of 8.4 solar constants for a selected design point of 500°K). At this time, the shield is deployed parallel to the panel and the effective array power output per solar cell area for the deployed shield configuration. A series of curves are displayed which are functions of: (1) configuration factor (φ) between array and Sun-shield, (2) number of Sun-shield foil layers (n), and (3) percentage of Sun-shield hole area which passes solar energy to the array. Configuration factor is defined as the percentage of thermal energy leaving the array that strikes the Sun-shield.

The general trends of the temperature and power output curves are as follows:

- Temperature decreases and power output increases as the Sun-shield/array spacing distance is increased (decreasing φ).

- Temperature decreases and power output increases as the number of Sun-shield layers (n) increase. Ten shield layers produce nearly the same results as an infinite number of shields.

- As the percentage of hole area in the shield is increased, more power output is produced up to approximately 40 solar constants. For solar constant values higher than 40, the higher percentage hole case produces less power output.

- Decreasing φ is more effective than increasing n.

The deploying shield design has several advantages over the tilting array design. One significant advantage is the elimination of the angle of incidence problem, all thermal calculations being performed for normally-oriented surfaces. However, analytical and experimental investigations of Sun-shield hole design would be required to insure that the proper illumination level is achieved at the array, and that no intense solar spotting results. At high solar-constant values, patterns of bright spots and shadows may produce undesirable thermal gradients on the array. Overlapping of the incident solar energy from the shield's holes is desired to produce approximate uniform illumination. The increasing decollimation of the Sun's rays at increasing solar constant positions helps obtain uniformity relative to the hole size and thermal gradients through the stack of shields does not cause significant misalignment.

Thermal Control Using Hybrid System of Array Tilting & Cylindrical Mirror. From both power output and thermal considerations, the method of tilting the solar array off-normal for near-Sun missions is very good. However, as the angle between the array normal and the Sun vector approaches 90° (as would be required for thermal control during very near-Sun missions) other problems will occur. The power output characteristics of solar cells at grazing Sun angles is not well known and the appropriate experimental programs would be extremely difficult to perform. Therefore, a practical approach might well be a hybrid system incorporating the benefits of an angular tilt system and a reflective system. Since the characteristics of solar cells are well known at grazing angles of up to 60° it would be advantageous to have the array operate at normal orientation at 1 solar constant, tilting off to an angle of 60° at some chosen point, and then fully tilting and receiving reflected solar energy beyond this point.

The power output plot of this system is shown in Figure 15.

Either of the above three methods of array temperature control could be used for the gallium-arsenide 0.09-AU array.

The charged-particle flux encountered by the vehicle on the 0.09-AU mission is greater than that encountered on any of the other three probe trajectories, but still not enough to degrade the performance of a gallium-

arsenide solar cell with 9 mils of fused-silica cover-glass shielding.

Assuming an $\bar{\alpha}/\bar{\epsilon}$ ratio of 0.7 for the array (which should be a practical value by the time of a 0.09-AU probe launch) and a packing factor of 0.9, the size of the array to supply 285 watts was determined. Using the array-tilting/cylindrical mirror method of temperature control described previously, it can be seen from Figure 16 that the minimum array output-power density occurs at the greatest probe-Sun distance (day 140). The minimum power density of 11.2 watts per square foot of active cell area. The packing factor of 0.9 then defines a total array size of 28.3 square feet.

At perihelion, the array has reached a maximum operating temperature of approximately 543°K and will supply 558 watts of output power. As with the other three solar-probe missions, a maximum power-point tracker would be used to obtain the predicted power.

Array operating temperature and array output-power density are plotted as a function of time in the 0.09-AU trajectory in Figure 16. Table 5 presents the gallium-arsenide parameters for a minimum output of 285 watts during the 350-day mission. The cost of the gallium-arsenide solar cells used for this mission is based on 1970 production. Array weight assumes a packing factor of 0.9 and 1.30 pounds per ft^2 of total array area.

Summary of Array Parameters for the Four Solar Missions

A comparison of the relative merits of a silicon and a gallium arsenide solar-cell array for the four Pioneer solar-probe missions discussed in this report is presented in Table 6. A hybrid array consisting of both gallium-arsenide arrays for the 0.51 and 0.291 AU missions; advantages of this type array are negligible for the 0.4 AU-mission and silicon solar cells will not produce power during the entire 0.09-AU mission.

The array characteristics presented in Table 6 are perihelion power output, array power density, array power-to-weight ratio, and solar cell cost-per-watt ratio.

The perihelion power output is the predicted maximum available array power output. For every array considered, this power output is greater than the design power of 55 watts for the 0.4-AU mission and 285 watts for the 0.5, 0.291, and 0.09-AU mission.

The array power density is defined as watts of array output per square foot of active solar-cell area. The values of power density shown in Table 6 are those calculated for the point in each trajectory when the solar array output is minimum.

Array power-to-weight ratio is defined as watts of array output

per pound of array weight. The array power is that power required by the mission (either 55 or 285 watts). Array weight is the total weight of the array including panel substrate, wiring, blocking diodes, shielding and bonding components, solar-cells and contacts, thermal coatings and supporting hardware. The weight of thermal control equipment (where applicable) is not included.

The solar cell cost-per-watt ratio is defined as the estimated cost of the bare-solar-cells purchased in production quantities in 1968, per watt of array power output, based on either 55 or 285 watts of array power. Cost of cells for the 0.09-AU mission is based on an estimate for 1970 production.

Each array compared in the table consists of 1 by 2 centimeter solar cells, 12-mils thick, having 9 mils of fused-silica cover-glass shielding. Efficiency of the silicon cells is 10.5 percent for a cover-glassed, module-assembled cell at $303^{\circ}K$ air-mass-zero conditions. Efficiency of the gallium-arsenide cells is 8.6 percent for a cover-glassed cell at $303^{\circ}K$ air-mass-zero conditions. The array packing factor, defined as the ratio of total active solar cell area to total array area, is 0.9 for each array in Table 6.

Conclusions

The results show that a solar-cell array is a feasible power source for solar-probe missions. The most severe environmental constraints imposed by the four missions considered will be the high temperature induced by proximity to the Sun. As high temperatures decrease solar-cell output, a thermal control system must be used for silicon solar-cell arrays at the 0.291-AU perihelion and gallium-arsenide solar-cell arrays at the 0.09-AU perihelion. Because of the greater temperature sensitivity of silicon solar-cells, their use is precluded for the 0.09-AU mission. Indications are that gallium-arsenide solar-cells, using suitable temperature control techniques, will be a practical power source for missions with solar approach distances down to 0.07-AU. Closer approaches will be feasible only if area, weight, or cost can be decreased.

Table 1

SILICON AND GALLIUM-ARSENIDE SOLAR-CELL ARRAY PARAMETERS FOR MINIMUM OUTPUT OF 55 WATTS DURING 0.4 AU MISSION

	Solar-Cell Efficiency Air-mass-zero	Perihelion Power (watts)	Active Cell Area on Cyl. Array (ft^2)	Cost of Solar Cells - 1968	Array Weight (lbs)
Si	10.5%	86	12.8	$29,700	14.2
GaAs	8.6%	140	13.8	$64,000	17.9

Table 2

ARRAY AREA AS A FUNCTION OF CLOSEST SUN APPROACHES FOR GALLIUM-ARSENIDE AND SILICON SOLAR-CELL SPINNING CYLINDRICAL ARRAYS

Closets Sun Approach (AU)	Packing Factor GaAs	Packing Factor Si	Active Cell Area (ft^2) GaAs	Active Cell Area (ft^2) Si	Total Array Area (ft^2) GaAs	Total Array Area (ft^2) Si
0.4	0.9	0.9	13.75	12.75	15.3	14.2
0.3	0.9	0.5	13.75	12.75	15.3	25.5
0.25	0.8	0.25	13.75	12.75	17.2	51.0
0.2	0.5	0.1	13.75	12.75	27.5	127.5
0.15	0.2	---	13.75	-----	68.8	----

Table 3

SILICON, GALLIUM-ARSENIDE, AND HYBRID SOLAR-CELL ARRAY PARAMETERS FOR MINIMUM OUTPUT OF 285 WATTS DURING 0.51 AU MISSION

	Perihelion Power (watts)	Active Cell Area on Array (ft^2)	Cost of Solar Cells - 1968	Array Weight (lbs)
Silicon Array	302	39.6	$92,000	51.5
GaAs Array	535	28.5	$132,000	41
Hybrid Array (70% Si- 30% GaAs)	357	31.7	$96,000	40.9

Table 4

SILICON, GALLIUM-ARSENIDE, AND HYBRID SOLAR-CELL ARRAY PARAMETERS
FOR MINIMUM OUTPUT OF 285 WATTS DURING 0.291 AU MISSION

	Perihelion Power (watts)	Active Cell Area on Array (ft^2)	Cost of Solar Cells - 1968	Array Weight (lbs)
Silicon Array **	600	33.5	$78,000+	41.3
GaAs Array ***	665	27.6	$129,000	40
Hybrid Array ***	328	27.2	$95,000	36.5

*   Array Weight for Packing Factor equals 0.9

**   Incidence Angle (θ) + 60°

*** Normal Orientation with Respect to Sun Vector

\+   Off-Angle Panel Orientation Mechanism Cost Not Included

Table 5

GALLIUM-ARSENIDE SOLAR-CELL ARRAY PARAMETERS FOR
MINIMUM OUTPUT OF 285 WATTS DURING 0.09-AU MISSION

	Perihelion Power (watts)	Active Cell Area on Array (ft^2)	Cost of Solar Cells - 1970	Array Weight (lbs)
GaAs Array	558	25.4	$100,000	36.8
Si Array	(Environment too severe for Silicon)			

Table 6

SYSTEM CHARACTERISTICS OF SILICON, GALLIUM-ARSENIDE, AND HYBRID SOLAR-CELL ARRAYS FOR THE FOUR SOLAR PROBE MISSIONS

	GaAs	Si	GaAs	Si	30% GaAs / 70% Si	GaAs	Si	50% GaAs / 50% Si	GaAs	Si
Perihelion (AU)	0.4	0.4	0.51	0.51	0.51	0.291	0.291	0.291	0.09	0.09
Minimum Power Required During Mission (watts)	55	55	285	285	285	285	285	285	285	285
Perihelion Power (watts)	140	86	535	302	357	665	600	328	558	---
Minimum Array Power Density 1. (watts/ft^2 active solar cell array)	4.0	4.3	10.0	7.2	9.0	10.3	8.5	10.5	11.2	---
2. (watts/ft^2, total array)	3.6	3.9	9.0	6.5	8.1	9.3	7.65	9.45	10.1	---
Array Power-to-Weight Ratio (watts/pound of array)	3.1	3.9	6.9	5.5	7.0	7.1	6.9*	7.8	7.7*	---
Solar Cell Cost-per-Watt Ratio ($1000/watt)	1.17	0.54	0.46	0.32	0.34	0.45	0.27**	0.33	0.35**	---

* Does not include temperature controlling mechanism weight.
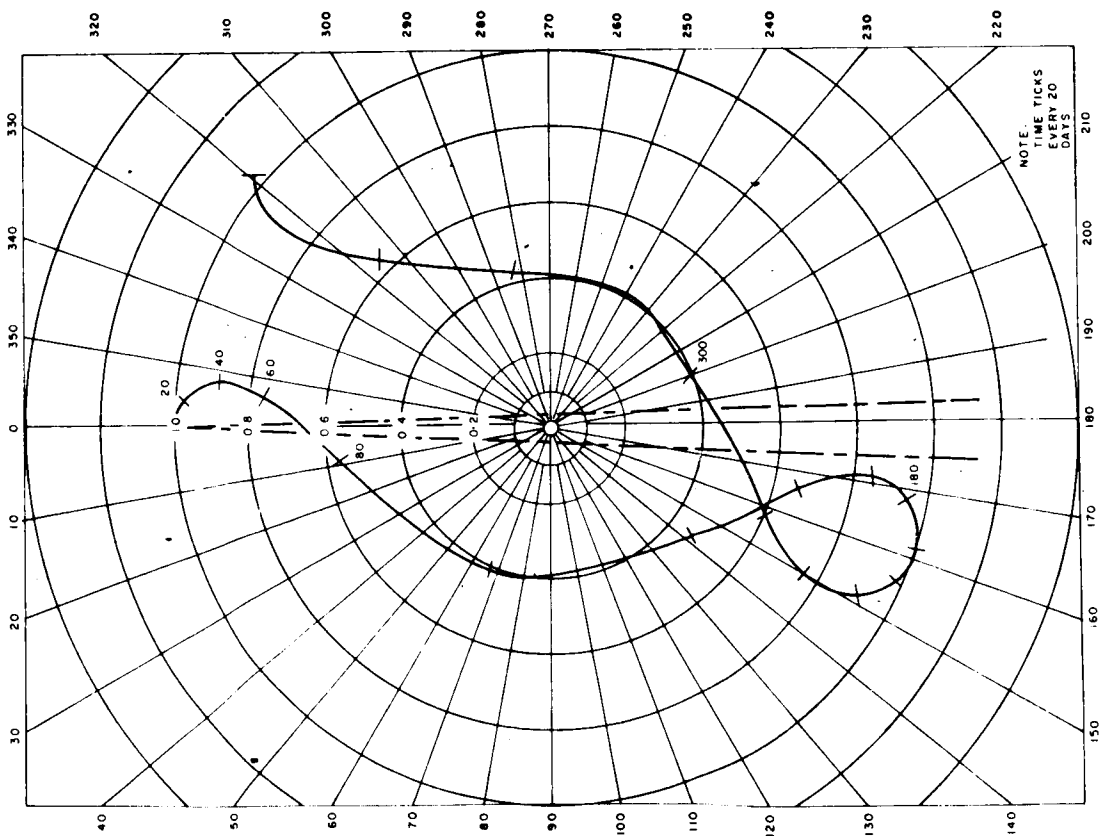
** Does not include temperature controlling mechanism cost.

Figure 1(b)

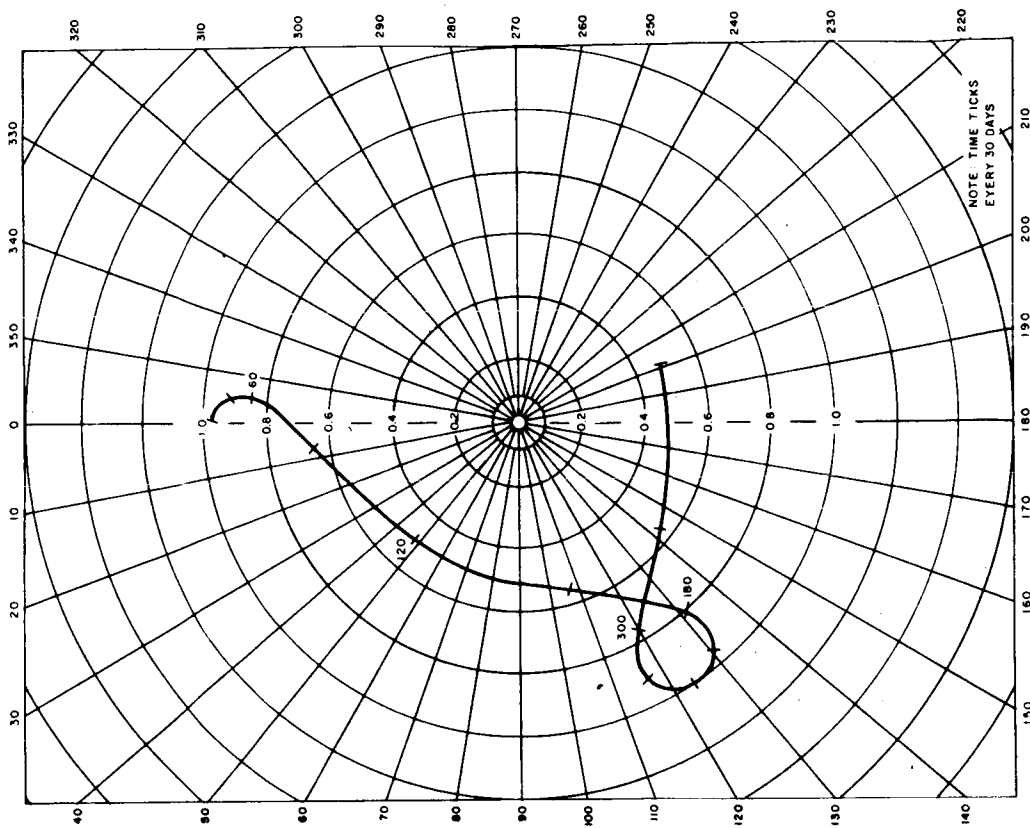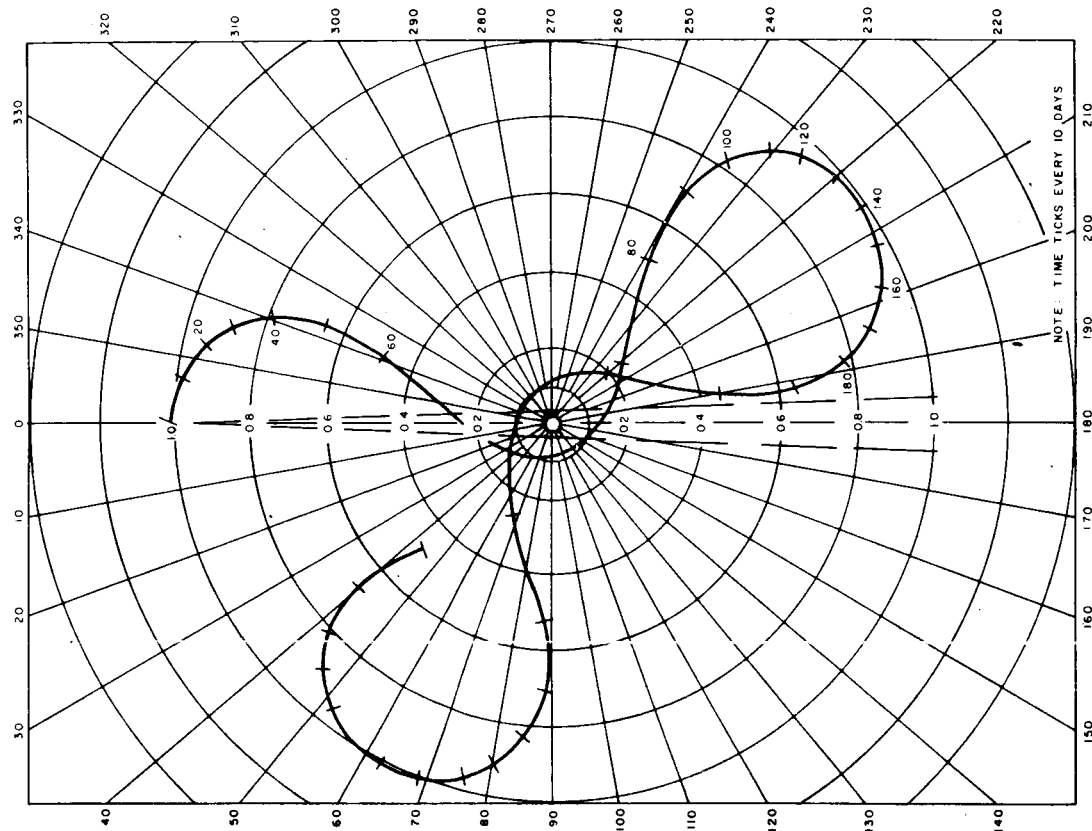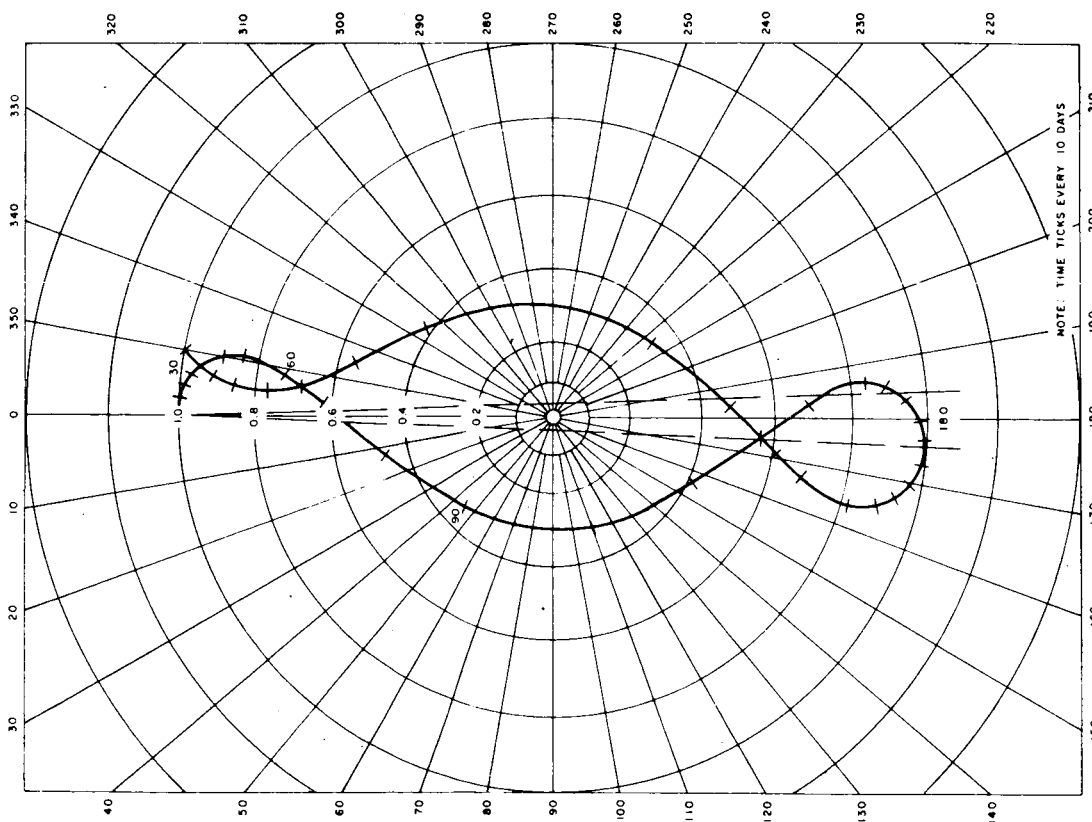Figure 1(a)

Figure 1(d)

Figure 1(c)

SPIN AXIS

$$\beta = \frac{\text{SOLAR CELL AREA}}{\text{TOTAL ARRAY AREA}}$$

$$0.1 \leq \beta \leq 1.0$$

INSULATED ARRAY
INTERIOR SURFACE

SUN VECTOR
PERPENDICULAR
TO SPIN AXIS

SOLAR CELL MODULES
IN GOOD THERMAL CONTACT
WITH HIGH CONDUCTIVITY
SUBSTRATE $\bar{\alpha} = 0.78$ $\bar{\epsilon} = 0.83$

LOW ABSORPTIVITY —
HIGH EMISSIVITY FINISH
ON SOLAR ILLUMINATED
SURFACE NOT COVERED
BY SOLAR CELLS
$\bar{\alpha} = 0.10$ $\bar{\epsilon} = 0.83$
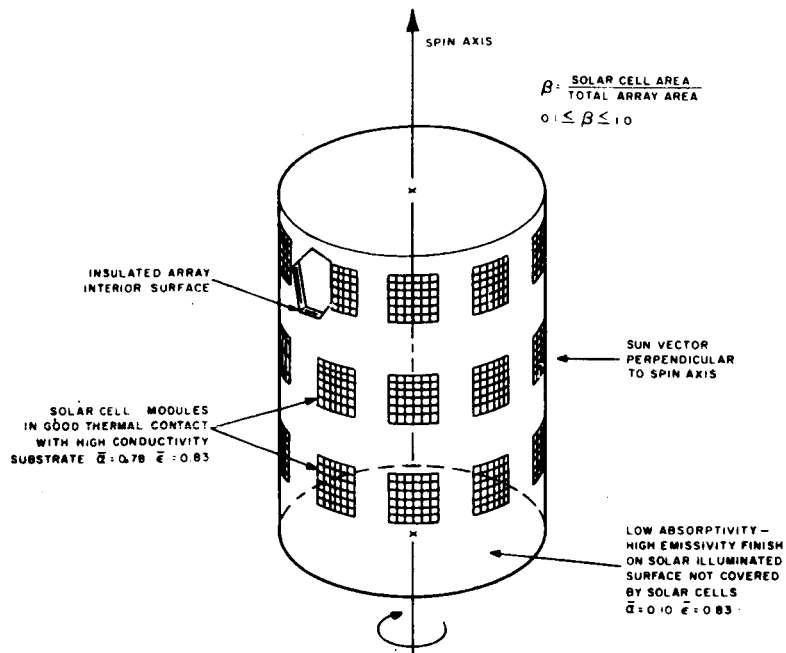
Figure 2.- Thermal analysis model of spinning cylindrical array.

SUN
VECTOR

PANEL
NORMAL

ISOTHERMAL
ARRAY

θ

TILT
ANGLE

ARRAY
ROTATION

FRONT SURFACE

$$\beta = \frac{\text{CELL AREA}}{\text{ARRAY AREA}} = 0.90$$

REAR SURFACE (FINISHED WITH BLACK PAINT)
$\bar{\alpha} = 0.93$
$\bar{\epsilon} = 0.93$

SOLAR CELL
$\bar{\epsilon} = 0.83$

$$\left(\frac{\bar{\alpha}}{\bar{\epsilon}}\right)_{\text{CELL}} = 0.7 \text{ OR } 1.1$$

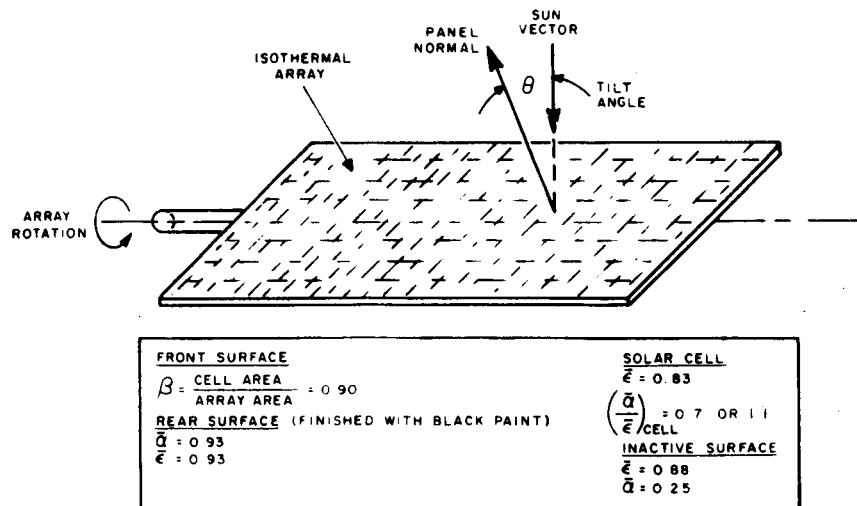INACTIVE SURFACE
$\bar{\epsilon} = 0.88$
$\bar{\alpha} = 0.25$

Figure 3.- Thermal analysis model of flat array with one axes
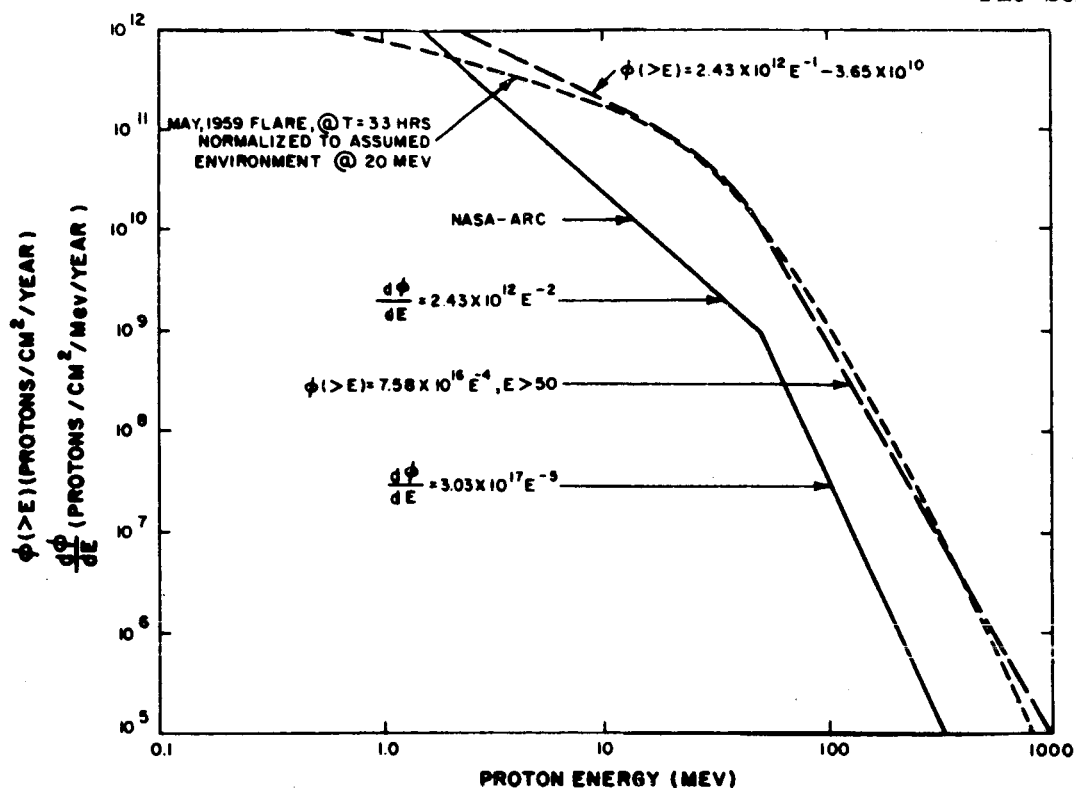rotational with respect to Sun vector.

Figure 4.- Omnidirectional solar proton environment in the vicinity of the Earth.

Figure 5.- Maximum power output of silicon and gallium-arsenide solar cells versus orbit time for 0.4 AU extended Pioneer trajectory.

Figure 6.- Array power output for gallium-arsenide cells as a function of solar intensity and packing fraction (β) on a spinning cylindrical array.
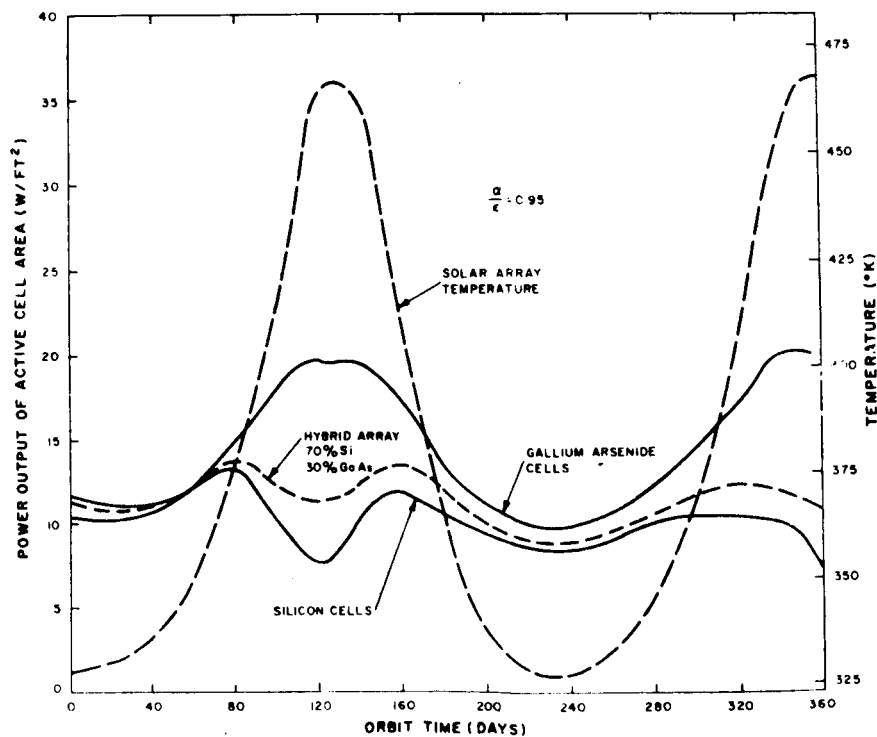
Figure 7.- Maximum power output of silicon and gallium-arsenide solar cells versus orbit time for 0.51-AU advanced Pioneer trajectory.
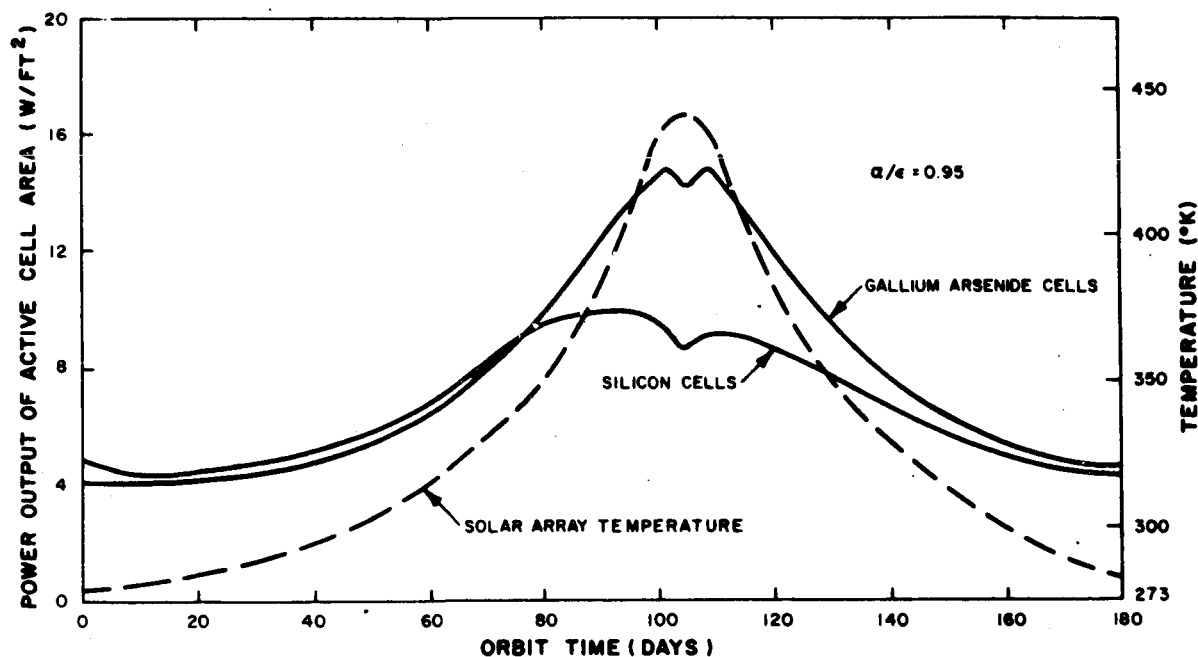
Figure 8.- Maximum power output of silicon and gallium-arsenide solar
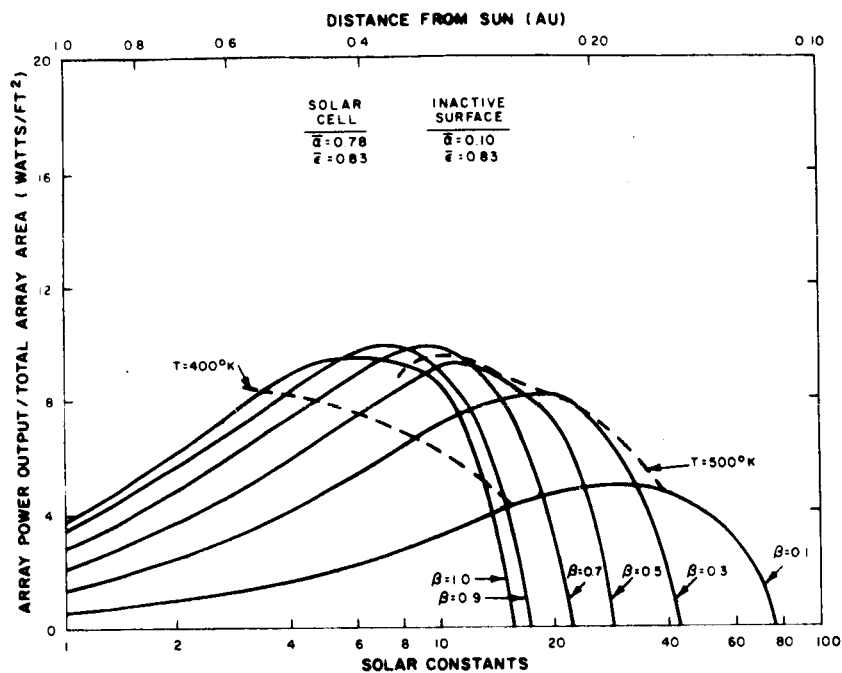cells versus orbit time for 0.291-AU advanced Pioneer trajectory.
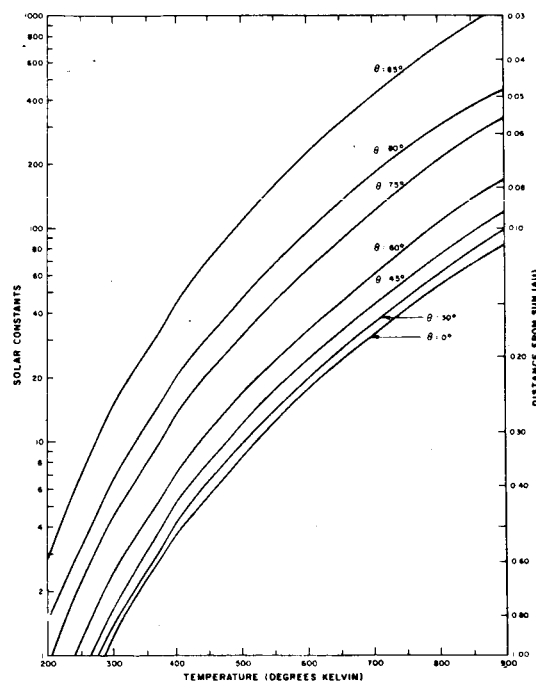
Figure 9.- Array temperature as a function of tilt angle (θ) and solar
intensity for gallium-arsenide cells, $(\overline{\alpha}/\overline{\epsilon})_{cell} = 0.7$.
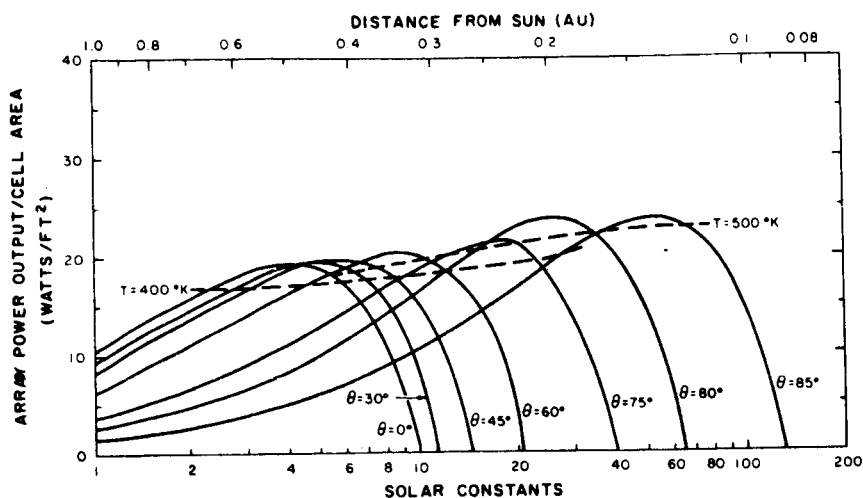
Figure 10.- Array power output as a function of tilt angle and solar intensity for gallium arsenide cells, $(\overline{\alpha}/\overline{\epsilon}) = 0.7$.
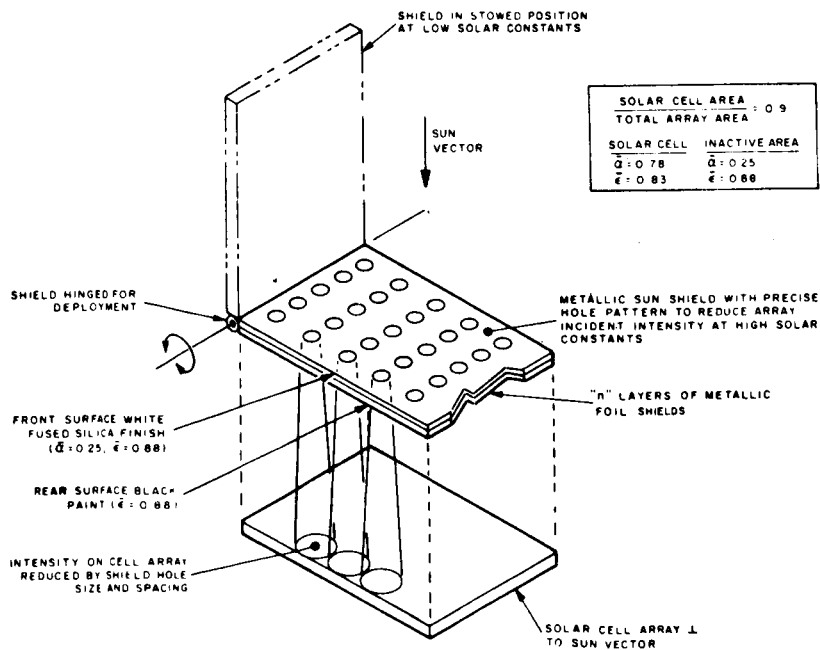
Figure 11.- Thermal analysis model of flat array with deployable, intensity-reducing Sun-shield.
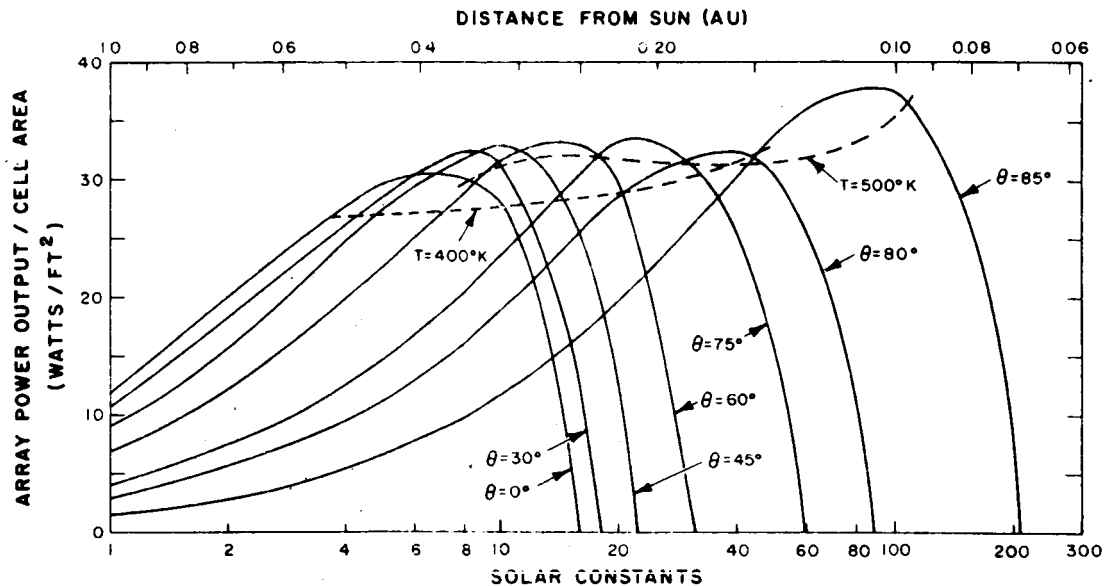
Figure 12.- Array power output as a function of tilt angle and solar
intensity for gallium-arsenide cells, $(\bar{\alpha}/\bar{\epsilon}) = 1.1$.
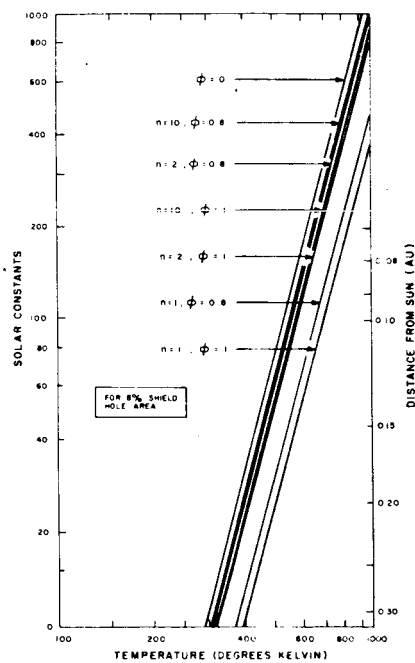
Figure 13.- Array temperature for gallium-arsenide cells as function
of solar intensity, configuration factor and number of shield
layers (eight-percent shield-hole area).
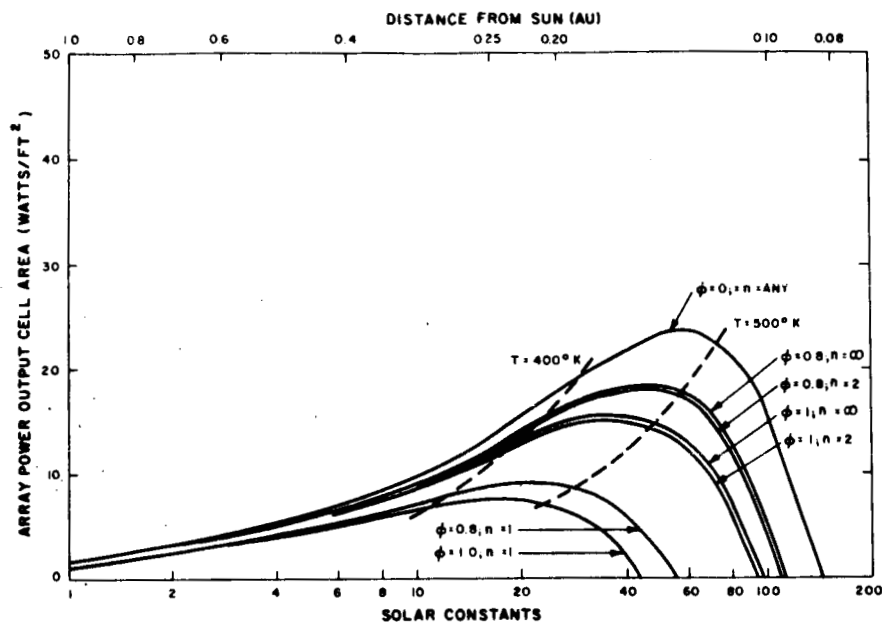
Figure 14.- Array power output for gallium-arsenide cells as a function of solar intensity, configuration factor, and number of shield layers (eight-percent shield-hole area).
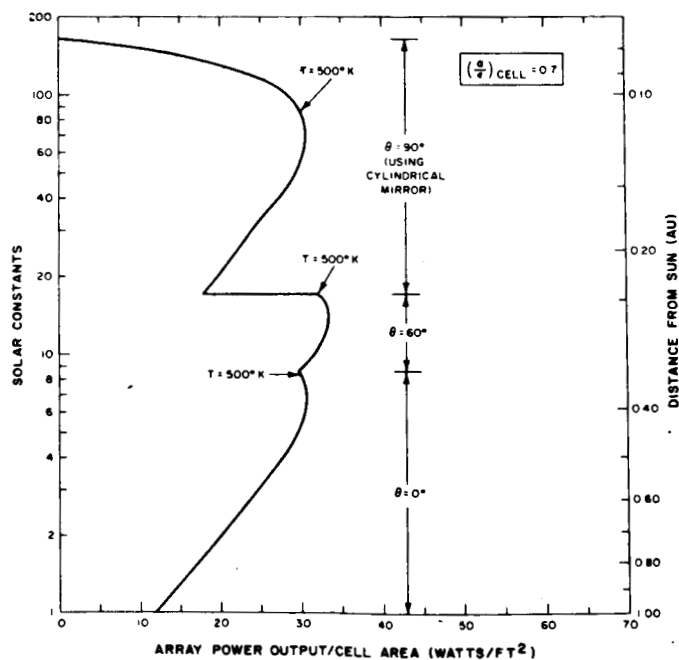
Figure 15.- Array power output for hybrid gallium-arsenide cell system as a function of solar intensity and array tilt angle $(\overline{\alpha}/\overline{\epsilon})_{cell} = 0.7$.
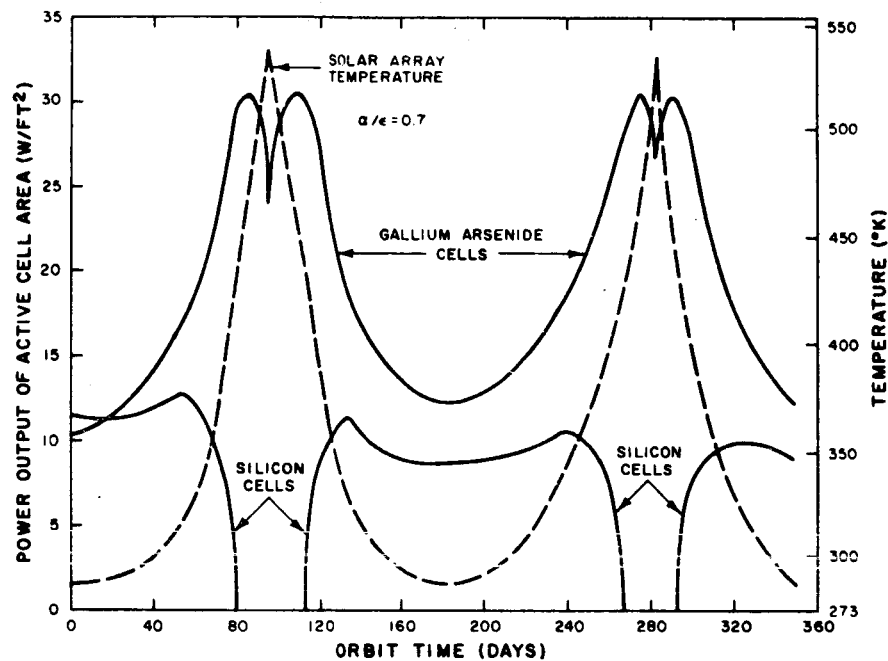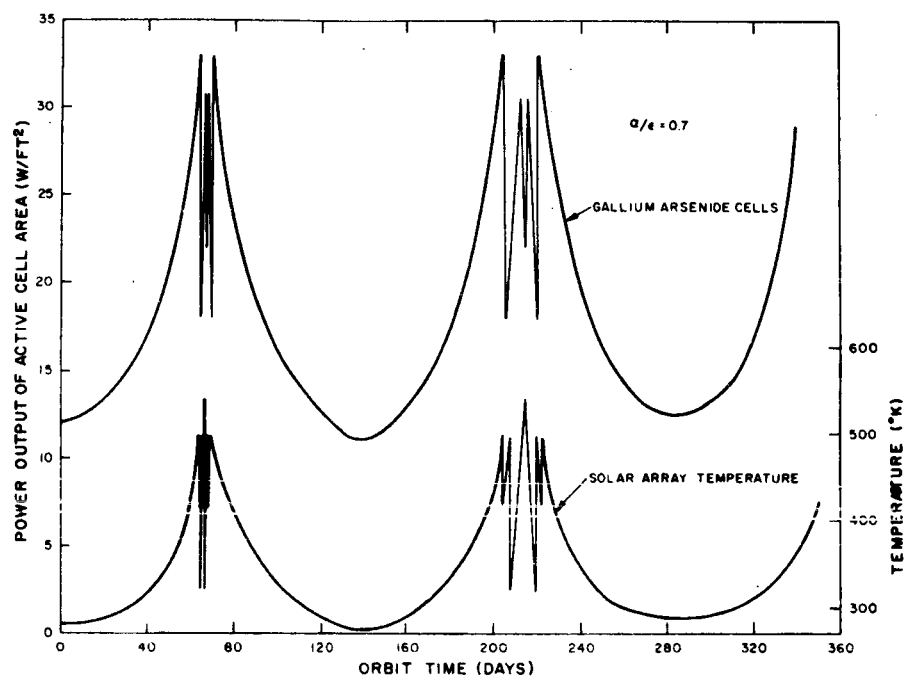
Figure 16.- Maximum power output of silicon and gallium-arsenide solar
cells versus orbit time for 0.09-AU advanced Pioneer trajectory.

Discussion

Voice (unidentified): Just a minor point on the question of angle of incidence, and the data that you were questioning. Although the angles which are shown are probably incorrect, they'd have to be stretched out, the actual thermal data is probably fairly close.

Foster: We have filters on the cells, and the angle problems I am concerned with are related to the filters.

Voice: The absorption of energy, however, is also less, and therefore the heating would be less.

Foster: It might work out.

Brandhorst - NASA-Lewis: Did you assume in the calculation that your short-circuit current of the cells would increase monotonically as a function of your solar constant increase?

Foster: I'll refer that to RCA.

Winkler - RCA: Let me answer that this way. We did the following. We started off by looking at the series resistance effects on the nonlinearity of short-circuit current with illumination, and then we looked at the kind of data that was available, in gallium arsenide particularly, as well as silicon. We then decided to mechanize the program, in which we assumed linearity but penalized the cell by not assuming the normal linear rise of the diode characteristic as the short-circuit current increments are applied. We calculated the two effects and they appeared to be comparable. Essentially, for ease of performing the first parametric calculations shown here, we did not allow the short-circuit current to saturate. However, I should point out that the maximum normal illumination we're talking about is in the order of a little over 10 suns, and really, the nonlinearity with careful control of series resistance is not bad up to those levels.

Mann - Spectrolab: You're talking about the effect on short-circuit current; actually, you made these measurements with maximum power, did you not?

Winkler - RCA: Yes, we did.

Mann: You assume that the numbers cancelled at 10 suns?

Winkler: Let me show you what I did. These curves are for 2, 4, 6, 8 suns and so on. We have taken this curve and rather than raising the diode characteristic uniformly as you should do and then subtracting the series resistance effect, we assumed that this was a ratio factor for simplicity in the computations. This wound up with something which was reasonably correct. If we allow the short-circuit current to rise, we wind up with a curve like this. Essentially, at the extremes and at the maximum power points, considering both intensity and temperature, we got an error that was quite small.

Mann: I don't agree.

N66-17350

RECENT DEVELOPMENTS IN LARGE AREA SOLAR CELL ARRAYS

Presented by

Kenneth A. Ray

Hughes Aircraft Company

Space Systems Division

El Segundo, California

20 October 1965

Abstract

A survey of power systems available to spacecraft designers in the next five years emphasizes the desirability of extending the space proven silicon solar cell into the multikilowatt range. The purpose of this paper is to review some recent solar cell array designs for both spinning satellites and oriented planar arrays. The basic design is outlined, calculated performance data are listed, the advantages and disadvantages are discussed, and the present status of development is described.

Several different configurations for spinning satellites are described with the associated range of specific power from 9.2 to 5.1 watts/pound and the packaging factor range from 383 to 61 watts/ cubic foot. A conceptual design for an oriented planar array is described, the component verification tests such as temperature shock and load deflection are described, and the preliminary calculations of array performance of 26 watts/pound are detailed.

Governing Parameters and Assumptions

The following are some basic parameters and assumptions that formulated the basis of the design study:

1. The satellite shall be cylindrical, 36 inches in diameter and 24 inches long, and in an equatorial earth orbit at 600 n.mi.

2. The deployment mechanism shall be capable of maintaining a rigid configuration in the earth's gravitational field.

3. The array shall be capable of positive deployment and of maintaining dimensional integrity while attached to the body of a spacecraft spinning at an initial rate (before deployment) of 80 to 160 rpm and a final rate (after deployment) of 20 to 40 rpm.

4. The deployment mechanism, wiring interconnections, and solar cells with attached 6 mil glass slips shall be included in the total weight.

5. The deployment mechanism shall be capable of reliable operation in the **hard** vacuum of space.

6. The packaged array shall be capable of withstanding shock, vibration, and accelerations such as might be experienced by arrays during launch.

A typical vibration schedule and input accelerations at the spacecraft interface will be as follows:

a. Sinusoidal tests:

Frequency, cps	Acceleration, g Thrust Axis, z	Transverse Axis, x and y
5 to 50	2.3	0.9
50 to 500	10.7	2.1
500 to 2000	21.0	4.2
2000 to 3000	54.0	17.0
3000 to 5000	21.0	17.0

Constant sweep rate of 2 octaves per minute.

RECENT DEVELOPMENTS IN LARGE AREA SOLAR CELL ARRAYS

Kenneth A. Ray*
Hughes Aircraft Company

Introduction

There exists today a need for a compact, lightweight space power source capable of providing hundreds of watts to kilowatts of electrical power that can be launched and deployed in a simple, reliable manner. Solar cells have been used in many space missions and have demonstrated long life (with adequate protection) and a high degree of reliability. However, up to now the packaging and deployment of large solar cell arrays have been a restricting design problem.

This paper summarizes some recent work directed toward the research and development of deployable large area arrays. The discussion is organized in two sections, one concerning work done on spinning satellite applications which was supported by NASA, Goddard Space Flight Center, Contract No. NAS 5-3989; and a section on oriented arrays currently under support by Air Force Aero Propulsion Laboratory, Contract No. AF 33(615)-2750.

Spinning Satellite Applications[1]

Study Approach

At the start of the program, outline drawings and descriptions of 14 different systems were prepared. It was decided to package the solar panels in the optimum manner for each individual system. Of the 14 systems shown on Figure 1, six were selected for further study. An additional system was subsequently added. Deployment systems were eliminated by considering the relative complexity of the deployment mechanism, the difficulty in achieving and maintaining the required rigidity, and the amount of satellite surface masked by the deployed array. Layout drawings were prepared for the seven systems. In order to make a valid comparison of the seven candidate systems, an effort was made to keep the deployed area approximately the same for each system. Two of the systems (4 and 6) are limited in size due to their geometry and therefore their deployed area is smaller. Of the seven systems, four (1, 2, 3, and 4) have flexible substrates and three (5, 6, and 7) are of conventional aluminum honeycomb type construction. Due to their advantage in weight, stowed volume, and growth potential, the four flexible systems were selected for detailed study.

---

*Senior Staff Engineer, Space Systems Division, Hughes Aircraft Company, El Segundo, California

describe the 14 different concepts that were considered. From this the seven systems selected for study in more depth are as follows:

System

1   Drum stowed concept - derived from
                     concept No. 9

2   Three flexible panels body stowed -
                     concept No. 11

3   Three panel common drum stowed -
                     derived from concept No. 9

4   Tri-nodal configuration - variation of
                     concept No. 6

5   Rigid multifold panels - concept No. 13

6   Rigid curved foldout panels (an added
                     concept to Figure 1)

7   Rigid telescoping panels - concept No. 12

The first four systems were studied in more detail since they showed the most favorable power-to-weight ratio, a favorable stowed volume configuration, good reliability, and favorable growth potential.

Comparison Chart

The objective of the study is to give careful consideration to any deployment system showing promise for application to spinning satellites. This consideration should be sufficiently detailed so that the parameters of each system could be evaluated separately. This is especially desirable since no specific mission was assigned to the study. The system comparison chart, (Figure 2) was considered to be the most efficient and satisfactory manner in which to list the important parameters of each system studied. A definition of the headings follows:

1. System description - self-explanatory

2. Dimensions and cubic feet - The dimensions are given for the deployed configuration and the volume is calculated for the stored condition.

b. Random test (each axis):

Frequency Range, cps	PSD, g^2/cps	Amplitude, g rms	Duration, minutes
20 to 2000	0.07	11.5	4.0

c. The above vibration levels are typical inputs to the spacecraft and are not necessarily the levels of acceleration that the solar cell assemblies will experience while mounted to the spacecraft. The actual level of acceleration is a function of the spacecraft structural response as well as input acceleration. Past experience indicates that amplifications of approximately 4 to 1 are possible within a frequency range of 50 to 200 cps.

7. All materials shall be nonmagnetic.

8. Materials shall be capable of withstanding humidity (up to 95 percent RH at 30°C for 24 hours).

9. The packaged arrays shall be capable of long-term (100 days) storage at temperatures which may vary from -20° to 60°C.

10. Materials shall be capable of withstanding radiations (including both ultraviolet and hard particles) experienced in space.

11. Materials shall be capable of withstanding hard vacuum conditions for extended periods (1 to 5 years) without excessive deterioration.

12. The extended array shall be capable of withstanding thermal cycling test at 10^{-7} Torr pressure from -70° to 70°C for 1000 cycles at a nominal rate of 2 hours per cycle.

13. Structure shall be capable of meeting the above conditions without degrading the performance of the attached cells.

Selection of Candidate Systems

In order to consider all possible candidates for a deployable solar array system, a large number of configurations was postulated and analyzed in the early phases of this study. From these a promising group was selected for a more detailed study. Figure 1 and Table 1

9. <u>Watts per square feet</u> - The average array output divided by the total deployed area.

10. <u>Watts per pound</u> - The average array output divided by the total weight.

11. <u>Watts per cubic feet stowed volume</u> - The average array output divided by the total volume of the deployment system when in the stowed or launch configuration.

12, 13, and 14.
Estimates of reliability, cost, and growth potential are of a relative nature since sufficient details do not exist to allow more and accurate estimates.

15. <u>Overall rating number</u> - A rating system devised to weight some parameters more heavily than others. The three parameters used, and their weighting factors, are given below.

Parameter	Weight Factor, W
watts/lb	10
watts/ft^3	8
watts/ft^2	3

A rating is calculated for three parameters of each of the seven systems using the following equation:

$$R = W \left[1 + \frac{A - B}{B} \right]$$

where

R = rating

W = weighting factor

A = value of parameter

B = average value of parameter for seven systems

The summation of the three rating numbers for each system yields an overall rating number. Table 2 shows the values for the seven systems.

3. Total weight, pounds - This includes all weight chargeable to the deployment system such as mounting brackets and hardware.

4. Deployed area, square feet - This is the total panel area including structural members such as support tubes and hinges, if used.

*5. Projected area, square feet - This is the component of the deployed panel area, on which solar cells are mounted, which is perpendicular to the sun's rays. The sun is assumed to be perpendicular to the spin axis of the satellite and the panels are assumed to be parallel to the spin axis.

*6. Array output watts - This is obtained by the following equation:

Array output = projected area (ft^2) x cell packing factor

x panel efficiency x[1 -0.005 (operating temperature

$-28^{o}C)$] x solar insulation $(watts/ft^2)$

A packing factor of 0.89 was used as a result of cell layout drawings.

A panel efficiency of 10 percent (air mass 0 at $28^{o}C$) was used and assumes an initial efficiency for the solar cells sufficient to yield this value after final assembly.

7. $\dfrac{P_{max} - P_{min}}{P_{ave}}$ - This is the cyclic variation in power output

obtained from the variation in 6 above.

8. Average panel operating temperature, ^{o}C - The calculation of the panel operating temperature assumed a solar absorptivity of 0.76 (effective) and an emissivity of 0.82; assumptions used in the calculations result in the maximum expected temperatures.

---

*5 and 6 are further delineated to show the maximum, average, and minimum values. These are a result of the rotation of the spinning satellite.

Design Verification Tests

Tests were conducted on the critical elements of the above designs to verify design adequacy and to obtain preliminary design data in areas where no data existed. A brief summary of these tests and results is listed below:

1. Tensile, compressive, and flexural tests of rigidized fiber-glas tubes. Tests conducted on polyester, polyurethane, and gelatin system showed excellent load carrying ability for the design requirements.

2. Outgassing of rigidizing systems. Tests conducted on the above resin systems in a vacuum system showed no measurable change in the output of a solar cell when exposed to possible outgassing impingement.

3. Tensile strength of flexible substrate materials. TFE impregnated 0.001 inch glass cloth tested in excess of 30 pounds per unit (width) in the preferred direction of weave.

4. Solar cell interconnection bending tests. Five different interconnection systems were tested. A seven cell module of 1 by 2 cm solar cells was repeatedly bent around a 4 inch radius. Of the five systems tested, the minimum number of bending cycles without failure was 1,310 and the maximum number was 71,000 for the optimum interconnection design.

Oriented Array Applications

Conceptual designs and preliminary analyses have been conducted on large area deployable arrays[2]. Additional work under Air Force APL contract AF 33(615)-2750 has resulted in a program to develop the technology and prove feasibility of a flexible, drum stowed, large area array. A demonstration model of approximately 50 ft^2 in area will be fabricated to allow verification of the design procedure and to show compliance with environmental tests. The following sections will summarize progress to date under Air Force contract.

Design Concept

The basic concept selected for the design verification study is described as follows: Dendritic solar cells, 1 by 30 cm, will be bonded to a flexible substrate member that supports the solar cells and associated wiring. In the stowed condition the array will be interwound with a thin flexible cushion that protects the solar cells.

Description of No. 1 Rated System

As shown on the system comparison chart Figure 2, system No. 2 received the highest rating of 33.7.

This design has three solar panels, 75 inches long by 24 inches wide, mounted 120 degrees apart and attached directly to the cylindrical surface of the spacecraft as shown in Figures 3 and 4. The substrate material is 0.0012 inch thick teflon impregnated fiberglas. Solar cells are mounted on both sides of this substrate on an area measuring 69.55 inches long by 20.18 inches wide. The solar panels are extended and supported with chemically rigidized fiberglas tubing which is attached to the two edges of the substrate. A 1/4 inch diameter aluminum spreader bar tube is attached to the fiberglas tubes at the end away from the spacecraft forming essentially a picture frame structure.

When stowed, the solar panels are wrapped around the 36 inch diameter body of the spacecraft. At this time, the support tubes will be flexible and in a flattened configuration. Thin sheets (0.150 inch thick) of polyurethane foam between the panels will cushion the solar cells. These sheets will be jettisoned when the solar panels are deployed. The solar panels will be held in place with a retaining hoop utilizing a release mechanism shown in Figure 5. This retaining hoop, made of the same material as the panel substrate, holds the solar panel in the stowed position and exerts a pressure of about 1 psi on the solar panels.

The first step in deployment of the solar panels will be to jettison the retaining hoop. Upon a signal the guillotine squib severs the safety wire and releases the ratchet assembly, thus allowing the leaf spring, shown in the top view of Figure 5, to exert a torque and unspin the 5/16 inch diameter tube. This motion releases the retaining hoop permitting it to be thrown off by centrifugal force. The solar panels are erected by pressurizing the support tubes, and chemically rigidizing them to complete deployment of the solar panels.

Chemical Rigidization System

The basis of the chemical rigidization systems is the preimpregnation of a plastic resin into a woven or sewn shape made of fiberglas or other woven cloth. The resin is stabilized in a highly viscous liquid condition so that the structure may be folded, compressed, wrapped, and otherwise packaged conveniently in a small volume. The structure is then deployed by the inflation of lightweight internal tubes of polyethylene. After the panels have been deployed, the tubes are chemically rigidized by ultraviolet activation of polyester resin and support the solar panels in the correct position.

The composite solar cell-substrate consisted of a TFE impregnated fiberglas cloth (overall thickness of 0.0012 inches) with a 1 by 30 cm dendritic solar cell cemented to one side and a 1 by 30 cm copper foil, 0.002 inches thick, cemented to the other side directly under the solar cell. This simulates the worst condition where the wiring harness of copper foil happens to pass along the entire length of one cell. Any one of several epoxy adhesive formulations, when used in the above composite, was capable of passing thermal shock tests from room temperature down to $-40^{\circ}F$. In subsequent tests to $-250^{\circ}F$, considerable delamination and cell breakage occurred. Several steps were taken to solve this problem. The best combination to date is the use of expanded copper mesh as the wire harness conductor, the use of a modified epoxy adhesive, and the careful control of the adhesive film thickness. This system has successfully passed the following thermal shock test:

Test Series

1. Low temperature shock   70 to $-100^{\circ}F$

2. Low temperature shock   70 to $-200^{\circ}F$

3. Low temperature shock   70 to $-250^{\circ}F$

4. High temperature shock   70 to $250^{\circ}F$

5. Low temperature soak $-250^{\circ}F$ for 2 hours

6. Temperature cycling   250 to $-250^{\circ}F$ for 3 cycles

7. Temperature cycling   70 to $250^{\circ}F$ - soak for one-half hour

                             $\begin{bmatrix} 250 \text{ to } -250^{\circ}F \text{ soak for one-half hour} \\ -250 \text{ to } 70^{\circ}F \end{bmatrix}$

Constitutes 1 cycle

Repeated for 6 cycles

The rate of temperature change was a maximum of $50^{\circ}F$ per min. These temperature shock tests are far more severe than what is expected in a typical earth satellite application.

Current-voltage curves were recorded on a 1 by 30 cm dendritic cell as the number of contacts to the n strip was varied. The results are shown in Figure 7 and on that basis a five contact configuration was chosen as optimum, considering power loss and assembly costs trade offs.

One of the wire interconnection configurations under consideration is a simple wire loop fabricated from No. 32 AWG tinned copper

An external shell will provide pressure to the rolled substrate on the storage drum. The interwound foam cushion, acting hydrostatically, will transfer the applied pressure uniformly through the wrapped-up substrate and prevent any relative motion between the substrate and the storage drum during the launch vibration and acceleration. Theoretical analysis has indicated that radial pressure of 0.6 to 1.0 psi will prevent relative movement of one substrate layer to the other when subjected to a maximum of 60 g acceleration.

The storage drum, substrate, and cover will be mounted by bearings to a structural member that will provide support for the deployment mechanism and mounting brackets. Deployment will be by positive acting extending members. The foam cushion will be rolled up on a takeup roll during deployment.

Demonstration Model

The demonstration model has been defined only to the extent of the overall dimensions and gross arrangement of parts. The storage cylinder length will be 6 feet. The diameter of the cylinder will be 6 inches. Two spring type, hollow extendible tubes will deploy each of two substrates at 180 degrees apart. Each substrate will be approximately 25 ft^2 in area. The exact size will depend on the output of the 1 by 30 cm dendritic solar cells available at the time of fabrication.

Two types of extendible tubes are under consideration: One is the DeHavilland STEM (Storable Tubular Extendible Member) device with six nested elements and the other is a Hunter Company spring that is wound at an angle to the longitudinal axis of the tube such that, when released from the flat coiled storage position, the spring forms a long conical tube. The Hunter Company has produced units capable of deployment to 50 feet and has run tests on deployment mechanisms similar to that shown in Figure 6.

Component Qualification Tests

A series of tests has been initiated to evaluate material and component suitability for long term operation in space. Most of the tests thus far have been on the dendritic solar cells, solar cell-substrate composite, wire interconnection bending, and array wiring harness configurations. Preliminary tests indicated that the low temperature shock test would be the most rigorous of all environmental tests and emphasis has been placed on this test.

will be deployed from two storage drums, with two panels from each drum deploying at 180 degrees from each other. The deployment mechanism considered here is the DeHavilland STEM device. Acceleration forces, related to typical attitude control systems, were considered as 0.003 g perpendicular to the panels, and 0.003 rad/sec/sec about the principal axis of symmetry parallel with the panels. The maximum panel deflection permitted was equivalent to 10 degrees displacement from the horizontal. Table 4 gives the weight breakdown for the Atlas-Centaur shroud design and Table 5 gives a corresponding break-down for the Saturn 1B design. The weight of the STEM elements has been calculated using available design data for the general application case and does not represent any design optimization. As an example, DeHavilland has recently produced a six element nested device whose load carrying ability can be tailored to match the application.

Conclusions

The design and test efforts described in this paper have indicated significant advancement in solar cell array performance combined with a fair degree of practicality. There is a high degree of confidence that the present development effort, supported by the Air Force APL, will result in a demonstration model that verifies the analytical predictions of the design approach and will ultimately result in workable solar cell arrays with specific power greater than 30 watts/lb.

Acknowledgements

The contribution and help from NASA, Goddard Space Flight Center, under the direction of Joseph Haynos, and Air Force Aero Propulsion Laboratory, under the direction of Joseph Wise, is gratefully acknowledged.

The author also acknowledges the contribution of many of the Hughes Aircraft Company personnel who participated in the NASA-Goddard contract and are engaged in the present Air Force, APL contract; and in particular the work of D. H. Winicur and W. D. Brown.

References

1. Ray, K. A., Keller, L. B., Syrovy, G. H., "Design and Evaluation study of Deployable Solar Arrays for Spinning Satellites," Hughes Aircraft Company Final Report SSD 4473R (October 1964).

2. Ray, K. A., Winicur, D. H., "A Large Area Solar Cell Array," AIAA Preprint No. 64-739 September 1964.

wire. The loops are made in jigs to avoid sharp bends and a test assembly of seven such cell interconnections has passed 80,000 cycles of repeated bending around a 4 inch radius. The spacing between solar cells is approximately 0.020 inch, therefore, the length of the interconnecting wires is very short.

Preliminary load tests on one candidate deployment device have been conducted. A Hunter Spring NEGATOR extendible boom was end loaded as a cantilever beam as shown in Figure 8. The spiral tube is made from a 301 stainless steel strip 0.004 inch thick and 4 inches wide. The diameter changes from 1 inch at the base to 0.46 inch at the tip. The tube is capable of extension to 106 inches from a package of 4 inches, and will support 1.6 pounds without collapsing. This sample boom is not the correct size for the demonstration model, however, data from the deflection tests will be used to determine the required boom dimensions.

Table 3 lists additional planned component qualification tests.

20 KW Design Considerations

A preliminary weight analysis was conducted on a 20 kw array in order to evaluate the growth potential of the general concept of the demonstration model. Two different shroud constraints were considered: the Atlas-Centaur and the Saturn 1B. The Atlas-Centaur shroud limits the length of storage cylinder to 11 feet and the Saturn 1B shroud allows a cylinder length of 18 feet.

The weight breakdown of the solar cell panel is given below:

0.008 inch thick 1 by 30 cm cell	0.00327 pound
0.003 inch thick coverglass	0.00136 pound
	0.00463 lb/cell
29.4 cells per square foot	0.136 lb/ft^2
Substrate (0.0015 inch thick)	0.012 lb/ft^2
Wiring and adhesive	0.020 lb/ft^2
	0.168 lb/ft^2

A panel performance of 10 watts/ft^2 is assumed at 50°C operating temperature and 95 percent packing factor*. This requires 2000 ft^2 deployed area for 20 kw power output. Four panels, each 10 by 50 feet,

---
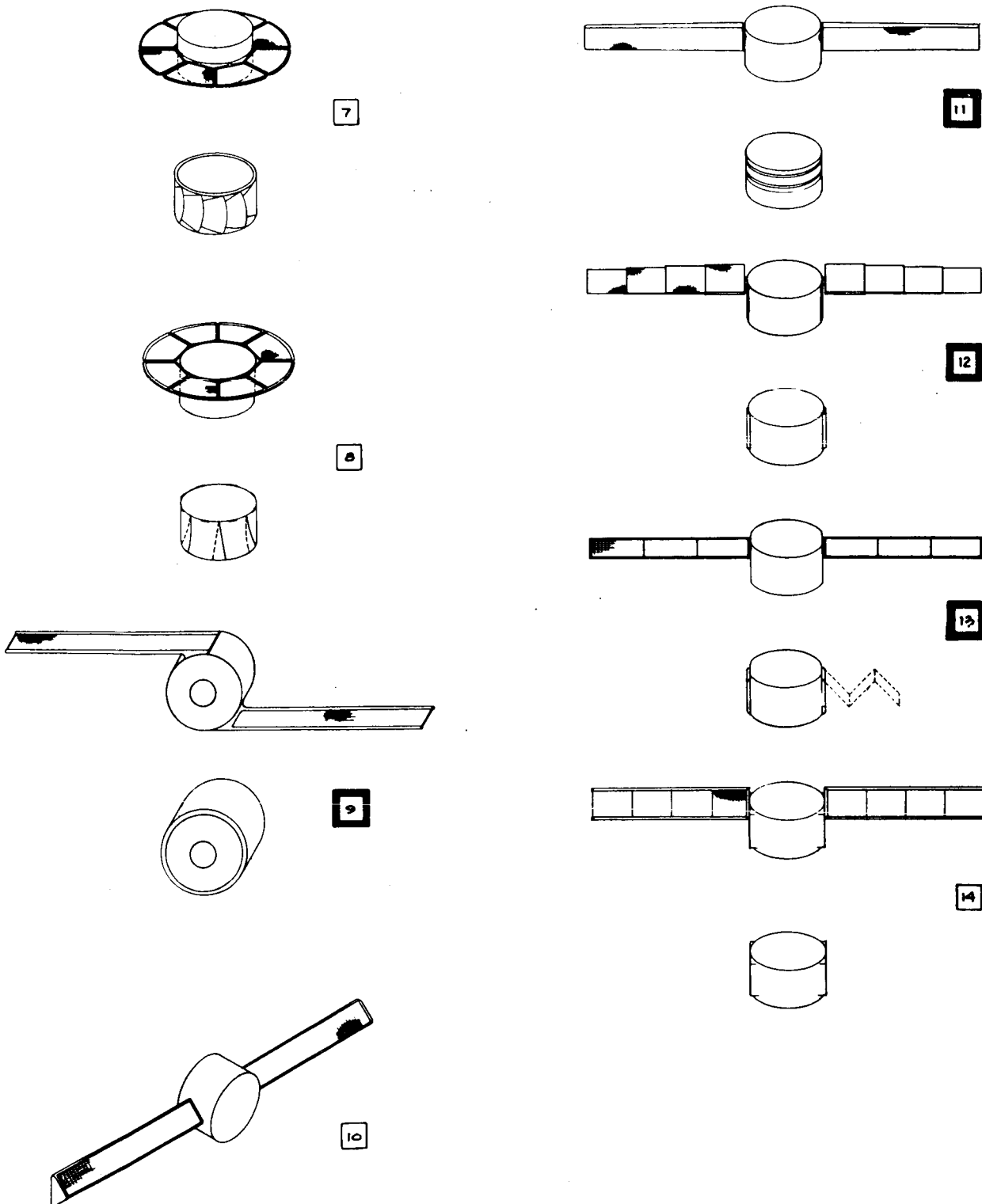
* Ratio of total cell area to total panel area.

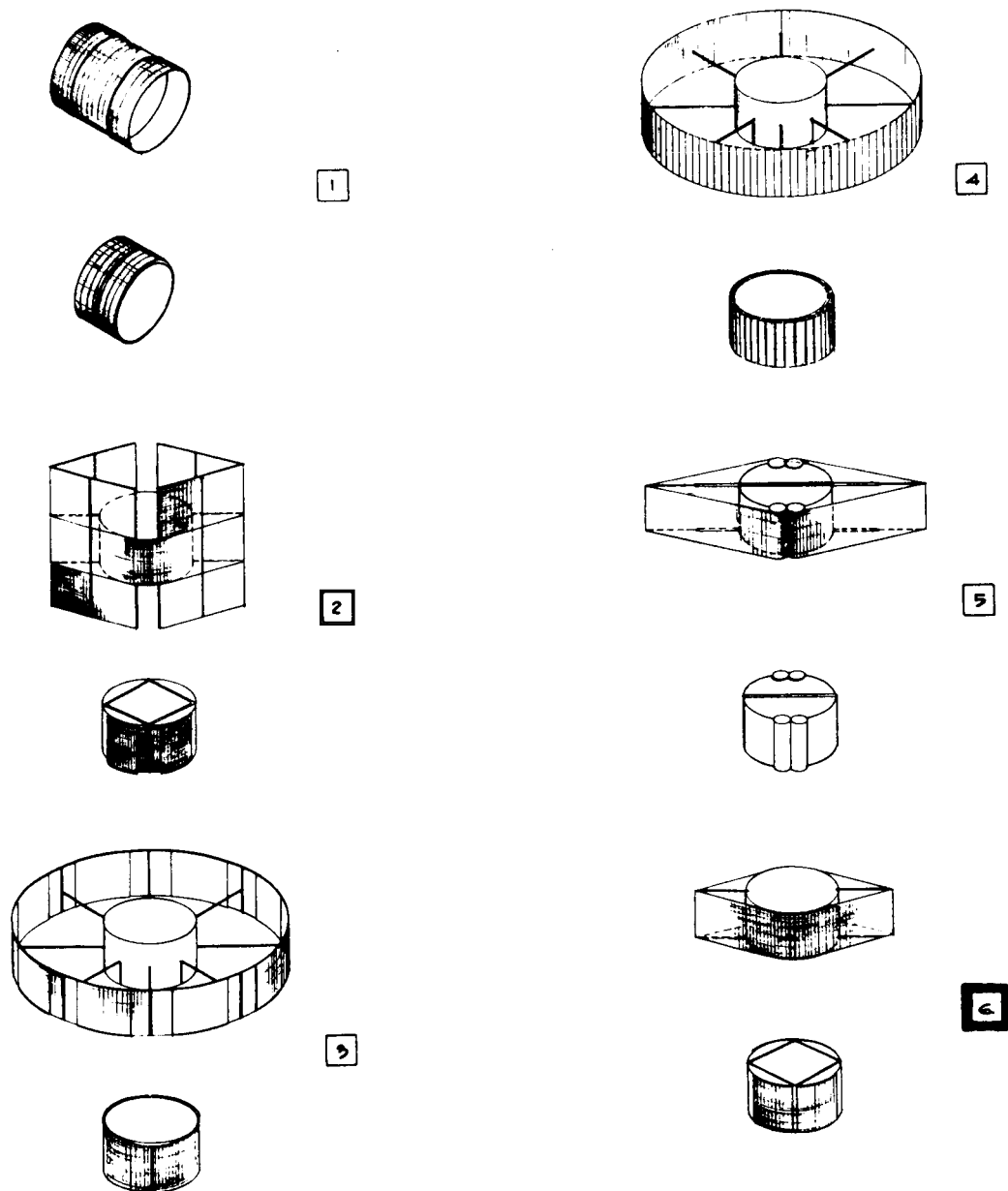Figure 1 b.   Preliminary Concepts for Deployable
Solar Array Study

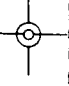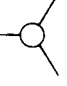Figure 1 a. Preliminary Concepts for Deployable Solar Array Study
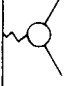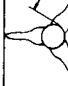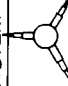
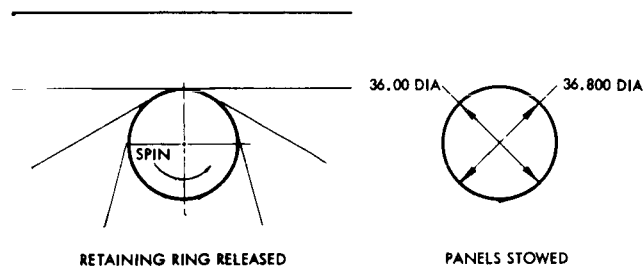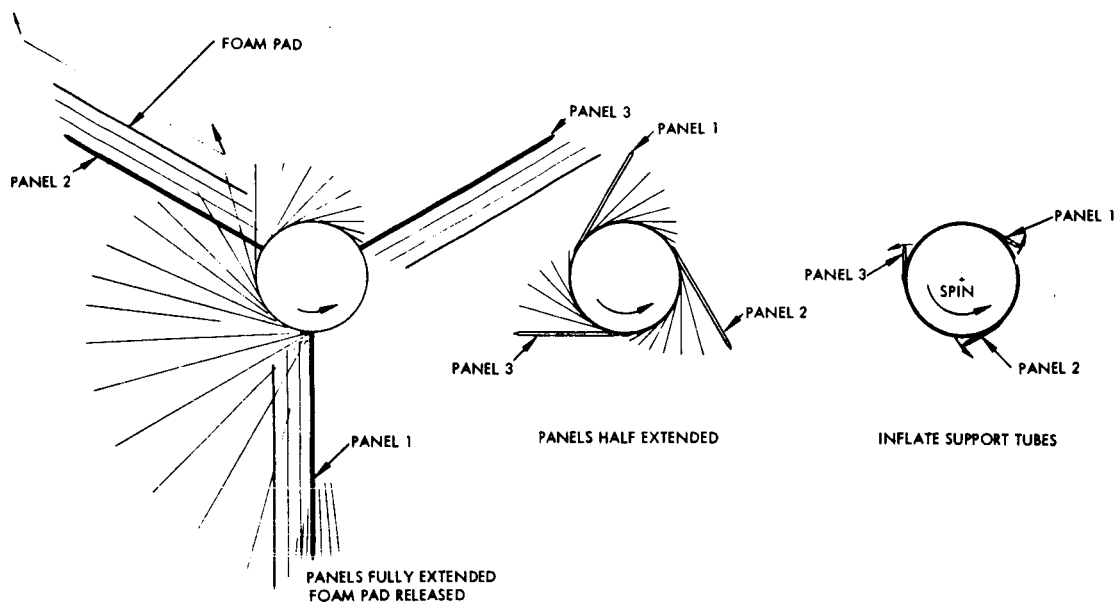| System Description	Dimensions ♦ Ft³	Total Weight Lbs	Total Deployed Area Ft²	Projected Area Ft² (Max/Avg/Min)	Array Output Watts	Pmax-Pmin / Pavg	Average Panel Operating Temp °C	Watts per Ft²	Watts per Lb	Watts per Ft³ (Stowed Volume)	Overall System Reliability Estimate	Cost Comparison	Growth Potential	Overall Rating Number
SYSTEM #1 — Four flexible panels cruciform configuration	4 Panels, each = 78 x 22, 2 drums, 6.00 dia x 22 long stowed dia (with 0.150 cushion + restraining hoop) = 0.04. Total stowed volume = 1.290 Ft³	22.6	95.3	20.0 / 17.9 / 14.2	202 / 181 / 143	.325	54	1.9	8.0	140	HIGH	LOW	EXCELLENT	19.9 (4)
SYSTEM #2 — Three flexible panels spacecraft body stowed	Each panel 78 x 24 (with tubes) stowed dia (with 0.150 cushion + restraining hoop) = 76.0. Total stowed volume = 0.450 Ft³	20.0	75.0	18.5 / 17.1 / 15.2	199 / 184 / 163	.196	43	2.5	9.2	383	HIGH	LOW	EXCELLENT	33.7 (1)
SYSTEM #3 — Three flexible panels drum stowed	Each panel 26 x 24 stowed dia (with 0.150 cushion + restraining hoop) = 9.96. Total stowed volume = 0.956 Ft³	21.5	88.0	18.5 / 17.1 / 15.2	199 / 184 / 163	.196	43	2.1	8.6	192	HIGH	LOW	EXCELLENT	23.4 (2)
SYSTEM #4 — Tri nodal configuration	Panel size = 25 x 24 stowed 0.7 = 2.7 tubes, 12 of 3/4 dia x 14 long. Total stowed volume = 0.56 Ft³	12.1	28.0	9.6 / 9.2 / 8.3	97 / 93 / 84	.179	54	3.3	7.7	158	FAIR	HIGH	LIMITED	22.0 (3)
SYSTEM #5 — Rigid panel multiple fold configuration	Each panel consists of (5), 12 x 24 segments. Total stowed volume = 1.33 Ft³	26.1	60.0	17.5 / 16.3 / 14.4	189 / 176 / 156	.187	42	2.9	6.7	132	LOW	MODERATE	LIMITED	18.9 (5)
SYSTEM #6 — Expanding rigid panel	Each panel consists of (6), 24 x 22 segments, length = 96.5 stowed 0.2 = 38. Total stowed volume = 1.19 Ft³	28.1	66.1	13.9 / 13.2 / 12.1	158 / 151 / 137	.139	32	2.3	5.4	126	LOW	HIGH	LIMITED	16.1 (6)
SYSTEM #7 — Rigid telescoping panels	Each panel consists of (9), 12 x 24 segments. Total stowed volume = 2.89 Ft³	34.7	60.0	17.8 / 16.4 / 14.6	193 / 177 / 158	.198	42	3.0	5.1	61	LOW	HIGH	LIMITED	13.5 (7)

Figure 2. System Comparison Chart

TABLE 1.   DESCRIPTION OF PRELIMINARY CONCEPTS FOR
DEPLOYABLE SOLAR ARRAY STUDY SHOWN ON FIGURE 1

Concept Number	Description	Comment
1	Cylindrical solar panels that telescope from satellite body	Adverse effect on moment of inertia
2	Folded flexible solar panels	Difficult to deploy
3	Solar panels that unfold to form larger cylinder	Inhibits installation of instrumentation on cylindrical surface of satellite
4	Same as concept 3 except smaller segmented panels	Same as concept 3
5	Flexible unrolling solar panels	Same as concept 3
6	Folded flexible solar panels	Modified and chosen for study; becomes system 4
7	Solar panels that fold from cylindrical surface of satellite then rotate into position	Limited to polar orbit and complex deployment
8	Solar panels that open similar to petals of a flower	Same as concept 7
9	Drum stowed flexible panels	Chosen for study; becomes system 3; a variation of this becomes system 1
10	Triangular solar panels that are folded closed and wrapped around the satellite when stowed	Requires change of angle between panels during orbit
11	Flexible solar panels that are wrapped around the satellite; deployed by pressurizing and rigidizing fiberglass tubes	Chosen for study; becomes system 2
12	Rigid telescoping solar panels	Chosen for study; becomes system 7
13	Foldout rigid solar panels; mechanical linked support beams	Chosen for study; becomes system 5
14	Foldout rigid solar panels; chemically rigid support beams	Variation of concept 13

TABLE 2. SYSTEM RATING METHOD

Weighting Factor = W

System Number	W = 10		W = 8		W = 3		Total Rating, R_T
	w/lb	Rating	w/ft^3	Rating	w/f^2	Rating	
1	8.0	11.1	140	6.6	1.90	2.2	19.9
2	9.2	12.8	383	18	2.45	2.9	33.7
3	8.6	11.9	192	9.0	2.09	2.5	23.4
4	7.7	10.7	158	7.4	3.32	3.9	22.0
5	6.7	9.3	132	6.2	2.93	3.4	18.9
6	5.4	7.5	126	5.9	2.28	2.7	16.1
7	5.1	7.1	61	2.9	2.95	3.5	13.5
Average	7.2	10.0	170	8.0	2.56	3.0	21.0

FOAM PAD

PANEL 3
PANEL 1
PANEL 2

PANELS HALF EXTENDED

PANEL 1
PANEL 3
SPIN
PANEL 2

INFLATE SUPPORT TUBES

PANEL 1
PANEL 3

PANEL 2

PANELS FULLY EXTENDED
FOAM PAD RELEASED

SPIN

RETAINING RING RELEASED

36.00 DIA
36.800 DIA

PANELS STOWED

ITEM	MATERIAL	
SUBSTRATE	0.0012 THICK TEFLON IMPREGNATED FIBERGLASS	0.051
CELL ASSEMBLIES	1,200 SEVEN CELL MODULES	4.842
WIRING HARNESS	COPPER	0.176
SUPPORT TUBES	0.250 DIA X 0.028 WALL ALUMINUM ALLOY	0.750
END SUPPORT	FIBERGLASS	0.045
BASE ATTACHMENT	ALUMINUM ALLOY	0.250
FOAM SHEET	FLEXIBLE POLYURETHANE FORM 0.150 THICK	0.360
RIVETS, THREADS, EPOXY AND MISC		0.020
WEIGHT ONE PANEL		6.484
WEIGHT THREE PANELS		19.452
TUBE PRESSURIZATION SYSTEM		0.300
RETAINING HOOP		0.238
	TOTAL WEIGHT	19.990

DIMENSIONS IN INCHES

Figure 3.   System 2 - Three Flexible Panels - Body Stowed

SUBSTRATE 0.0012 THICK
TEFLON IMPREGNATED
FIBERGLASS

ALUMINUM ALLOY ANGLE
0.040 X 0.500 X 0.500
BONDED AND RIVETED TO SUBSTRATE

18.00 R
(REF)

SECTION A—A

SYM ABOUT ℄

(ONE 7 CELL MODULE)

SOLAR CELLS-
BOTH SIDES

0.020

0.050 ──────2.85──

SUBSTRATE

DOUBLER

0.788

TUBE FLANGE
BONDED TO
SUBSTRATE

TO PRESSURIZATION

MANIFOLD

PRESSURIZATION TUBE AND
OUTLET FITTING

STOWED POSITION

RIGIDIZED TUBE (1.00 DIA)
INFLATED POSITION

FIBERGLASS SLEEVE

TUBE TO BE REINFORCED IN THIS AREA

1.40

69.55

74.00

PANELS ERECTED AND RIGIDIZED

600 SOLAR CELL MODULES EACH SIDE OF EACH PANEL
1200 SOLAR CELL MODULES PER PANEL
3600 SOLAR CELL MODULES
TOTAL (EACH MODULE - 7 INDIVIDUAL CELLS)

36.00 dia

RIGIDIZED TUBE

22.80

24.00   600 - SEVEN CELL
MODULES EACH FACE   20.18

DIMENSIONS IN INCHES

Figure 4.   System 2 - Panel Details - Body Stowed

SAFETY WIRE

LEAF SPRING

ALUMINUM ALLOY
RATCHET ASSEMBLY

A

0.0012 THICK TEFLON
IMPREGNATED
FIBERGLASS SHEET

GUILLOTINE SQUIB

SQUIB HOLDER

A

GUILLOTINE SQUIB

SECTION A-A

SPACECRAFT BODY
OR SOLAR ARRAY STORAGE DRUM

0.012 THICK
SHOWN OUT OF SCALE

5/16 OD X 0.028 WALL
ALUMINUM TUBE

LOWER LAYER TO BE
BONDED TO TUBE

SECTION B-B
SCALE 4/1

B

B
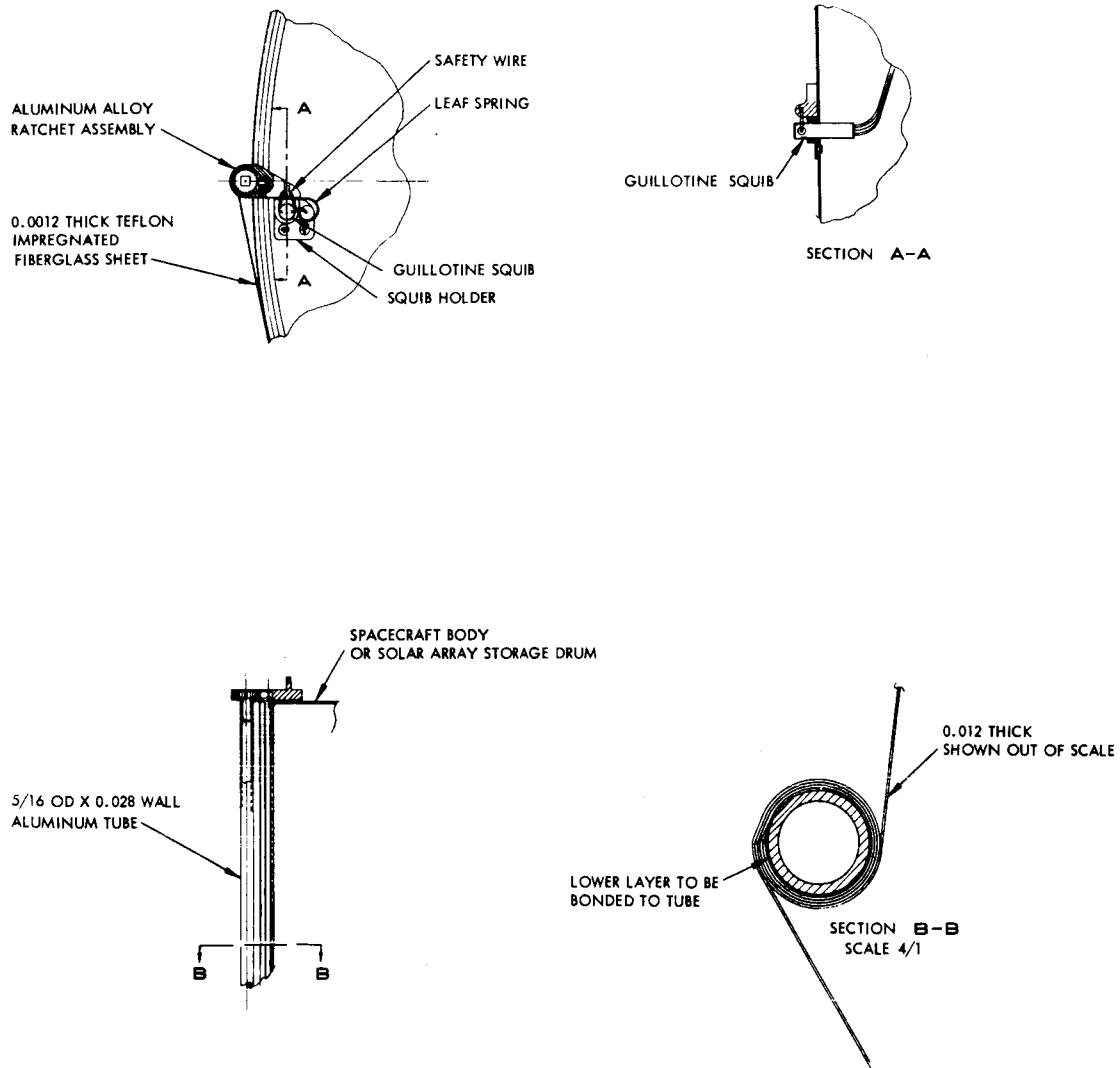
WEIGHT - POUNDS

DIMENSIONS IN INCHES

	36 INCH DRUM	6 INCH DRUM
5/16 DIA X 0.028 WALL ALUMINUM TUBE	0.058	0.058
RATCHET ASSEMBLY ALUMINUM	0.030	0.030
SQUIB	0.055	0.055
SQUIB HOLDER	0.010	0.010
SPRING, RIVETS, SAFETY WIRE	0.010	0.010
RETAINING HOOP	0.075	0.016
TOTAL	0.238 POUNDS	0.179 POUNDS

Figure 5. Retaining Hoop - Flexible Solar Panels Systems
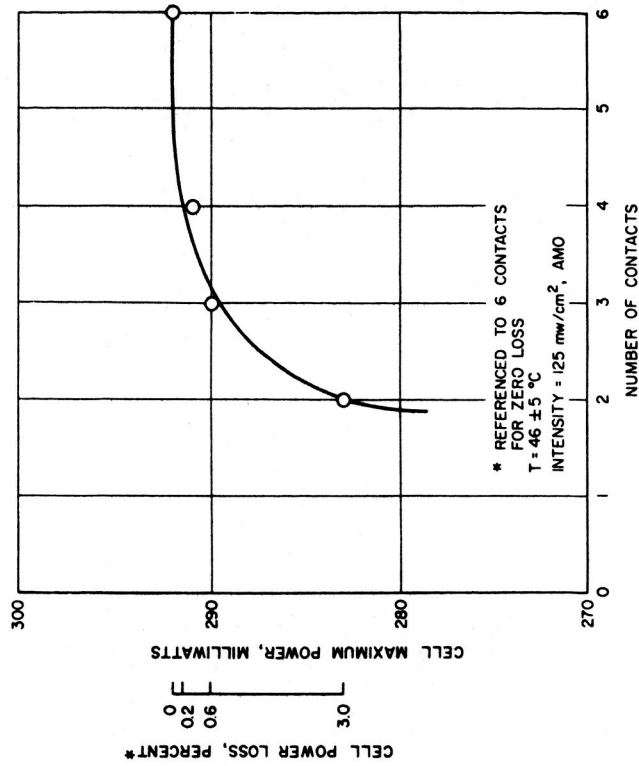
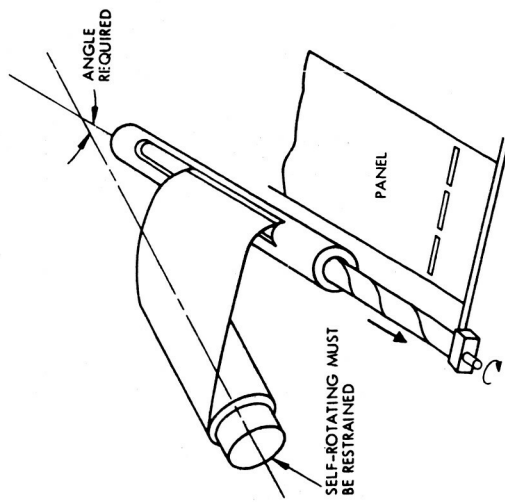Figure 7.   Cell Power Loss versus Number of Contacts

Figure 6.   Hunter Spring Deployment
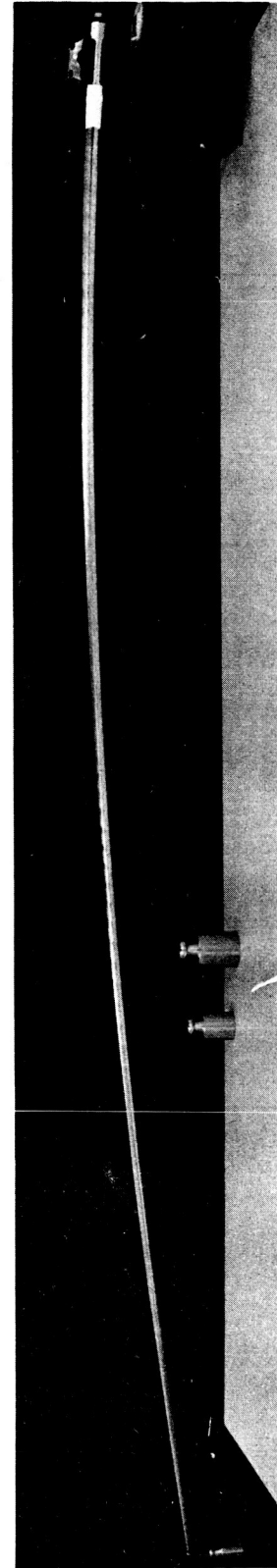   Mechanism

Figure 8.   Deflection Test on Hunter Negator Extendible Boom

TABLE 3. COMPONENT AND SUBASSEMBLY QUALIFICATION TESTS

Test Number	Test Objective	Test Specimen Description	Test Environment	Test Evaluation Criteria
1	Evaluate use of modified epoxy for cell-to-substrate bond.	1 x 30 cm dendritic cell bonded to 0.0015 inch TFE substrate using modified epoxy.	250 to -250°F temperature cycling at 50°F/min 14.7 lb/in^2 pressure (1 atmosphere).	Visual inspection.
2	Evaluate effect of adhesive voids in cell-to-substrate bond.	Same as 1 except adhesive will be spotted on cell back surface.	Same as 1.	Visual inspection.
3	Evaluate effect of increased substrate rigidity due to bus wiring on cell-to-substrate bond.	Same as 1 except strip of 0.002 inch copper foil will be bonded to substrate rear surface using modified epoxy.	Same as 1.	Visual inspection.
4	Evaluate bus wiring-to-substrate bond.	0.002 inch copper foil bonded to 0.0015 inch TFE substrate using modified epoxy.	Same as 1.	Bond peel strength measurement before and after environmental exposure.
5	Evaluate substrate-to-substrate bond.	0.0015 inch TFE substrate segments bonded together using modified epoxy.	1) Same as 1. 2) UV exposure in vacuum.	Tensile strength measurement before and after environmental exposure.
6	Evaluate effect of wire mesh contact through substrate.	0.005 inch x 0.5 inch wire mesh contact inserted through slit in 0.0015 inch TFE substrate and bonded in place using modified epoxy.	Same as 1.	Tensile strength measurement before and after environmental exposure.
7	Evaluate change in substrate α, ϵ after UV exposure.	0.0015 inch TFE substrate material bonded to tinned copper sheet using modified epoxy.	UV exposure in vacuum.	α and ϵ measurements before and after environmental exposure.
8	Evaluate wire mesh-to-substrate bond.	0.005 inch wire mesh bonded to 0.0015 inch TFE substrate using modified epoxy.	Same as 1.	Bond peel strength measurement before and after environmental exposure.
9	Evaluate thermal control paint adhesion to substrate.	0.001 and 0.002 inch coats of organic and inorganic white paint on TFE substrate.	Bend tests.	Visual inspection.
10	Determine α and ϵ of thermal control paints.	TFE substrate segment bonded to tinned copper sheet and coated with thermal control paint.	None.	α and ϵ measurements.
11	Determine cell cracking strength and radius in 1 cm dimension.	1 x 2 cm dendritic cell bonded to TFE substrate using modified epoxy.	Bend tests around a cylindrical surface along 1 cm	Cracking strength versus cylinder radius.

TABLE 4. FOUR PANELS — EACH 10 X 50 FEET

4 panels	336 pounds
8 STEM elements (1.5 inch diameter x 0.010 inch wall)	100
8 STEM mechanisms (100 x 1.5)*	150
2 drums (10 inch diameter x 0.08 inch wall Al)	59
8 cushions (0.080 inch thick)	34
2 covers	23
4 takeup spools	15
4 rewind mechanisms	10
Structure	24
Bus bars	13
Total	764 pounds

$$\text{Watts/pound} = \frac{20,000}{764} = 26.2$$

*Mechanism weight is estimated as 1.5 times STEM weight.

TABLE 5. FOUR PANELS — EACH 18 X 28 FEET

4 panels	336 pounds
8 STEM elements (1.25 inch diameter x 0.005 inch wall)	22
8 STEM mechanisms (22 x 2)*	44
2 drums (14 inch mean diameter x 0.125 inch wall Al)	240
8 cushions (0.080 inch thick)	34
2 covers	20
4 takeup spools	15
4 rewind mechanisms	6
Structure	20
Bus bars	13
Total	750 pounds

$$\text{Watts/pound} = \frac{20,000}{750} = 26.7$$

*Mechanism weight is estimated as twice STEM weight.

Discussion

Reynard: Any questions?

Vineyard - TI: (inaudible) Did you consider any cells other than the dendritic cell...?

Ray: We originally looked at 1 by 2 cm cells and 2 by 2 cm cells and actually did physical tests on both of these cells. As I said, the present effort is based on the use of the dendritic 1 by 30 cm cell only, but previously to this, we have looked at these other cells. We've put 2 by 2 cells around an 8-inch storage drum, and done some compression testing and found no problem.

Hamilton - IDA: Ken, I don't understand what you mean in reference to the pressure levels for the compression testing of the cells. Could you explain that a little bit, please?

Ray: It's understandable, because I went over this rather hurriedly. What I didn't dwell upon and what's in the paper and in the previous reports at greater length, is the fact that when you roll up this system on this storage drum, there has to be some means to compress these rolled-up layers. There is a polyurethene foam pad that is in between the solar cell substrate assembly for cushioning. We found it is possible to compress this type of sandwich construction with pressures necessary to prevent relative motion of the rolled-up layers during the worst extremes of launch vibration and acceleration, something up to 60 g's. We have measured coefficients of friction of actual substrates, and based on this, we calculated the force required to prevent the layers from moving relative to one another. And it turns out to be somewhere around 0.6 psi. We've put upwards of 1 and 2 psi on rolled-up systems in the laboratory with no damage to either solar cells or interconnection wiring. Now, in an effort to find out what the cell will do, since no data were available on the ability of cells to withstand cracking when subjected to uniform pressure over cylindrical surface, we loaded these up in various ways, one the vacuum bag method. We have put 14 psi on a cell, using the vacuum bag method on the 6-inch drum, and had no problem. Does that explain it?

Hamilton: Yes.

Winkler - RCA: You mentioned the six-tenths of a psi pressure. I'm wondering whether you have perhaps neglected to note that your substructure has to be able to take six-tenths of a psi, or whatever, and there may be some configurations which you want to use where they don't - I mean, there are a lot of structures for space that won't take a half a psi necessarily by - for other design reasons. So you may have to add another 30 or 40% or some such number.

Ray: It's a good point, Woody. However, the mode of failure of the
storage tube is not one of compression failure by buckling. We have
done quite a thorough analysis of the vibration test that we're going
to subject the demonstration model to - and the critical loading will be
in vibration at right angles to the long axis of the cylinder. The
actual bending of the storage drum is the designing feature, not the
compressive forces. This drum will be 6-foot-long for the demonstra-
tion model, and right now the thickness of the storage drum is set
something around 0.020 inch. If it changes it will change from
manufacturing considerations not from a design consideration.

Haynos - GSFC: Would you go into a little more detail on this ex-
tendable boom, not the De Havilland?

Ray: You mean the Hunter?

Haynos: Yes, the Hunter one - that's it.

Ray: The Hunter boom is composed of 4 mil material and it can be available
in 2 mil material. That one in the slide has about a 60% overlap as the
spiral layers go out. These booms have been built by Hunter in various
lengths. We have had several samples to play with, up from 3-foot
extensions to 10-foot extensions. They have a considerable extension
force available. They can be deployed either by collapsing - as I said,
like a drinking cup - and letting them spring out in a fully deployed
position. Or there's another method that Hunter has used, and we're very
attracted to it in that the coil of spring steel is wound on a storage
coil, and from there it is allowed by a motor to go into a cone slot and
form the spiral. And this has attractiveness of controlling the rate of
deployment. So essentially you have two cones at some 30 degrees to one
another. One cone contains the stored-up steel tape; it comes off of
this into a guide and forms a long tube. In the paper, I think I have
a picture of the mechanism that Hunter has used to deploy this.

Haynos: Thank you.

Johnson - Bellcomm: This Hunter boom - is this similar to the jack-
in-the-box DeHavilland type boom?

Ray: I don't believe it is because, if I remember the jack-in-the-box
DeHaviland boom, the boom is attached to the vehicle, and the spool
and everything just flies out. And this is not like that. So, in that
respect it's not similar. In the respect that this is steel tape,
prestressed to conform to certain dimensions and when released will spring
to the desired dimension, it might be called similar. However, we've
rejected the jack-in-the-box approach since, as far as we know, the spool
has to travel outward as the boom deploys.

Johnson: One more question. Do you feel that your solar arrays are
present state of the art?

Ray: I'd like to have you define about what our solar arrays are. Right now our solar arrays are on paper.

Johnson: Do you feel that these arrays can be built now for spacecraft?

Ray: OK. Are you asking, do we feel that what we've described can be built, and the answer is certainly yes. We've built small models within the lab having some 700 cells on them, and have been subjected to inhuman abuse and have come through fairly well. The weight estimates and the calculations for the larger arrays look sufficiently attractive, so that there doesn't seem to be any real constraint that we can see which would prevent these arrays from being built tomorrow, if you want to set up a fabrication effort.

Johnson: Thank you.

Reynard: We'll let the next author at least raise a question. Did you have a question?

Ratcheson - Boeing: I just wonder if I understood the last question and the last answer. I think the question was - do you think that the building of a, say, 20 KW array of this type is state of the art today? You could start doing it and develop it and build it within a couple of years? Was your answer in that regard?

Ray: I feel it can be done.

Ratcheson: Thank you.

A FIFTY KW, TWENTY WATT PER POUND SOLAR CELL ARRAY FEASIBILITY STUDY

Presented by

William I. Ratcheson

Space Division

The Boeing Company

20 October 1965

III. Structural Support
IV. Deployment and Jettison Mechanisms
V. Ground Support Requirements

The leading components of each subsystem were integrated and synthesized
into several array configurations; two of which are shown on Figure 2.
Each of these configurations were evaluated and compared as shown in
Figures 3 and 4.

The folding modular array consists of trapezoidal panels joined to-
gether by hinges and latches, folded in the stowed position and deployed
by one of several actuating systems. The trapezoidal panels best utilize
the available conic envelope under the shroud.

Several panel configurations including aluminum and beryllium flat
sheet stringer, aluminum concentrator, and semirigid panels were analyzed.
Only the aluminum concentrator and beryllium semirigid panels were capable
of meeting the 20 watt per pound conversion ratio requirement. Sufficient
area of concentrator panel could not be stowed in the available envelope to
meet the 10 and 50 kilowatt power requirements.

Beryllium and aluminum support structure were compared. Aluminum with
a modulus of elasticity of 10×10^6 and a specific density of 0.10 pounds
per cubic inch could not meet the weight requirement. Beryllium with a
modulus of 43.5×10^6 and a specific density of 0.067 pounds per cubic inch
proved best. The choice of beryllium will result in higher cost for fab-
rication of a prototype array because of special tooling and facility
requirements. Beryllium with a modulus of 43.5×10^6 and a specific
density of 0.067 pounds per cubic inch proved best. The choice of beryl-
lium will result in higher cost for fabrication of a prototype array
because of special tooling and facility requirements. Other new components
selected during the trade studies include 8 mil N on P back connected sili-
con solar cells and 4 mil microsheet cover glasses. These components
provided the best power per pound ratio within the expected state-of-the-
art as of January 1, 1966.

For the rollup type array, combinations of rigid panels and curtain
panels were considered. The rigid panels would be capable of sustaining
the retro-loads imposed during injection into the Mars orbit. H-film
substrates mounted to collapsible type booms were configurated. Two
substrate concepts were considered. One used H-film corrugations bonded
to a flat sheet of H-film, for solar cell support, and in the other the
cell stack and H-film substrates were protected by foam rubber between
the rolled up layers. Beryllium copper DeHavilland STEM type, and col-
lapsible closed section booms, and telescoping aluminum booms were con-
sidered for deployment and structural support. Figures 3 and 4 summarize
the trades that were conducted.

Based upon these studies, the baseline array configuration was defined
by JPL and The Boeing Company. The preliminary design illustrated in
Figure 5 consists of a four armed folding modular array using semirigid
fiberglas substrates. Rectangular panel shapes joined by hinges were

A FIFTY KW, TWENTY WATT PER POUND SOLAR CELL ARRAY FEASIBILITY STUDY

William I. Ratcheson
Solar Array Project Engineer
Space Division
The Boeing Company

In 1965, The Boeing Company, under contract to Jet Propulsion Laboratory, conducted a study to determine the feasibility of fabricating solar arrays capable of generating from 3 to 50 kilowatts of power with a minimum conversion ratio of 20 watts per pound; representing about twice the presently achievable ratio. The arrays would be used to drive electric propulsion systems and provide all other electric power on unmanned Mars orbiting spacecraft. Concurrently, contracts were awarded to two other contractors to develop the spacecraft and mission feasibility. Interface coordination with JPL and the associate contractors was a significant program element.

The plan to meet the program objectives included these major items.

1. Definition of the problem by determining the environmental, mission and interface requirements.

2. Data collection and evaluation of state-of-the-art components, materials and processes that were appropriate to the configuration of large solar arrays.

3. Use of this material to develop several feasible configuration alternatives for cell stack modules, support structure and deployment mechanisms. These component and subsystem configurations were synthesized into array configurations which were compared to the requirements in order to select a near optimum configuration.

4. After establishment of a baseline configuration, preliminary designs were developed for a 10 KW and a 50 KW array.

5. Finally, a power conversion ratio, schedule, and cost evaluation of each design was performed.

In cooperation with Jet Propulsion Laboratory and the mission contractors, a detailed statement of array requirements from fabrication through mission completion were developed and is summarized in Figure 1.

Concurrently, evaluations of the following major elements of the array were conducted.

   I. Solar Cell Modules
  II. Electrical Bus System

auxiliary panels are released mechanically and deployed by redundant torsion springs.

The Jettison System, employed just prior to the Mars injection orbit, is squib actuated. Spring driven torsion bars unclamp the outboard sub-panel assemblies from subpanel No. 1 and compression springs then disengage the electric power plugs and slowly separate the assemblies. Deployment cables are cut by squib driven guillotines. Dual squibs and bridge-wires are used at all points for reliability.

The electrical power subsystem consists of the solar cell modules and power busses to generate the required power and carry the current to the interface at the spacecraft-array joint. Power conditioning is provided on the spacecraft. 28-volt power is provided by sub-panel No. 1 for telecommunications and the scientific and engineering experiment package. The spacecraft bus receives 100-volt power for the electrical propulsion engines.

Panel temperature, deployment completion, and separation complete sensors are provided on each panel assembly. Current and voltage sensors for each assembly are provided on the spacecraft power busses.

Ground Support Requirements from fabrication through development, qualification and acceptance testing phases have been developed.

Interfaces

Compatible envelopes for the array stacks and the spacecraft structure and subsystems in both the stowed and deployed positions have been deter-minded. Physical and functional interfaces for the 400 cycle deployment motors and locations for the cables have been established.

The structural loads imparted at the array-spacecraft attachment have been calculated. The dynamic input from the launch vehicle and spacecraft to the stowed array has been specified in the design require-ments. The deployed array has been designed to meet stiffness require-ments which preclude coupling with the spacecraft Guidance and Control System.

The electrical interface between the 28 and 100 volt bus system of the array and the spacecraft has been defined and documented. The array bus system will terminate in NAS 1600 connectors and power will then proceed to the spacecraft bus and power conditioning equipment.

One major interface problem remains unresolved. The effective dis-persion angle of particle emission from the ion engines remains undefined. The possibility of impingement causing degradation to structural or electrical components of the array is to be examined by an engine-solar panel test at the spacecraft study contractor's facility.

utilized to minimize design and fabrication problems. The main deployment subsystem consists of 4 two-stage electric motor drive gear boxes actuating a pulley cable concept. The preliminary analysis indicated that the baseline concept would meet the 20 watt per pound power to weight requirement. The 107 square foot panels can be fabricated with less difficulty than the large, 833 square foot roll-up panels. The pulley-cable deployment system which was compared to torsion springs and bourdon tubes, demonstrated light weight and satisfactory reliability and is composed of essentially state-of-the-art components.

Two prototype preliminary conceptual designs were completed in this program. The array designed for installation of a spacecraft launched by a Saturn IB/Centaur provides 47.7 kilowatts of power at a sun-probe distance of one astronomical unit. This is achieved through the deployment of 4944 square feet of gross area, or 4433 square feet of active solar cell area. The total array weight has been calculated to be 2125.6 pounds for a power conversion to weight ratio of 22.4 watts per pound. If a weight contingency of 10 percent were added for unknowns in the design, a ratio of 20.4 watts per pound would be achieved. Sufficient storage space exists under the shroud to add an additional subpanel assembly to each panel. This would provide approximately 500 square feet of additional deployed area for a 52 kilowatt power output for the array. The second array designed is installed on a spacecraft launched by an Atlas/Centaur and provided 10 kilowatts of power at one astronomical unit. The structural, mechanical, and electrical subsystems are identical in principle to the Saturn IB/Centaur launched array. It provides power at 1.0 AU at a 19.9 watts per pound conversion ratio.

The array consists of four folding panel assemblies. Each assembly then consists of subpanel number 1 and subpanel assemblies 2 through 5 Each subpanel assembly has a main panel and two auxiliary panels. The entire array is made up of only three different panel sizes to minimize tooling and spares problems.

During the preliminary design period, engineering efforts have been concentrated on the four major array subsystems, necessary sensors, the ground support system, and the interfaces of these systems with the spacecraft.

Primary structure consists of beryllium panel spars and intercostals. Critical loads are imposed by the launch mode with the retro maneuver imposing additional requirements on sub-panel No. 1. In the launch mode each folding array stack is clamped together by tension tie rods at two points and the four stacks are tied together at these points. The stacks are then tied to the spacecraft through hinges at the aft end.

The subpanel assemblies are deployed by a cable pulley system driven by four electric motors and harmonic drive gear boxes. Electric power is provided by spacecraft batteries. Each motor is capable of driving two panel assemblies providing redundant deployment capability. The

have given us a high level of confidence that a 20 watt/pound solar array for the particular mission defined in the criteria and requirements statement can be achieved.

Several development problems require resolutions. Among these are:

1. The availability of 8 mil cells with 11.8% nominal efficiency at air mass 1 in the quantity required.

2. Four mil cover glasses are available from a single source only at present. Funding to vendors may be required for process technique improvements to increase production quantities of these two items for flight article fabrication.

3. The verification of the dynamic analyses through test is required because of the inability to predict the array damping factor with a high degree of confidence.

4. Manufacturing processes for beryllium frame - fiberglas substrate assembly techniques and solar cell stack bonding and soldering must be developed.
    Small scale substrate assembly will be developed during the sample panel fabrication in the next few weeks.
    Cell bonding and soldering processes will be developed to a hand assembly level by the sample panel fabrication.

An analysis of production problems for full scale prototype arrays has been made and major problem areas have been defined. A cost and schedule evaluation for development and fabrication of prototypes has also been made. It is estimated that a 50 kilowatt flight article could be developed within 32 months from go-ahead.

Three one-square foot panels are being fabricated. These will demonstrate the feasibility of the cell mounting and soldering techniques. It is also planned for one panel to be incorporated in an ion engine test to ascertain the effects of ion impingement. The panels can also be used for thermal, thermal shock, and acoustic testing.

Two small scale hand operated array models are being fabricated to illustrate the launch packaging, deploying, and latching principles of the array design.

A final report summarizing the analyses, designs, and evaluations will be made to JPL and NASA at the conclusion of the program.

Deployment Reliability

Deployment system reliability was calculated using failure rate data from the Boeing Data Bank. The estimate is based on 100 percent array deployment. Using this assumption and the available data for typical components a reliability of 0.997 was calculated. However, the data is based on more severe service than the array should experience including infant mortality, wearout, and fatigue. If it is assumed that the actual array failure rates are 25 percent of those represented by the data used, the reliability figure is increased to 0.999.

Jettison Reliability

The pyrotechnic initiators are considered critical. Four completely redundant pyrotechnic severing devices are used. Failure of the firing charge is the predominant failure mechanism. The failure rate for firing was increased from 1×10^{-4} to 1×10^{-3} failures per trial to account for 350 days exposure to the space environment.

Electrical Bus Reliability

The predominant failure point for the electrical bus system is considered to be the bus connections to solar cell modules at the diodes. All these connections are redundant resulting in a negligible probability of failure for the mission.

Solar Cell Modules Reliability

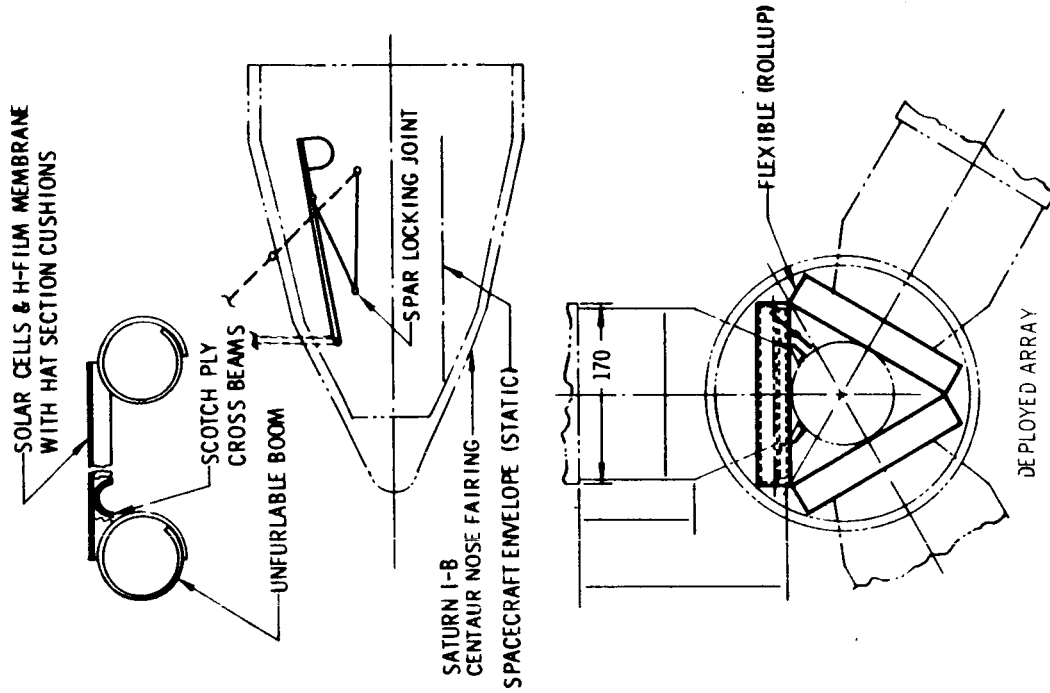The assumptions used in the module reliability analysis were:

1. The principal mode of failure is open circuit in individual cells. The number of short circuits will be negligible.

2. The failure rate for the individual cell is 0.1×10^{-6} failures per hour.

3. Cell failure rate is constant with respect to time, and failure occurrence is random with respect to location in the array.

4. Blocking diode failure rate is 0.05×10^{-6} failures per hour.

The module under consideration has a basic grouping of seven cells in parallel. Occurrences of two cell failures in the same seven-cell group are very unlikely to occur. Failures of one cell in a group are more numerous. For a reliability of 0.999 a power loss of approximately 1.5% can be expected at the end of 350 days for the electrical subsystem.

Summary

To sum up, the design efforts and analyses that have been conducted

ROLLUP ARRAY

- SOLAR CELLS & H-FILM MEMBRANE WITH HAT SECTION CUSHIONS
- SCOTCH PLY CROSS BEAMS
- UNFURLABLE BOOM
- SPAR LOCKING JOINT

SATURN I-B
CENTAUR NOSE FAIRING
SPACECRAFT ENVELOPE (STATIC)

FLEXIBLE (ROLLUP)

170

DEPLOYED ARRAY

FOLDING ARRAY

- FOLDING MODULAR SOLAR ARRAY
- SPACECRAFT ENVELOPE STATIC
- PAYLOAD DYN. ENVELOPE SATURN IB CENTAUR

₵ SYM

SOLAR ARRAY STOWED

PAYLOAD SHROUD

JETTISON AT
HINGE 4 PLACES
AND 4 AUXILIARY PANELS

53'
DEPLOYED LENGTH

₵ SYM

₵ HINGE

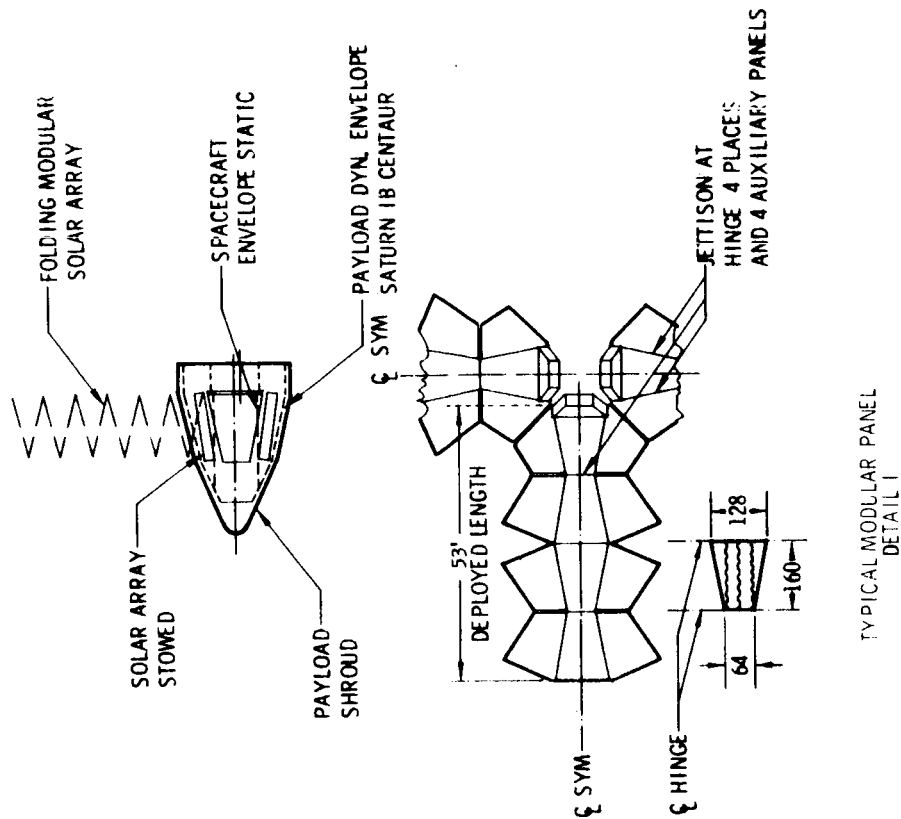TYPICAL MODULAR PANEL
DETAIL I

128
160
64

FIGURE 2

CRITERIA AND REQUIREMENTS

- MISSION PROFILE

  - 71 THRU 75 TIME PERIOD
  - AMR DIRECT LAUNCH
  - 350 DAYS TO ENCOUNTER
  - 140 DAYS OPERATION IN MARS ORBIT
  - SATURN IB/CENTAUR LAUNCH VEHICLE
  - ATLAS/CENTAUR LAUNCH VEHICLE

- POWER PROFILE

  - 50 KW AT A SUN-PROBE DISTANCE OF 1 A.U.
  - 1.1 KW AFTER MARS ENCOUNTER (AT A SUN-PROBE DISTANCE OF 1.67 A.U.)
  - POWER CHARACTERISTICS FOR OPTIMIZATION

- STRUCTURAL AND ENVIRONMENTAL

  - NATURAL
  - INDUCED

- INTERFACES

  - PHYSICAL
  - FUNCTIONAL

- MANUFACTURING AND DEVELOPMENT

  - AUTOMATION OF CELL MODULE ASSEMBLIES
  - REPAIR CAPABILITIES
  - ASSEMBLY AND INSTALLATION TECHNIQUES
  - QUALITY CONTROL
  - TEST REQUIREMENTS

- RELIABILITY

  - ELECTRICAL
  - MECHANICAL
  - STRUCTURAL

- CONFIGURATION AND ENVELOPE

  - DISCOVER-SERIES LANDER

    - SC-1 FOLDING MODULAR
    - SC-2 FOLDED DISC
    - SC-3 ROLL-UP

- APOLLO SERIES

  - 1000# LANDER

- GROWTH CAPABILITIES INCLUDING 4 TO 6000# LANDERS

  - SC-1 AND SC-3 APPEAR TO BE ADAPTABLE TO THESE ENVELOPES

FIGURE 1

ROLLUP CONFIGURATION TRADES STUDY

ITEM	LBS/ SQ FT	RELIABILITY RATING	STATE OF ART RATING	WATTS/LB	TOTAL KW POSSIBLE
STIFFENED PANEL	.249	1	C		50
UNSTIFFENED – FOAM PAD AND STORAGE DRUMS	.245	2	C		50
AS STRUCTURE					
STEM BOOM	.059	1	A		
CLOSED TUBE BOOM	.059	1	C		
TELESCOPING BOOM	.035	2	A		
AS DEPLOYMENT SYSTEM					
STEM BOOM	.079	1	A		
CLOSED TUBE BOOM	.079	3	C		
TELESCOPING BOOM	.083	2	A		
BUSES	.025				
TOTAL ARRAY USING STEM BOOM	.412	1	C	25	50
TOTAL ARRAY USING CLOSED BOOM	.412	3	C	25	50
TOTAL ARRAY USING TELESCOPING BOOM	.392	3	C	26.2	50

FIGURE 4

FOLDING MODULAR TRADES SUMMARY

ITEM	LBS/SQ FT	RELIABILITY RATING	STATE OF ART RATING	ESTIMATED PERFORMANCE WATTS/LB	TOTAL KW POSSIBLE IN ENVELOPE
CONCENTRATOR PANEL	.263	1	A		45
SEMI-RIGID PANEL (CELL STACK AND SUBSTRATE)	.211	2	B		50
BERYLLIUM SUPPORT STRUCTURE FOR CONCENTRATOR	.108		B		50
BERYLLIUM SUPPORT STRUCTURE FOR SEMI-RIGID	.208		B		
MOTOR DRIVE DEPLOYMENT	.023	1	A		
BOURDON TUBE DEPLOYMENT	.028	2	B		
SPRING & DAMPER DEPLOYMENT	.025	1	B		
MISCELLANEOUS	.030				
BUSES	.025				
TOTAL ARRAY FOR CONCENTRATOR CONCEPT (MOTOR DRIVE)	.449	1	A	19.9	45
TOTAL ARRAY FOR SEMI-RIGID CONCEPT (MOTOR DRIVE)	.497	2	B	21.9	50

FIGURE 3

FEASIBILITY STUDY

20 WATT/POUND SOLAR CELL ARRAY
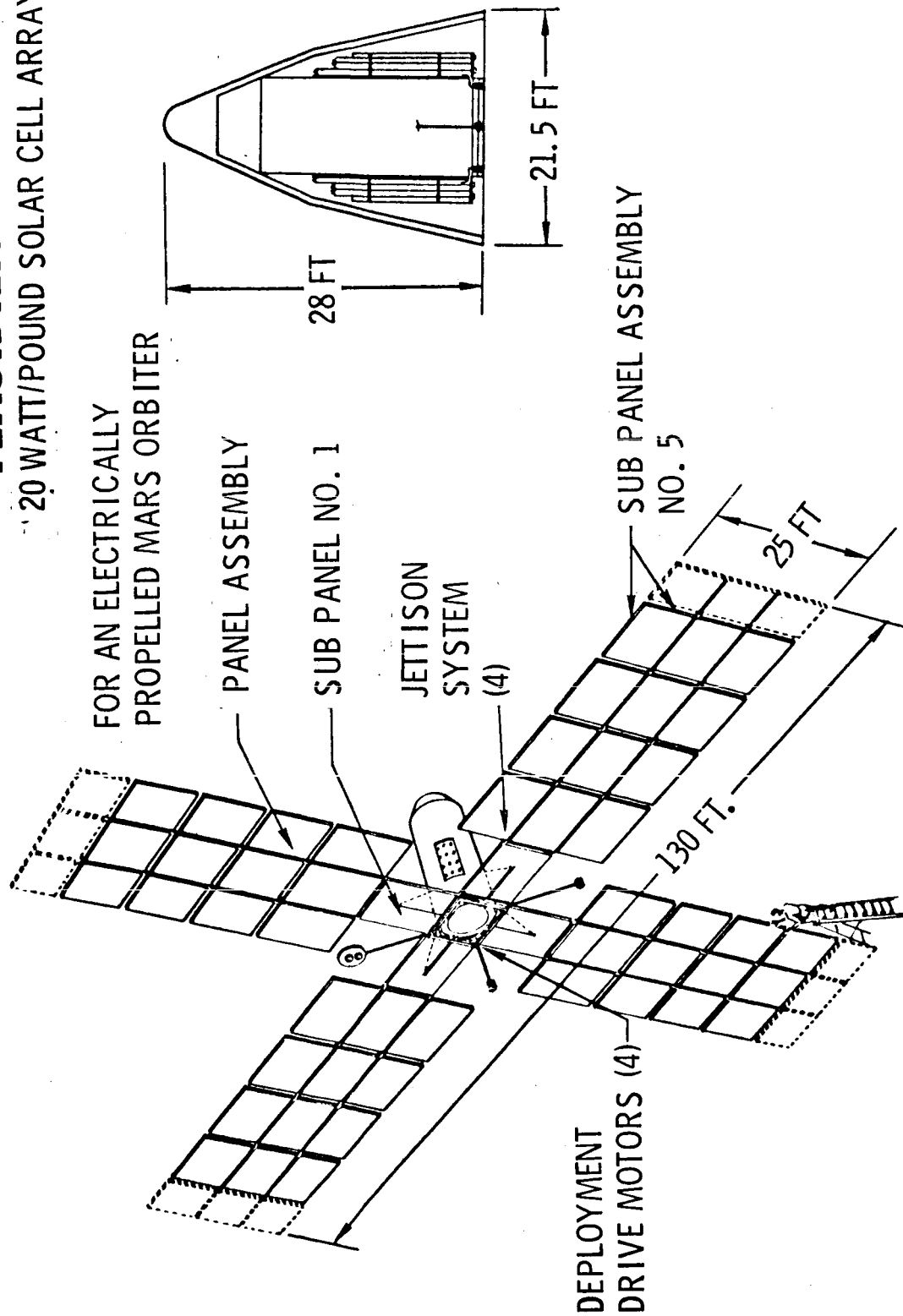
FOR AN ELECTRICALLY
PROPELLED MARS ORBITER

28 FT

21.5 FT

PANEL ASSEMBLY

SUB PANEL NO. 1

JETTISON
SYSTEM
(4)

SUB PANEL ASSEMBLY
NO. 5

25 FT

130 FT.

DEPLOYMENT
DRIVE MOTORS (4)

FIGURE 5

Acknowledgement

Summary

An analytical study has been performed to determine the feasibility of using a positionable despun thermal shield to control the temperature and power of a solar array used for spacecraft on-board power during a 0.2 AU mission. The results of the study indicate that such a mission is feasible using body-mounted N/P silicon solar cells with blue-red full-cell-response bandwidth filters.

A cylindrical spacecraft with a Pioneer configuration, spinning about its axis at 60 RPM, was used in the study; the selected thermal shield consisted of two counter-rotating cylindrical surfaces with a radius only slightly larger than the spacecraft and rotating about the spacecraft spin axis.

Solar array temperature, thermal shield temperature, and system power output are given as a function of shield position and solar distance for N/P silicon solar cells with full-cell-response bandwidth blue-red filters. Voltage-current curves are given as a function of solar distance for this cell-filter combination.

It is shown that the required power generation level of 60 watts can be maintained throughout the mission. With the solar shield opening programmed to optimize power, a minimum power of 72 watts is available at 1.0 AU and a maximum power of 325 watts obtains at 0.2 AU. The solar array reaches a maximum temperature of 88°C (190°F) at 0.2 AU.

Both the cell and the filter selected on the basis of this study are production items available at relatively low cost.

N66-17352

THE FEASIBILITY OF A PROGRAMMED HEAT SHIELD FOR

SOLAR CELL PERFORMANCE CONTROL

Presented by

J. W. Fairbanks

Texas Maritime Academy

Texas A&M University

College Station, Texas

20 October 1965

drical surface which rotates with respect to the cylindrical spacecraft. This configuration is probably the simplest and most direct method of effecting the shield. However, this concept has a serious drawback. Power produced by the solar cells on the cylindrical surface of the spacecraft is an inverse function of the angle of incidence between the solar flux and the normal to the surface of each cell; at large incidence angles, the cell power approaches zero. Also, the large shifts that occur in the spectral transmission of filters when the incidence angle is large affects both heating and adhesive degradation. With this configuration, a relatively large number of cells must be exposed at any given power level; as a result, cell temperatures will be higher and, consequently, photovoltaic performance will be degraded. Also, a large number of exposed cells will receive solar energy at large incidence angles and will thus be operating inefficiently or not at all.

Configuration 2 (shown in Figure 2) consists of two counter-rotating cylindrical surfaces which rotate with respect to the spacecraft. This method eliminates the drawbacks cited for configuration 1. With this configuration, cell performance can be maximized with a minimum effective exposure. This is the recommended configuration, and it will be used throughout as the reference concept.

Nominal dimensions of the solar cell covered cylindrical spacecraft are 36 inches in diameter by 30 inches in length. The cylindrical surface is spinning at 60 + 10 RPM and is normal to the incident solar radiation at all times during flight.

The thermal shield will consist of a nonmagnetic framework supporting a typical 1/4-inch thick multilayer insulation blanket. The properties of the insulation will be:

$$\text{density} = 5 \text{ lb/ft}^3$$

$$\text{thermal cond.} = 0.005 \text{ Btu/hr} \cdot \text{ft.} \ (^{\circ}\text{F/in})$$

The shield will be bearing supported at one end and will rotate independently of, but colinear with, the spacecraft cylindrical axis.

Surface properties of the shield will be:

Externally exposed surface (space side)

$\alpha_S = 0.10$
$\epsilon_H = 0.80$ $\quad \left\{ 70^{\circ}\text{F} \leq \text{T} \leq 500^{\circ}\text{F} \right.$

Surfaces facing spacecraft

$\epsilon_H = 0.05$

The shield is considered to be thermally isolated from the spacecraft, excepting radiation coupling.

THE FEASIBILITY OF A PROGRAMMED
HEAT SHIELD FOR SOLAR CELL
PERFORMANCE CONTROL

Michael W. Cobb
W. Scott Cummings
Philco Corporation
A Subsidiary of Ford Motor Company
WDL Division
Palo Alto, California

John W. Fairbanks
Assistant Professor
Texas Maritime Academy
Texas A&M University
College Station, Texas

Introduction

Near solar space probe missions are desirable for the purpose of col-
lecting needed scientific data. However, during such a mission, spacecraft
temperatures will be high. Solar cells are the conventional power source
for extended space missions, but they do not operate efficiently at high
temperatures -- in fact, they have a temperature limit beyond which no
power is produced.

The purpose of the present investigation was to determine the feasi-
bility of extending the useful range of solar cells to include near solar
missions. The suggested means for accomplishing this end -- a close-
mounted despun heat shield -- is applicable only to a spinning spacecraft
with body-mounted cells.

The feasibility of this technique is established on the basis of the
results of a combined thermal and photovoltaic analysis which considers a
spinning cylindrical spacecraft with a Pioneer configuration. Solar array
temperature, thermal shield temperature, and system power output are pre-
dicated as a function of shield position and solar distance; voltage-
current curves are estimated as a function of solar distance.

System Description

The purpose of the thermal shield is to control the temperature of the
solar cells by minimizing the effective number of cells exposed to the inci-
dent flux during a near-solar mission. Figures 1 and 2 suggest two possible
configurations which could be used to satisfy the thermal shield require-
ments.

Configuration 1, (shown in Figure 1) consists of a single hemicylin-

S_d = solar constant at distance d from the sun

$\quad$ = 442 Btu/hr $\cdot$ ft^2 at 1 AU

$\quad$ = 2760 Btu/hr $\cdot$ ft^2 at 0.4 AU

$\quad$ = 11000 Btu/hr $\cdot$ ft^2 at 0.2 AU

α_{Si} = solar absorptance of node i

T_1 and T_2 are desired as functions of the shield angle (2θ), the solar distance, and the surface properties of the spacecraft and shield. The resulting equations are:

$$\sigma T_2{}^4 = \frac{\epsilon_E A \, q_{Si} + [A (\epsilon_{13} + \epsilon_E) + \epsilon'_{13} A'] \, q_{S2}}{A \left\{ A \left[\epsilon_E(\epsilon_{13} + \epsilon_{23}) + \epsilon_{13}\epsilon_{23}\right] + \epsilon'_{13} A'(\epsilon_E + \epsilon_{23})\right\}} \qquad (2)$$

$$\sigma T_1{}^4 = \frac{(\epsilon_E + \epsilon_{23}) \, A\sigma T_2{}^4 - q_{S2}}{\epsilon_E A} \qquad (3)$$

where:

$\epsilon_E \doteq \left[\dfrac{1}{\epsilon_1} + \dfrac{1}{\epsilon_2} - 1\right]^{-1}$ = effective emittance^2 between nodes 1 and 2.

ϵ_{ij} = emittance of that portion of A_i that "sees" node j.

ϵ'_{13} = emittance of ends of cylinder.

A = πrh = one-half the area of the cylindrical surface of revolution. Also, either surface of the shield.

A' = $2\pi r^2$ = total area of the ends of the cylinders.

T_1 = temperature of node 1, $^{\circ}$R

T_2 = temperature of node 2, $^{\circ}$R

The following surface properties were used:

ϵ_{13} = ϵ_{12} = 0.875 (solar cells with 0.4 to 1.1 μfilters).

ϵ'_{13} = 0.875 (arbitrarily taken equal to ϵ_{13})

ϵ_{21} = 0.05

ϵ_{23} = 0.80

α = 0.10

The solar cell array is thermally isolated from the spacecraft structure. A total of 10,368 silicon solar cells are arranged uniformly on the cylindrical surface of the vehicle. They are connected in 48 strings of 4 (parallel) by 54 (series) cells. All 54 cells of a given series will be in a single line parallel to the vehicle axis.

Thermal Analysis

A general thermal analysis of the spacecraft/shield system was performed for the purpose of establishing temperature levels and ranges. The resulting thermal model is also used in the detailed analysis of the power system. The thermal analysis treats both spacecraft and shield as isothermal; this assumption is shown to be valid for the spacecraft by considering the effect of its spin rate. Radial and circumferential gradients in the shield are also considered; as a result, the analysis is shown to be conservative.

Both spacecraft and shield are assumed to be isothermal in the thermal analysis which follows. Figure 3 is a schematic description of the thermal model. The following assumptions were made in the development of the thermal model:

- The heat shield is attached to the spacecraft by a thermally non-conducting support.

- The shield may be interposed between the spacecraft and the Sun to any extent desired.

- Both spacecraft and shield are isothermal bodies.

- The shield is mounted in close proximity to the spacecraft.

- The total surface area of the shield is equal to the area of the cylindrical surface of revolution of the spacecraft.

- The solar absorptance of any surface is independent of the incidence angle of the solar vector.

- The effective temperature of deep space is absolute zero.

The solar energy absorbed by node i is:

$$q_{Si} = A_{pi} \, S_d \, \alpha_{Si}$$

where

A_{pi} = projected area of node i as seen by the sun

$= 2rh \sin \theta$ for node 1, the spacecraft

$= 2rh \, (1 - \sin \theta)$ for node 2, the shield.

details of the analysis are given in Reference 1. The assumption of an isothermal shield provides conservatism in the photovoltaic calculations which are a function of cell temperature.

The effect of circumferential* gradients will only be significant with the shield closed, or nearly closed. Consideration of these gradients will reduce the lower limit of the predicted temperatures. As a result, a further degree of conservatism is included in the analysis of the system.

Multiple reflections of solar radiation between the shield and the spacecraft have not been considered in this analysis. However, the geometry of the selected configuration (Figure 2) is such that very little solar radiation will enter the space separating the shield and the spacecraft.

The thermal analysis of this study is essentially conservative in the sense that predicted solar array and thermal shield temperatures are higher than those which actually will occur. The assumption of an isothermal spacecraft is valid for the purposes of this exposition.

Photovoltaics

Parameter investigation and system design of solar cell arrays have been primarily concerned with operation in near-earth environments. Consequently, there is a paucity of data regarding high-temperature photovoltaic operation under conditions of intense solar illumination. Several parameters that can be neglected for near-earth missions become quite significant for a near-solar mission. For example, silicon solar cells, body-mounted on an unshielded cylindrical spacecraft, approach zero power output between 0.5 and 0.4 AU because of temperature limitations.

The performance of silicon solar cells is discussed below, with an emphasis on near-sun operation. The discussion includes consideration of spectrally selective filters, cover glass adhesives, and particle radiation damage. State-of-the-art components and techniques are stressed throughout.

A 1 by 2 cm, 10 Ω-cm N/P silicon solar cell with 10.7 percent conversion efficiency at 28°C and air mass zero was selected.

Silicon Solar Cells

Solar cell selection was based on the following criteria:

- Performance Reliability

  1. Elevated temperatures

  2. Very high intensity

---

* Circumferential is defined herein as on the circumference of the thermal shield (or spacecraft), and in a plane perpendicular to the centerline of the spacecraft.

Calculated quantities are:

ϵ_E = 0.0496

A = $\pi r h$ = 11.78 ft^2

A' = $2\pi r^2$ = 14.14 ft^2

Predicted temperatures are given by Figure 5.

In order to simplify the thermal model of the spacecraft, it was assumed that the spacecraft was isothermal. This assumption was examined to determine its validity.

The following assumptions were made in the analysis:

(i)   Solar cells are mounted on a cylinder composed of aluminum honeycomb sandwich construction. The facings are 10-mil aluminum sheets; the core is 1-mil aluminum foil; and the sandwich is 0.250-in thick.

(ii)   It is assumed that axial temperature gradients are negligible and all circumferential heat transfer occurs in the facings (this assumption will cause large gradients).

(iii)   The heat capacity of the honeycomb is assumed to be that of the aluminum facings. (This assumption will also give circumferential gradients larger than actual since the heat path is considered to be entirely within the facings. This neglects the capacity of the core and its bonding agent; thus, giving a lower capacity than actually obtains.)

(iv)   The surface of the cylinder is assumed to be thermally isolated from the interior of the spacecraft.

Solar heating of a rotating cylindrical space vehicle has been considered analytically by Charnes and Raynor[3]. An analysis based on their work (described in detail in Reference 1) indicates very small temperature gradients (less than 1 percent of the average spacecraft temperature over any quadrant of the surface).

Thus, in the real case (with the thermal shield, increased capacitance of the spacecraft, heat transfer in the honeycomb, etc.) circumferential temperature gradients in the spacecraft surface are negligible. This result obtains at all solar distances of interest in the present study.

The analysis above assumed an isothermal heat shield. In fact, a radial temperature drop will exist in the shield which will have the effect of lowering the temperatures of the solar cell surfaces (node 1). Radial[*] temperature gradients in the shield have been considered analytically;

──────────────────────

[*] Radial is defined herein as in the direction of the radius of the cylindrical spacecraft.

3. Particle radiation resistance

• Flight Quantity Availability

• Cost

• Current state-of-the-art.

It should be noted that several manufacturers of solar cells rate their cell conversion efficiency by considering only the exposed active cell surface area instead of the total surface area of the cell. This covered surface area varies slightly with the manufacturer, but is generally about 3 to 5 percent of the total cell surface area. In the present analysis, the conversion efficiency is applied to the total surface area of the cell.

Although large-area solar cells provide several advantages, they were not considered because of excessive cost. Bulk single-crystal gallium arsenide solar cells are an alternative to silicon cells. Although they provide a conversion efficiency advantage at very high temperature, they are not considered herein because of deficient performance in the temperature range of interest and excessive cost.

Solar Cell Spectrally Selective Filters

Solar cell conversion efficiency is essentially inversely proportional to the cell's temperature; silicon cells approach zero efficiency at approximately 868°R (209°C). Hence, it is desirable to operate a solar array at as low a temperature as possible.

The most successful solar cell thermal control technique is the installation of cover glass slides with spectrally selective multilayer interference filters and antireflective coatings which selectively reflect wavelengths not photovoltaicly convertible.

An ideal filter would transmit solar radiation only in the wavelength region within the spectral response of the solar cell. Unfortunately, real filters include undesirable characteristic transmission bands in the near-IR and IR regions beyond the cell's response region; this is illustrated in Figure 4. Most earth-orbiting spacecraft utilize a "blue filter" which rejects solar energy on the shorter wavelength side of the cell's response bandwidth. Suppression of both the shorter wavelength and some of the solar energy just beyond the cell's long wavelength response can be accomplished by using a filter with a larger number of layers; this filter is called the "blue-red filter". Thelan[4] identifies this characteristic as a single suppression band. This filter is used extensively in the present analysis, and is identified as filter No. 3.

Three commercially available filters are compared in Table 1. Based on the analysis which follows, the best filter for the present

mission would be a full-cell-response-bandwidth blue-red filter similar to filter No. 3, with a triple suppression band characteristic.

TABLE 1

FILTER COMPARISON

	Filter No. 1	Filter No. 2	Filter No. 3
λcut-on (Microns)*	0.5	0.71	0.42
λcut-off (Microns)*	0.82	1.06	1.02
IR Suppression	Tripleband	Tripleband	Singleband
Availability	6 Weeks	6 Weeks +	2 Weeks
Relative Cost	4.5**	4.5**	1.0
Flight Proven	No	No	Yes

* 50% Transmission Point

** Plus Developmental Cost

As the angle of incident illumination (i.e., the angle between the incident illumination and a normal to the solar cell filter surface) increases, filters exhibit a characteristic shift to shorter wavelengths accompanied by decreased transmission. It should be noted that a sharp decrease in transmission occurs above approximately 45 degrees.

A filter cut-on shift to shorter wavelengths can be extremely detrimental to the performance of an array, since the optical adhesives are UV sensitive.

The incidence angle effects discussed above are increased by the adhesive and represent a strong argument for the configuration shown by Figure 2. It is imperative that the incidence angle be kept less than approximately 30 degrees.

System Analysis

System power and electrical output are considered below in terms of the active control parameter (shield position) and the solar distance. The shield angle (2θ) is used as the specification of shield position.

Power Analysis

The maximum power output per unit projected area of the solar array was determined as described below:

$$\frac{P}{A_p} = SZ\eta_S \, \eta_T \, \eta_{FB} \tag{4}$$

where

P   = power output

A_p = projected surface area = $2rh \sin \theta$

S   = incident solar flux

Z   = Packing factor -- the fraction of the total spacecraft surface (excluding ends) covered with solar cells

η_S = bare solar cell conversion efficiency at air mass zero and 28°C

η_T = cell temperature efficiency

  = $1 - 0.00545 \, (T - 301^\circ K)$ for 10.7% N/P silicon cells

η_{FB} = efficiency ratio, filtered to bare cell

$$\doteq \frac{\int_{\lambda_1}^{\lambda_2} T_\lambda \, r_\lambda^* \, S_\lambda \, d\lambda}{\int_0^\infty r_\lambda^* \, S_\lambda \, d\lambda} \tag{5}$$

T_λ = spectral transmittance of filter

r_λ^* = normalized solar cell spectral response

  = $\dfrac{(r_\lambda)_{max}}{r_\lambda}$

S_λ = spectral solar intensity distribution

It is apparent from equation (4) that cell stack temperature is a very influential parameter in the performance of the solar array.

The thermal analysis together with accurate thermal absorptance (α_{ZT}) values for the cell stacks with filters will provide a better estimate of the operating temperatures of the cells. The cell stack absorptance can, in the present case, be represented as the difference between the total absorptance of the cell stack (α_{ZA}) and the energy converted by the cell into electricity:

$$\alpha_{ZT} = \alpha_{ZA} - \eta_{FB} \, \eta_T \tag{6}$$

An analytic approach leading to equation (6), and utilizing commonly measured, parameters, results in the following equations;

$$\alpha_{ZA} = 0.05 \sum_{\lambda=0}^{\infty} [1 - (p_{ZA})_{\lambda}] \, (1 + A_{\lambda}) \tag{7}$$

$$\eta_{FB} = \frac{\sum_{\lambda=0}^{\infty} [1 - (p_{ZA})_{\lambda}] \, r_{\lambda}^{*} \, S_{\lambda}}{\sum_{\lambda=0}^{\infty} r_{\lambda}^{*} \, S_{\lambda}} \tag{8}$$

The data for the filter were based on spectrophotometer measurements of a fabricated unit. Johnson's data were used for the solar spectral distribution (S_{λ}). The solution of equations (7) and (8) considered the solar spectrum in 5 percent energy increments:

The cell stack temperature is obtained from a trial and error solution using the absorptivity given by equation (6) as α_{Sl} in equations (1), (2), and (3).

In Reference 1, the above power analysis was performed for the indicated N/P silicon solar cell with each of the three filters considered in Table 1. The results presented herein are only for the most promising combination, which used filter No. 3.

Refernce (1) also provides details of the numerical calculations for the power analysis, including performance data for the cell stack components. It was found that:

$$\alpha_{ZA} = 0.682$$

$$\eta_{FB} = 0.901$$

and

$$Z = 0.85$$

$$\eta_{S} = 0.107$$

Using the absorptivity equation (6),

$$\alpha_{ZT} = 0.682 - 0.901 \, [1 - 0.00545(T-301)]$$

cell stack temperatures were calculated. These results are presented by Figure 5. The maximum calculated cell temperature is approximately $190^{O}F$; the maximum temperature of the thermal shield will be about $380^{O}F$.

Using the power equations:

$$P = (2rh \sin \theta) \, S \, (0.107) \, \eta_{FB} \, [1 - 0.00545(T-301)]$$

$$= 336 \, S \sin \theta \, [1 - 0.00545(T-301)],$$

the power output of the solar array was computed for three solar distances (1, 0.4, and 0.2 AU). These results are presented in Figure 6.

Figure 7 shows the shield angle required for maximum and minimum (60 watts) power from 1.0 to 0.2 AU. Figure 8 provides the maximum power available from the array, for each of the filters considered, as a function of solar distance; this figure provides a basis for selecting filter No. 3. These results show that the minimum power of 60 watts can be maintained for all systems considered, and under all conditions, with the exception of operation with filter No. 2 at 1 AU where the corresponding power is about 52 watts.

Voltage-Current Curves

Voltage-current curves have been estimated for the solar array with filter No. 3 as a function of shield angle and solar distance. The results of this calculation, details of which are provided by Reference 1, are given in Figure 9.

The given analysis does not include losses or degradation of efficiency from the following: assembly losses, diode losses, random open circuit losses, UV adhesive transmission degradation, solar flare degradation, micrometeorite erosion, and operation off of the maximum power point.

Discussion

A number of assumptions and simplifications have been made to facilitate the power and voltage analysis of the system. Consequently, the given results should be considered as a good first approximation of the system performance.

Refinements which could be incorporated in the analysis include: using a larger number of iterations on temperature; accounting for temperature dependent properties such as the shift in the spectral response, r_λ^*, with temperature; including incidence angle effects; allowing for the effects of UV and particle radiation; and allowing for other miscellaneous losses. These refinements would reduce uncertainties resulting from a lack of knowledge of actual component (adhesives, filters, cover glasses) performance in a space environment (i.e., a vacuum with combined UV, particle, and thermal radiation).

Conclusions

The primary conclusion resulting from the analysis reported here is that using a positionable despun thermal shield to expose body-mounted

N/P silicon solar cells at near normal incidence angles, a 0.2 AU mission is feasible in terms of thermal and photovoltaic performance for the spacecraft configuration specified.

In addition, the following conclusions are made:

a) The recommended cell for the solar array is a 1 by 2 cm N/P silicon solar cell with a 10.7 percent conversion efficiency at $28^{\circ}C$ and air mass zero.

b) A currently available and reliable full-cell-response bandwidth blue-red filter with a single IR suppression band would perform satisfactorily on the stated mission. For improved performance, the same filter with triple suppression should be investigated.

c) A minimum power of 60 watts and a minimum voltage of 24 volts can be maintained throughout the mission. Switching may be required to maintain the minimum voltage at 0.2 AU.

d) Near the sun, a considerable power surplus is available.

e) Shield angles near the sun are small, thereby minimizing the effective exposure of the cells. Thus, incidence angle effects and solar array temperatures are minimized and photovoltaic operation is optimized.

f) As a result of the spacecraft spin rate, the solar array is essentially isothermal.

g) The maximum temperature of the solar array will be approximately $190^{\circ}F$. The maximum temperature of the thermal shield will be about $380^{\circ}F$.

h) The shield configuration using two counter-rotating despun shields rotating about the spacecraft spin axis, provides the performance optimization noted above.

References

1. Cobb, M. W., Cummings, W. S., and Fairbanks, J. W.; The Feasibility of a Programmed Heat Shield for Solar Cell Performance Control, WDL-TR2633, Philco Corporation, WDL Division, Palo Alto, California October 15, 1965.

2. Charnes, A. and Raynor, S., Solar Heating of a Rotating Cylindrical Space Vehicle, ARS Journal, May 1960.

3. McAdams, W. H., Heat Transmission, McGraw-Hill Book Co, Inc., 1965.

4. Thelan, A., Multilayer Filters with Wide Transmittance Bands, Journal of the American Optical Society, Vol 53, No. 11, November 1963.

Bibliography

1. Arveson, J. C., Neel, C. B., and Shaw, C. C.; Preliminary Results from a Round-Robin Study of UV Degradation of Spacecraft Thermal Control Coatings; NASA SP-55, Symposium on Thermal Radiation of Solids; San Francisco, California, March 1964.

2. Baker, J.K., Temperature Control Techniques for Solar Energy Converters, Tech. Report ADS-TR-61-689, February, 1962.

3. Cherry, W. R., Solar Cells and the Applications Engineer, Astronautics and Aerospace Engineering, May, 1963.

4. Cooley, W. C. and Janda, R. J.; Handbook of Space Radiation Effects; NASA SP-3003, Office of Scientific and Technical Information, NASA, Washington, D. C.; 1963.

5. Fairbanks, J. W. and Piccianno, W.; Comet and Close-Approach Asteroid Mission Study, Vol. 7, Power, WDL-TR2366, Philco Corporation, WDL Division, Palo Alto, California, January, 1965.

6. Johnston, P. A., Laboratory Experiments on the Performance of Silicon Solar Cells at High Solar Intensities and Temperatures, NASA TN D-2733, Ames Research Center, Moffett Field, California, March, 1965.

7. Kuyminski, H. W., McKendry, F. J., Oblinger, C. R., and Topfer, A. R., Development of Improved Gallium Arsenide Solar Cells, Contract NAS 5-9006, RCA, Direct Energy Conversion Department, Mountaintop, Pa., February, 1965.

8. Loferski, J. J., Theoretical Considerations Governing the Choice of the Optimum Semiconductor for Photovoltaic Solar Energy Conversion, Journal of Applied Physics, Vol. 27, No. 7, July, 1956.

9. Loferski, J. J., Recent Research on Photovoltaic Solar Energy Converters, Proc. of the IEEE, May, 1963.

10. Luft, W., Advanced Energy Conversion, Vol. 5, pp. 21-41, Pergammon Press, 1965.

11. Martin, J. H.; Teener, J. W., and Ralph, E. L., Some Effects of Electron Irradiation and Temperature on Solar Cell Performance, Heliotek Technical Paper B101A, 21 May, 1963.

12. Neustien, J., Selected Notes on Space Power Systems, Electro-Optical Systems, Inc., Presented at Stanford University, 23 February, 1965.

13. Rappaport, P., Solar Cells 1963 -- A Status Report, RCA Direct Energy Conversion (Company Brochure), RCA Laboratories, Princeton, N. J., April, 1964.

CYLINDRICAL
SPACECRAFT

THERMAL
SHIELD

THERMAL
SHIELD

SPACECRAFT

SHIELD
PIVOT

SHIELD FULL OPEN
(ζ = 180°)

SHIELD HALF OPEN
(ζ = 90°)
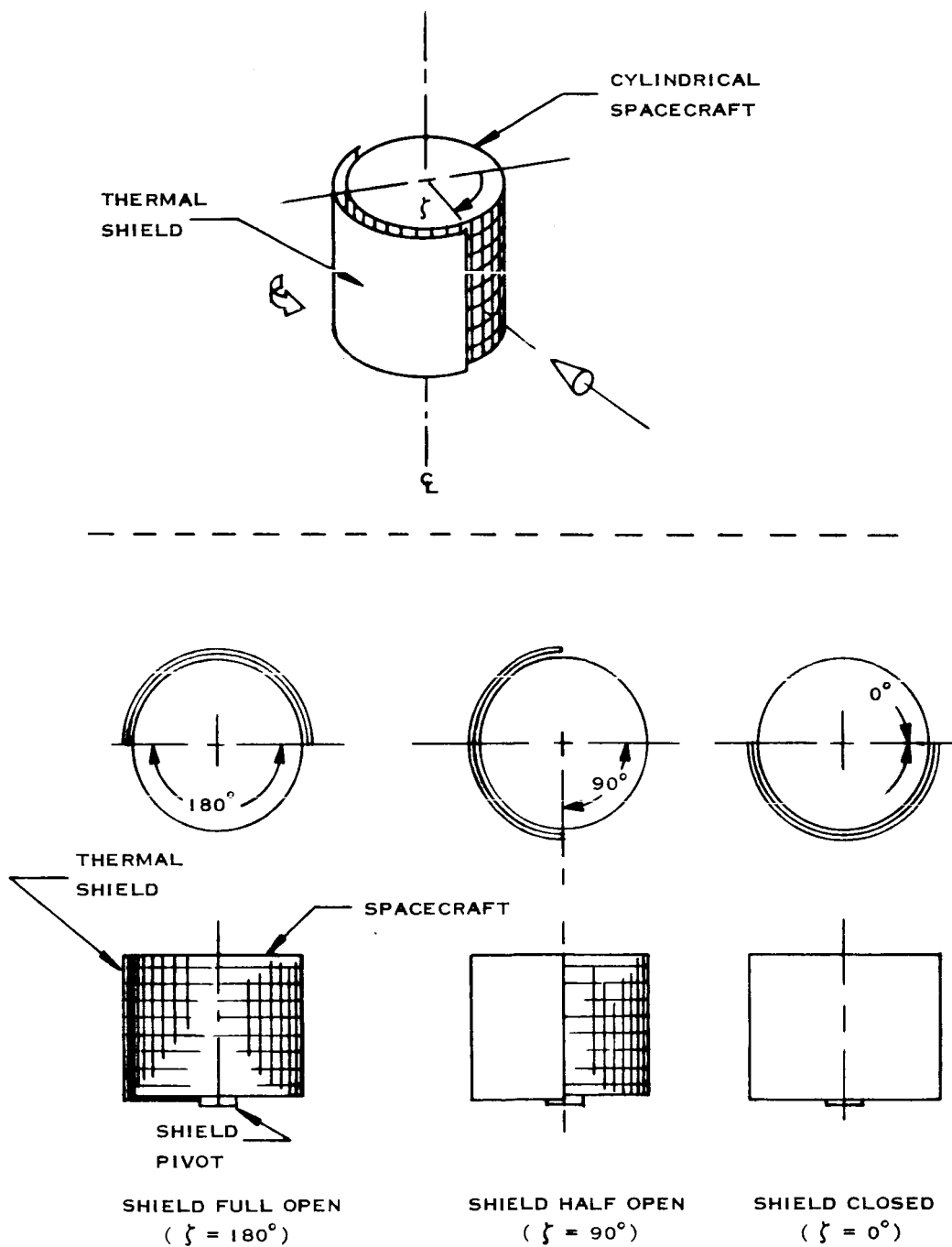
SHIELD CLOSED
(ζ = 0°)

Figure 1 - Configuration Schematic - Single Active
Thermal Shield (Configuration 1)

14. Wise, J. F., Radiation Effects on Solar Cells , Technical Memorandum ASRPP RM 63-41, Aeronautical Systems Division, Air Force Systems Command, Wright-Patterson Air Force Base, Ohio, June, 1963.

15. Wolf, M., and Rauschenbach, H., Series Resistance Effects on Solar Cell Measurements, Advanced Energy Conversion, Vol. 3, pp. 455-479, Pergammon Press, 1963.

TOP VIEW

SPACECRAFT
(NODE 1)

SHIELD
(NODE 2)

2θ

UNIT
SOLAR
VECTOR

SIDE VIEW

SPIN AXIS

SHIELD

2.5
FT

SPACE-
CRAFT

UNIT
SOLAR
VECTOR

₵

3 FT
DIA.
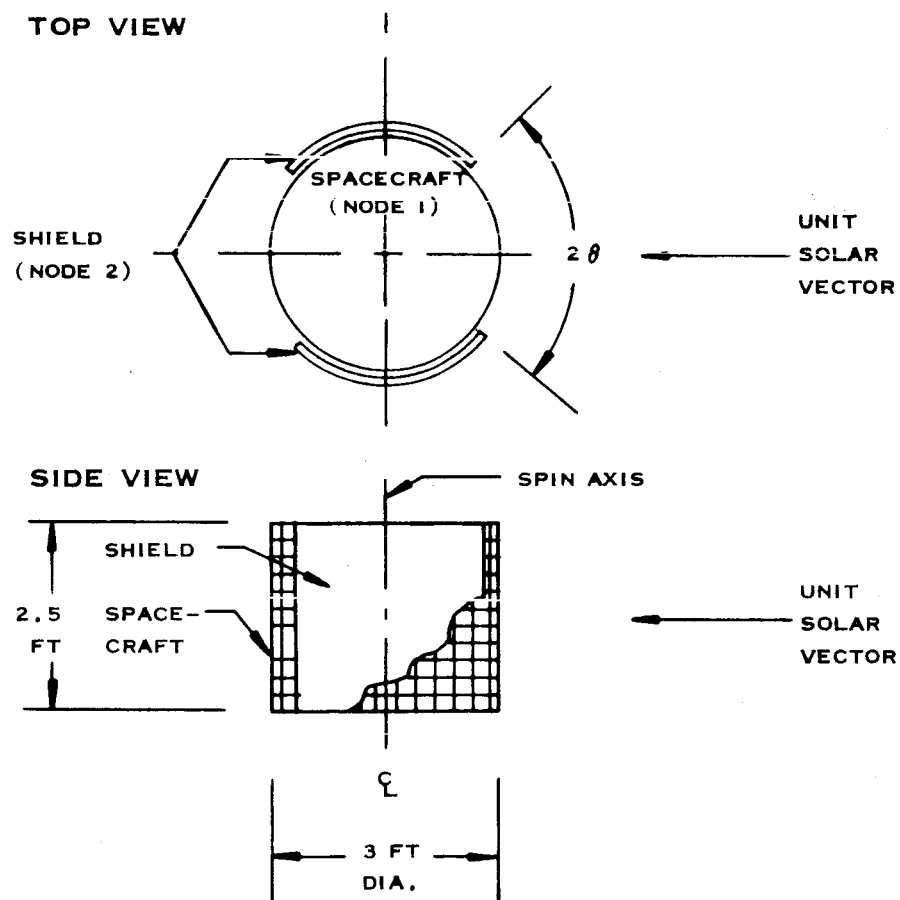
Figure 3 - Spacecraft and Shield Schematic of Thermal Model
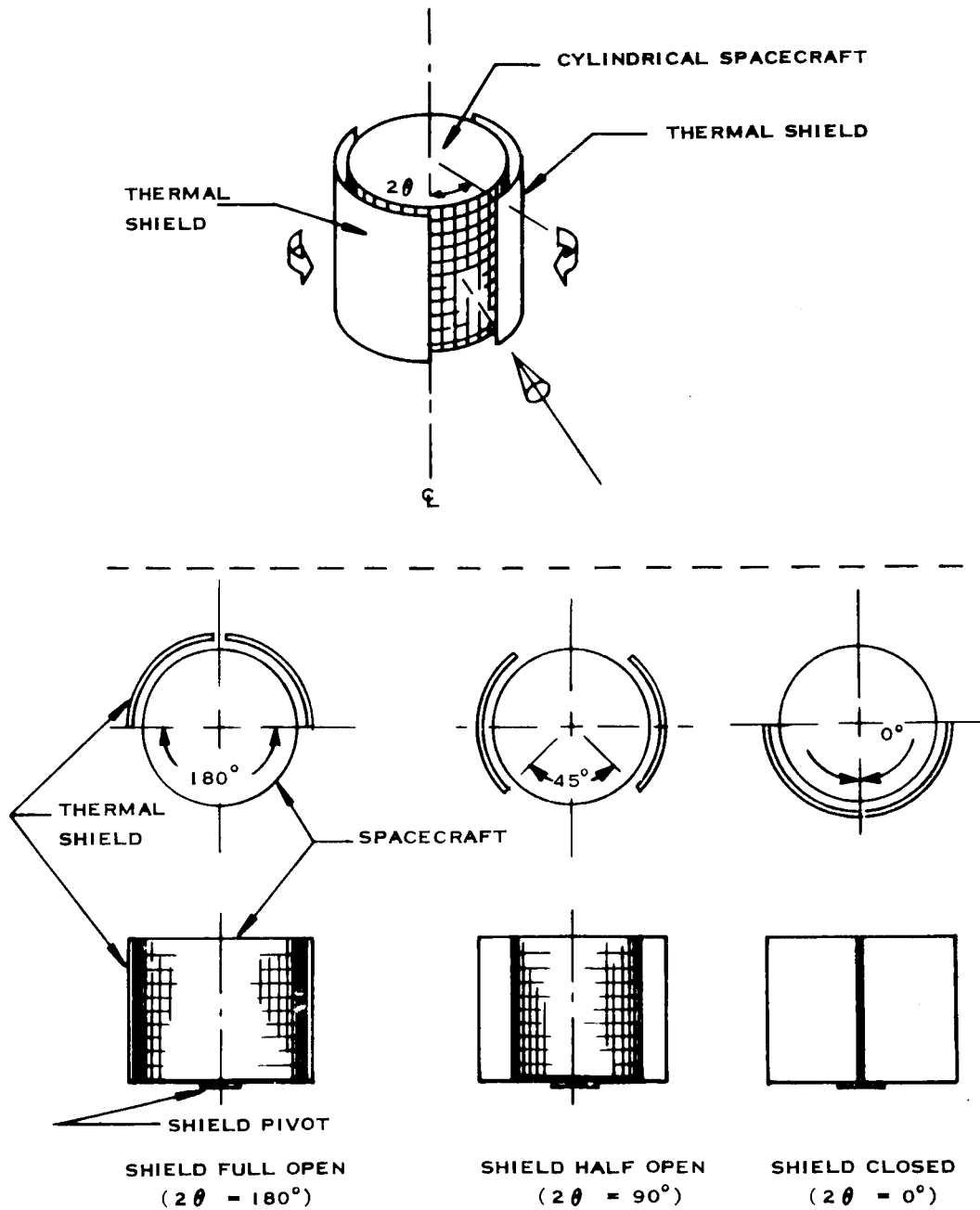
Figure 2 - Configuration Schematic - Active Shield Consisting
of Two Counter-Rotating Shields (Configuration 2)
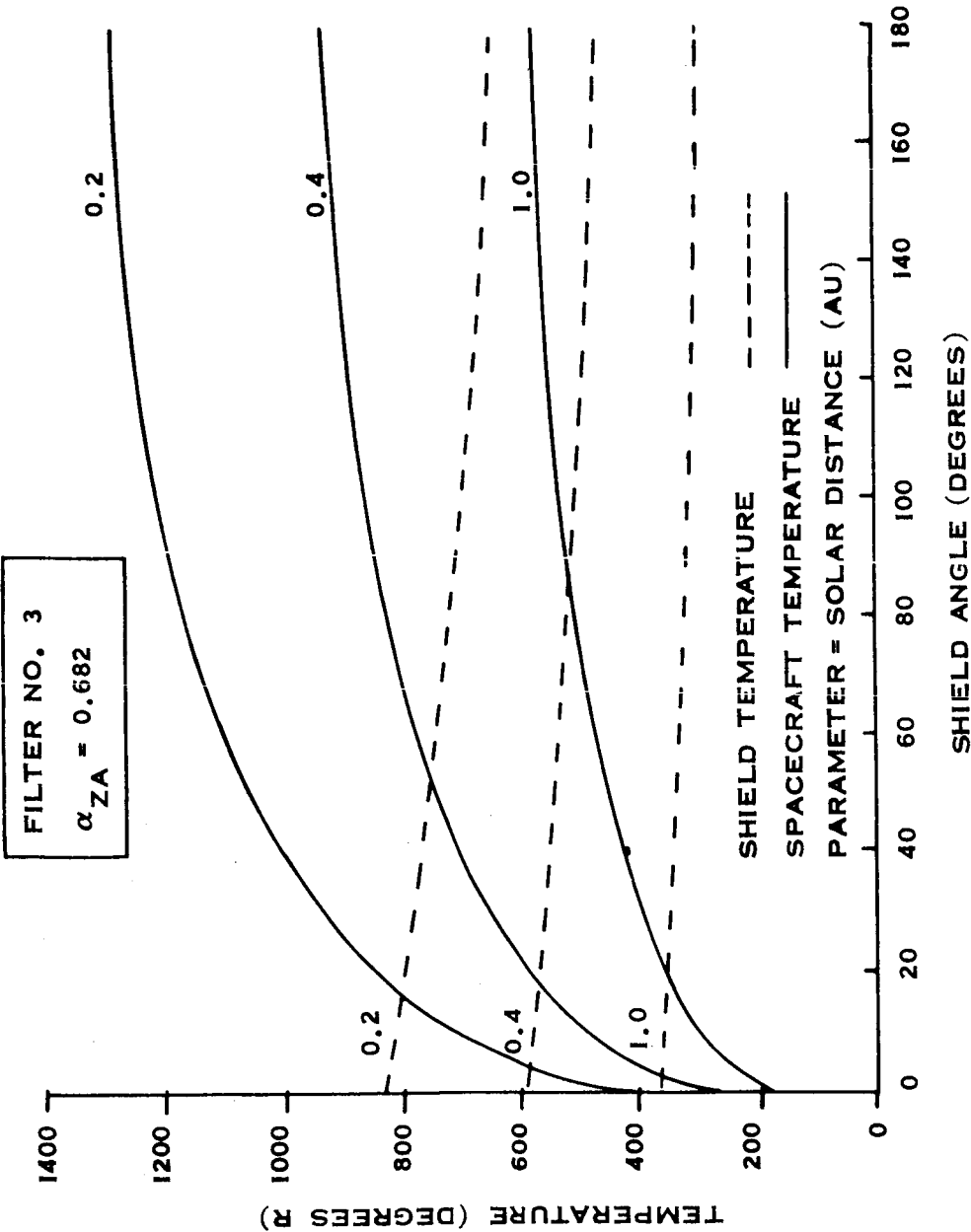
Figure 5 - Shield and Spacecraft Temperature vs. Shield Angle No
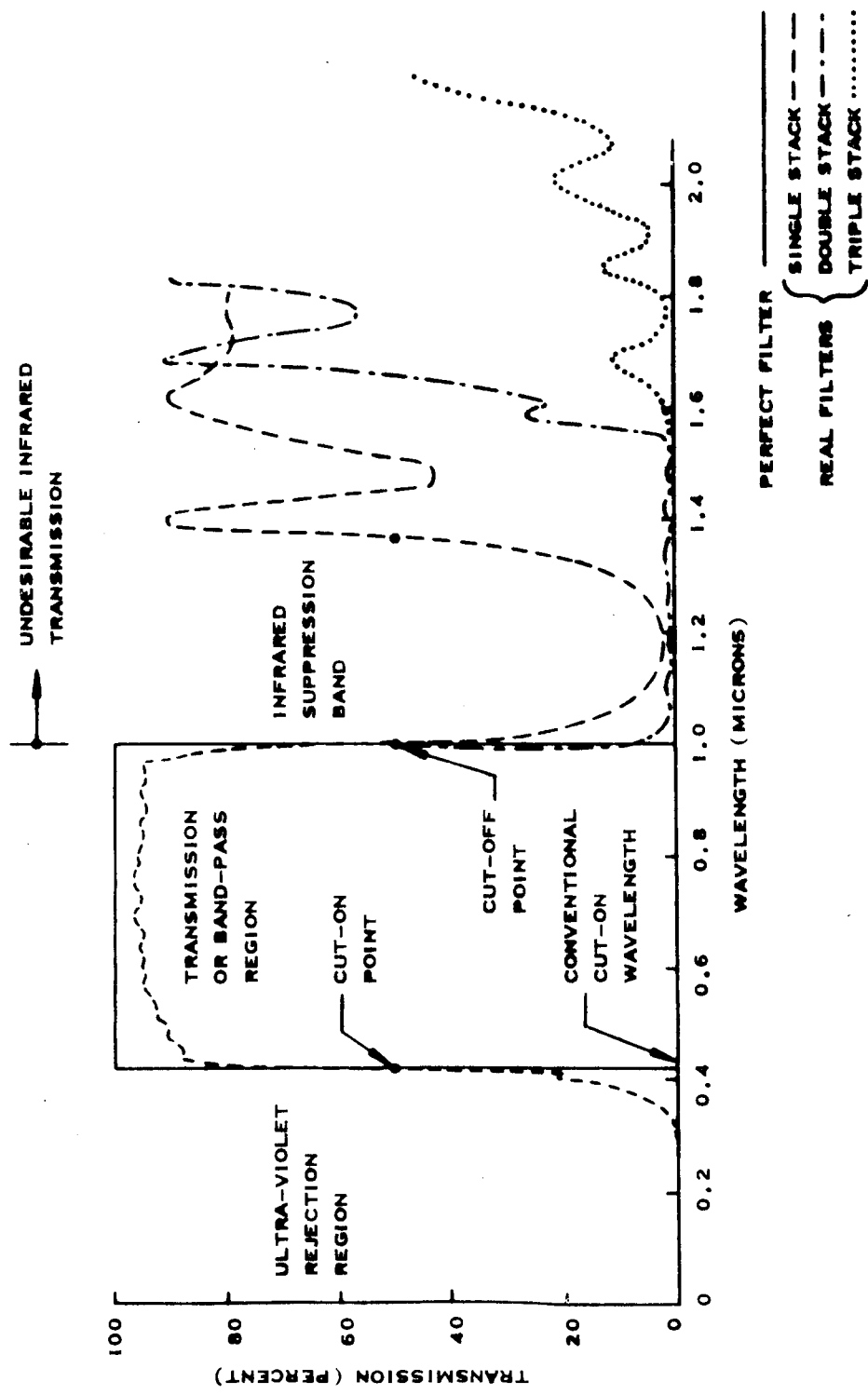Radiation from Ends of Satellite

Figure 4 - Perfect and Real Filter Characteristics (Silicon Solar Cells)
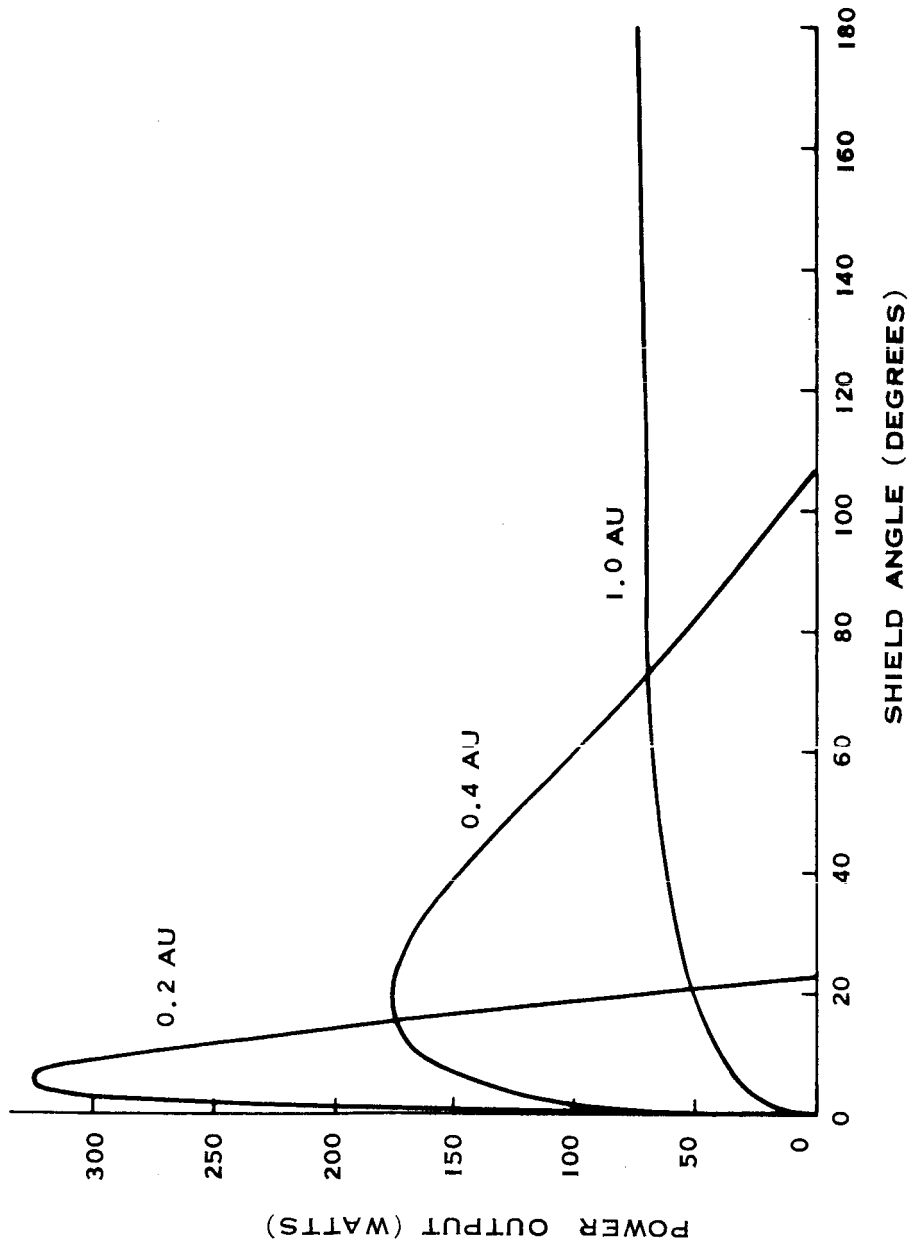
Figure 6 - Power Output vs. Shield Angle N/P Silicon Solar Cells with Filter No. 3
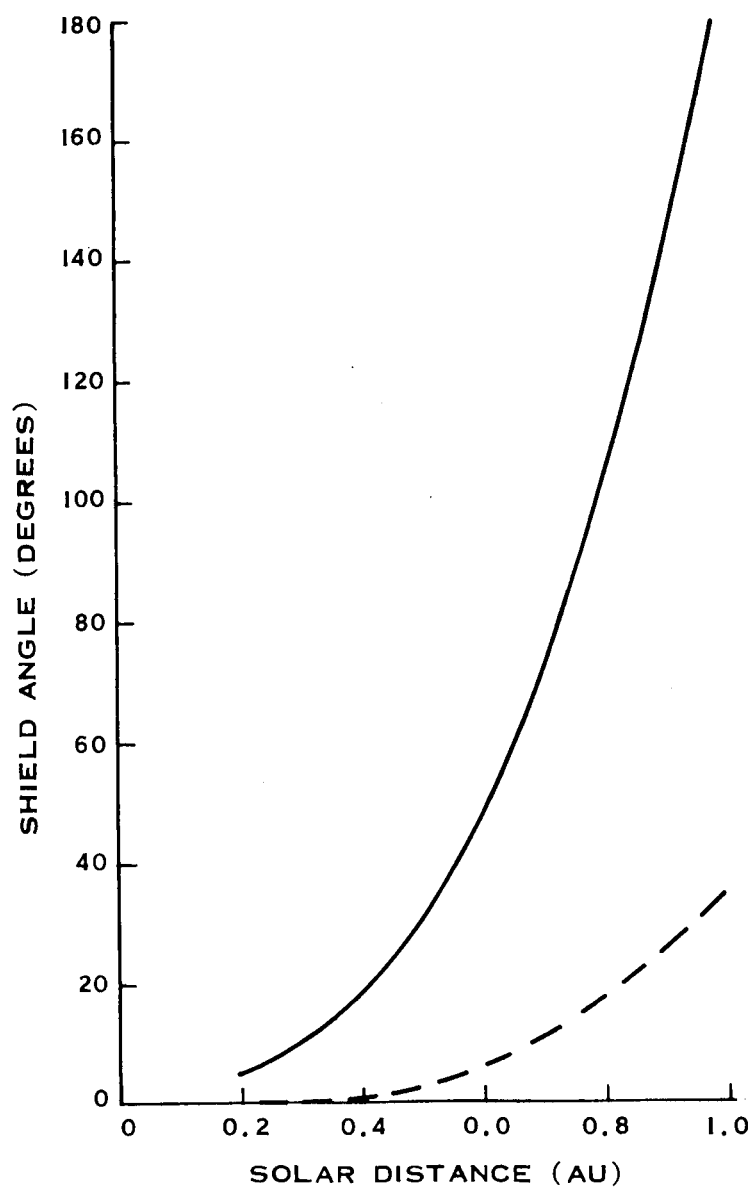
Figure 7 - Shield Angle vs. Solar Distance N/P Silicon
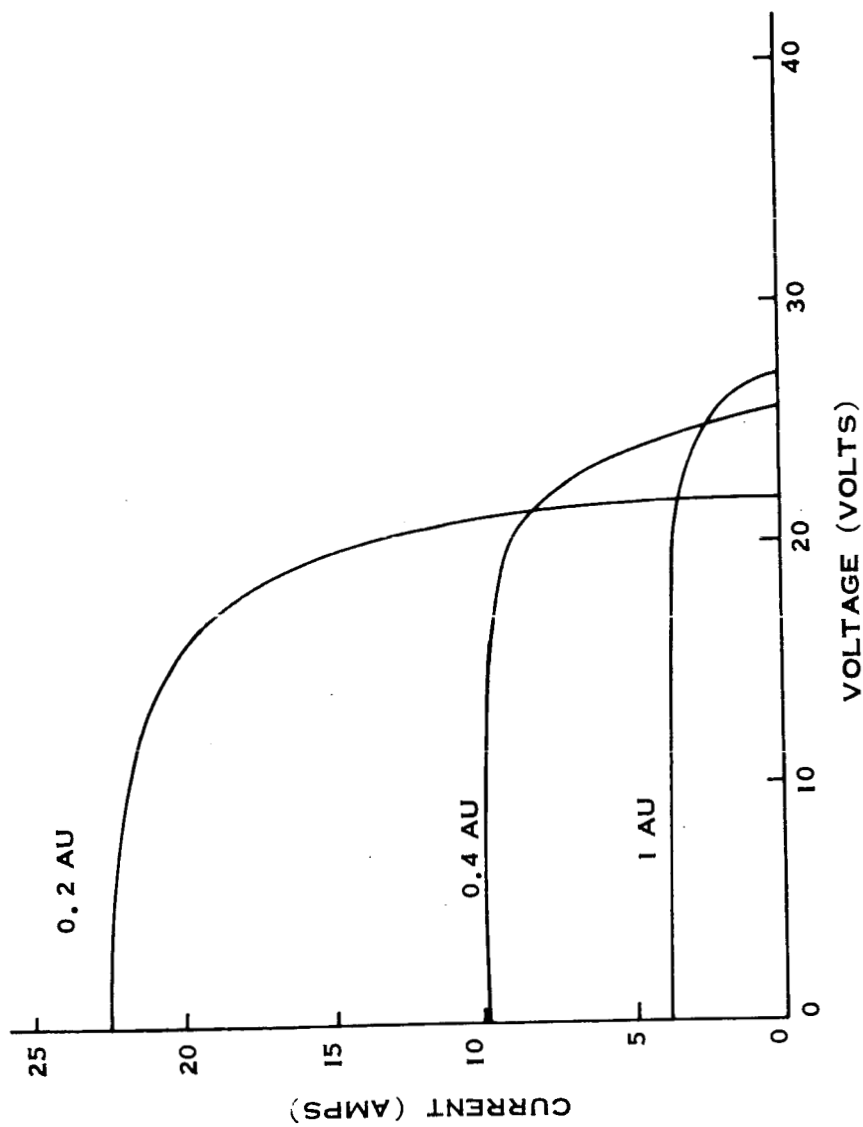Solar Cells with Filter No. 3

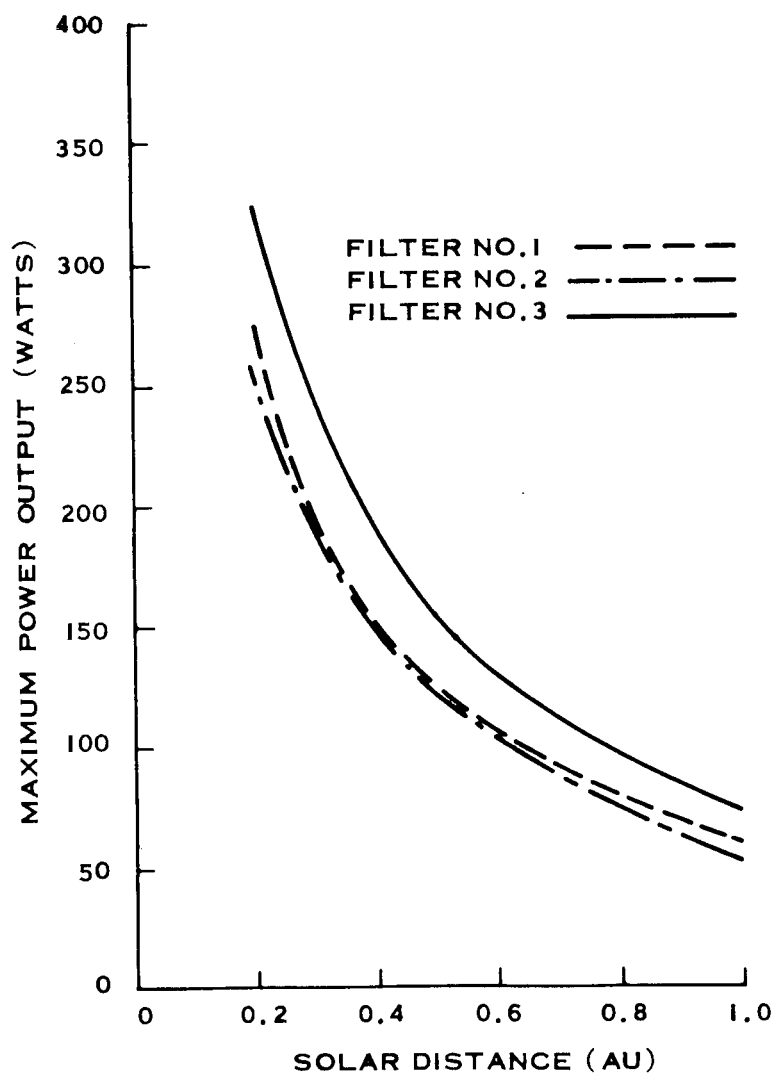Figure 9 - Voltage-Current Curves N/P Silicon Solar Cells with Filter No. 3

Figure 8 – Maximum Power Output vs. Solar Distance

Closing Remarks

by

Paul Rappaport
IEEE Program Committee Chairman

In spite of the vital job solar cells have already done in space, we in the solar cell field still seem to be battling to stay alive! We don't seem to have a high level national spokesman, and in view of Dr. Townsend's remarks and Mr. Finger's remarks I would say we need one. Short of that, we should all attempt to make sure that the systems people are aware of the real potential of solar cells!

Single crystal silicon cell arrays have been engineered today to deliver power in the kilowatt range with power to weight ratios of 15-20 w/lb. This is a moving target and p/w ratio of 25 w/lb should be possible within a few years. As we have seen in this meeting, film type cells are coming along very well and certainly cell p/w ratios of over 100 w/lb are possible. The system p/w ratio would of course be less but appreciably higher than 25 w/lb. Systems in the tens of kilowatt range could fly before 1970!

Radiation damage is no longer a serious problem. The reliability of solar cell systems is in the 5-10 years range. Storage batteries are the real weak link in systems where they are needed. Most of the competing systems I know of will have difficulty attaining over 5 year life. Perhaps Pu^{238} isotope systems using Si-Ge thermoelectrics will compete in reliability, although the power to weight ratio will be ten times poorer.

The cost of $1000/watt that Mr. Finger mentioned last night is an antiquated number. Here again, solar cells are a moving target! An oriented array system today cost perhaps $400/watt, standardization could reduce costs, and I dare say that if the volume demand were great enough where high power systems were required that this price could be reduced by an appreciable amount.

I am not trying to say that solar cells are the be-all and end-all in space power systems. Other systems are very important and should be developed, but for solar powered missions, solar cells stand alone in reliability, weight and availability for high power (tens of Kw) systems. In spite of this, the industry has literally been scrounging to stay alive. Something's wrong, the funding has been low and decreasing and some of you in this room should be thinking about what can be done to correct this situation!